NASA-CR-193480

OSU-ECE Report NASA 93-03

Final Report on

NONLINEAR STABILITY AND CONTROL STUDY OF HIGHLY MANEUVERABLE HIGH PERFORMANCE AIRCRAFT

(NASA Grant No. NAG-1-1081)

Date: July 20, 1993

R.R. Mohler, Principal Investigator

Oregon State University
Department of Electrical and Computer Engineering
Corvallis, OR 97331-3211

(503) 737-3470/3617

Graduate Research Assistants: S. Cho, C. Koo, R. Zakrzewski, D. Collins
Undergraduate Participants (NSF Support): J. Young, H. Travis, S. Bloom
Visiting Researchers: M. Boasson, A. Khapalov

OSU-ECE Report NASA 93-03

Final Report on

NONLINEAR STABILITY AND CONTROL STUDY OF HIGHLY MANEUVERABLE HIGH PERFORMANCE AIRCRAFT

(NASA Grant No. NAG-1-1081)

Date: July 20, 1993

R.R. Mohler, Principal Investigator

Oregon State University
Department of Electrical and Computer Engineering
Corvallis, OR 97331-3211

(503) 737-3470/3617

Graduate Research Assistants: S. Cho, C. Koo, R. Zakrzewski, D. Collins
Undergraduate Participants (NSF Support): J. Young, H. Travis, S. Bloom
Visiting Researchers: M. Boasson, A. Khapalov

TABLE OF CONTENTS

1. PROJECT SUMMARY

This project is intended to research and develop new nonlinear methodologies for the control and stability analysis of high-performance, high angle-of-attack aircraft such as HARV (F18). The present report summarizes past research (reported in our Phase 1, 2, and 3 progress reports) and provides more details of final Phase 3 research.

While research emphasis is on nonlinear control, other tasks such as associated model development, system identification, stability analysis, and simulation are performed in some detail as well. Table 1-1 provides an overview of various models that have been investigated for different purposes such as an approximate model reference for control adaptation, as well as another model for accurate rigid-body longitudinal motion. Only a very cursory analysis has been made relative to type 8 (flexible body dynamics). Standard nonlinear longitudinal airframe dynamics (type 7) with the available modified F18 stability derivatives, thrust vectoring, actuator dynamics, and control constraints are utilized for simulated flight evaluation of derived controller performance in all cases studied here.

Past research indicates that nonlinear control can be utilized effectively to control high-performance aircraft such as HARV (F18) for rapid maneuvers with large changes in angle of attack (α) — cases where classical linear feedback control (without gain scheduling) can yield poor performance or even instability. Even nonlinear feedback controllers that were generated in conjunction with a linear model reference (and without multiple regression terms) failed for certain high-α maneuvers but with added nonlinear reference terms they lead to successful control. More recent results, however, indicate that even the nonlinear feedback controller generated in conjunction with a higher-order (more delay terms) linear model-reference is quite effective for the cases considered in Section 6. On the other hand, it is shown that further performance gains may be realized with the addition of bilinear and higher nonlinear terms in the model reference for control adaptation as for previous studies.

As a benchmark for judging controller performance, and also as a basis for future designs and for pilot-manipulated control, optimal control is studied in some detail, as summarized in Section 3. The derived algorithms for minimum-time control and for minimum quadratic state-error control both consider the full nonlinear dynamics with applicable control (magnitude and rate) constraints. The software has been generated in C language and can be applied virtually to any aircraft control or other plant.

The time-optimal control from an initial trim state (at 15,000 ft altitude and mach 0.3) with $\alpha(t_0) = 5°$ to $\alpha(t_f) = 60°$, with thrust $T(t_0) = 3{,}000$ pounds and $T(t_f) = 18{,}000$ pounds, takes place about 1.8 sec without any efforts to hold $\alpha(t)$ for $t > t_f$. On the other hand, a quadratic-performance controller completes the maneuver in about 2.5 sec with a normal peak acceleration (n_z) of about 2.5 g

Table 1-1. Aircraft Models

Type	Purpose	Remarks/Limitations
1. Linear perturbations desired α, M, h*	Local control, check of nonlinear system, application of well developed linear control methodologies Local stability	Only valid for small maneuvers Special case of types 2-5
2. Gain scheduled (nonlinear function of α) from 1	Gain-scheduled adaptive control based on well developed methodologies Simplified description of complex system Approximate stability	May have stability problems with small number of reference states and/or large fast maneuvers
3. Volterra series† a) at reference states b) general case	Nonlinear adaptive control via cross-correlation and/or á priori dynamic structure Stability approximation Simplified dynamic description of complex system	Non-orthogonal series approximation Sufficiency of 2 or 3 kernels Large computation time for adaptation
4. Bilinear system a) continuous b) BARMA 5. Polynomial time series	Nonlinear adaptive control via model reference identification (NLMRAC) Stability approximation Simplified dynamic description	Large computation time Bilinearizing controllers may be more practical than linearizing ones Polynomial approximation may be more accurate but more time consuming than linear or bilinear approximation
6. Neural network	Potential application to adaptive control	Probably less accurate than 4 or 5 for a given data set but accuracy may be more robust outside the available data set
7. Nonlinear ordinary differential equation model	Accurate approximation to fast large maneuvers for "final" design and simulation Stability	Neglects flexible modes and other complications
8. Nonlinear partial differential equations model	Allows the treatment of distributed external stresses and local pressures as well as internal stresses and deformations	Computations are time consuming Overall model complexity Allows one to treat flutter and distributed control strategies, etc.

*α is angle of attack, M mach number, and h altitude
†Wiener series can be used for orthogonal representation

and a q_{max} (maximum pitch rate) of about 60°/sec. The α response is quite smooth with less than 10% overshoot and a rise-time of about 1.8 sec (see Section 3.4).

All the high-performance controllers studied seem to mimic the optimal control policy by operating in saturation for most of the trajectory. Switching times of the stabilator and the thrust vector motion is somewhat critical as generated by the appropriate feedback.

The stringent requirement to control α and not allow drastic changes in pitch for $t > t_f$ suggests the use of a terminal sliding-mode control which is studied for the whole maneuver in Section 7. While the results are preliminary, the method shows promise.

The adaptive controls studied in Section 6 perform very well and only a little slower than optimum. It is expected that further investigation of practical nonlinear feedback control will lead to an even simpler and better closed loop system. Then effectiveness for trajectory following in general needs to be studied.

The neural-net controller which is trained off-line on the simulated optimal policies perform quite effectively despite the preliminary nature of derivation. For example, such neural-net generated policy controls HARV (F18) from a $\alpha = 5°$ trim state to 70° in about 4.5 sec. It should be realized that, in a general sense, neural-net-based controllers typically are a form of nonlinear adaptive controllers with the neural-net an appropriate nonlinear model consisting of layers of adjustable parameters with their outputs summed and processed through nonlinear limiting functions such as sigmoidal ones. The other adaptive controllers here are based on polynomial (with linearity a special case) discrete approximations with varying degrees of lag terms. Project publications (in addition to the semiannual progress reports) are listed in Appendix A along with research contributors.

2. INTRODUCTION

Nonlinear control of high-performance aircraft such as HARV (F18) has been demonstrated with accurate computer simulations to be effective by this project as well as others such as Ostroff [2.1] and Buffington, Sparks, and Banda [2.2]. The difference between our controllers and the latter two is that the latter generate the nonlinear feedback gains to account for certain (assumed known) nonlinear plant dynamics. Reference [2.1] utilizes numerous trim-state linearization studies to determine the required gains in conjunction with a flight-test proven PIF controller which is able to successfully control HARV from $\alpha(t_0) = 5°$ trim to about 60° in about 5 sec. Reference [2.2] is based on a linear H_∞ design in conjunction with trim-state linearized dynamics and an appropriate nonlinear gain scheduled according to dynamic pressure variation. The latter study only considers a maximum change from $\alpha(t_0) = 10°$ to $\alpha = 20°$ in about 3 sec with a rise time of 1 sec, $q_{max} \sim 14°$/sec, and $n_z \sim 1.5$ g. While neither of the latter two are nearly minimum-time maneuvers as demonstrated here, they probably represent the best controllers based primarily on linear design methodology in conjunction with somewhat ad-hoc nonlinear correction.

2.1 References

[2.1] A. J. Ostroff, "High Alpha Application of Variable-Gain Output Feedback Control," *J. Guidance, Control & Dyn.*, Vol. 15, 491-497, 1992.

[2.2] J. Buffington, A. Sparks, and S. Banda, "Full Envelope Robust Longitudinal Axis Design of a Flight Aircraft with Thrust Vectoring," *Proc. IEEE American Control Conf.*, San Francisco, 1993.

3. OPTIMAL CONTROL

3.1. General Concept

This section discusses research on optimal control of longitudinal aircraft dynamics. Since the objective of the project is to develop high performance control algorithms, it is natural to investigate the possibility of obtaining the highest possible performance — through optimal control theory. While optimal control may be useful in its own right, the emphasis here is in using the optimal control as a yardstick to judge our more practical designs and as a base for their synthesis such as by neural nets. Understanding how the formulation of the optimal control problem affects the behavior of optimally controlled aircraft is crucial to a successful application. In this work two most commonly used performance criteria are investigated: minimum time performance index and integral quadratic performance index.

Even if the correspondence between the problem formulation and actual optimal performance is well understood, still practical application of optimal control theory sometimes may seem questionable. Most significantly, optimal control depends upon exact knowledge of the dynamics of the controlled plant. While this assumption may be quite realistic in some applications, parameter uncertainty arises for high performance aircraft due to stability derivative uncertainty, nonuniform (geometrically) fluid flow, etc. Also, for a nonlinear system, the actual calculation of the optimal controls usually involves an iterative numerical algorithm. Even in case of a relatively uncomplicated model, as longitudinal aircraft dynamics, on-line optimization may require computational capabilities of the order precluding any realistic practical applications. Furthermore, unlike for linear systems, optimal feedback synthesis for a nonlinear plant may be almost impossible. There are numerous optimization techniques available that solve open-loop optimal control problems efficiently. However, there are few methods to solve the closed-loop synthesis problem. Theoretically, the very existence of a unique optimal feedback is not even certain for some nonlinear systems [3.6]. These three points make one raise a question: If the available aircraft model is highly uncertain and feedback control policy is sought that must be implementable in real-time using an on-board computer is it at all logical to investigate optimal control? It is argued here that in spite of those doubts the study of optimal controls can answer important questions and be utilized in the design of feedback controllers.

First of all, optimal trajectories provide the upper bound for the performance possible achieved by the investigated aircraft. Since the solution of the optimization problem is obtained with full and exact information about the plant dynamics, no other control algorithm can possibly result in better performance in terms of a particular criterion. Thus the optimal trajectories can serve as benchmark tests for feedback controllers developed using other design methodologies. With the limit of performance available, it is

easier to assess the degree of improvement of one control scheme over another. This alone seems to be an objective important enough to justify the investigations that will follow.

Second, optimal trajectories demonstrate what type of control actions are required to achieve high performance. In particular, optimality is often achieved with extremal values of control signals. Current practice in aircraft control design is to use gain scheduling of linear controllers, and often the point is made of avoiding the saturation of actuators (e.g. [3.4]). This is motivated by the fact that saturation results in loss of linearity of the controller and invalidates the theory underlying the design. The issue emphasized here is that, since the aircraft dynamics during large maneuvers can hardly be described by a linear model, the struggle to maintain linearity of the controller is somewhat unnecessary. As it is demonstrated below, almost always maximum admissible control effort is required for both time-optimal control and integral-quadratic criterion minimization. Thus, to utilize existing control capabilities fully to their limits, it is necessary to use nonlinear control algorithms, which take into account limits of control signals and of their change rates. Investigations of optimal open-loop trajectories may also answer the questions which of those constraints are most critical for which types of maneuvers. This may provide some guidelines for the designers of the actual aircraft about possible ways of enhancing optimal aircraft performance.

Third, open-loop generated optimal trajectories may be used for synthesis of feedback controllers. One such possibility, discussed in detail in Section 4, is to approximate optimal feedback mapping using a number of optimal trajectories as learning data used for nonlinear function fitting. A particular implementation of such approximation proposed in this report is by artificial neural networks. Another way to utilize information about optimal trajectories is to use them as reference tracking signals in output feedback controllers. Formation of reference signal out of command signal is one of the major difficulties in model reference control. Common practice is to use linear reference models. As discussed above this may lead to unnecessarily conservative performance, particularly close to the target value of the output. A solution to this problem may be the utilization of optimal trajectory as the demanding, yet possible to track, reference signal. Difficulty with on-line generation of an optimal output trajectory may be circumvented by some kind of interpolation between a number of optimal trajectories, pre-calculated off-line for different command signals. Again, the artificial neural network approach is one possible implementation of this idea.

To investigate the issues raised above a large number of optimal trajectories was calculated in the open-loop mode using numerical optimization techniques. The following sections discuss in detail optimal control problems solved, the actual algorithms used for solution, and the results of simulations.

3.2. Methodology

The optimal control calculations were performed for the fourth-order nonlinear model of longitudinal dynamics augmented with dynamics of three actuators including their saturation. Two types of optimal control problems are solved, time-optimal problem and integral quadratic performance index minimization, with controlled output variable being either the angle of attack or pitch rate. The following subsections give precise problem statements and discuss the numerical methods used.

3.2.1. Aircraft Model

The model of the aircraft used is the full nonlinear longitudinal dynamics of a modified F 18 (HARV), described in Appendix B. The general form of the models is:

$$\mathbf{dx/dt} = \mathbf{f(x,u)} \tag{3.1}$$

with state vector $\mathbf{x} = [\alpha, q, \theta, v]^T$, control vector $\mathbf{u} = [\delta_h, T_M, \delta_v]^T$, α — angle of attack, q — pitch rate, θ — pitch angle, v — total velocity, δ_h — elevator angle, T_M — thrust magnitude, and δ_v — angle of thrust vector. In practice, thrust magnitude is controlled typically by the pilot through the throttle, so generally it should be treated as a given, time-varying parameter, rather than a feedback control signal. Here, the objective is to obtain the performance limits for the aircraft and to manipulate T_M optimally. Control signals are assumed to be subject to the following constraints:

$$\begin{aligned} -24° \;&\le\; \delta_h \;&\le\; 10° \\ 3{,}000 \text{ lbs} \;&\le\; T_M \;&\le\; 18{,}000 \text{ lbs} \\ -20° \;&\le\; \delta_v \;&\le\; 20° \end{aligned} \tag{3.2}$$

Additionally, model (3.1) was extended with dynamics of the actuators for δ_h, T_M, and δ_v. Dynamics of T_M is assumed to be linear of the first order with time constant 1s. Time constants for δ_h and δ_v are 1/30s, but there are constraints for their rates of change: $|d\delta_h/dt| \le 40°/S$, $|d\delta_v/dt| \le 40°/S$. This results in nonlinear dynamics model for δ_h and δ_v. The saturation of rate of change is modelled in a smooth way to make the gradient calculations in optimization methods possible. The actuators were modelled as:

$$\begin{aligned} d\delta_h/dt &= g\left(-30\delta_h + 30u_{\delta_h}\right) \\ d\delta_v/dt &= g\left(-30\delta_v + 30u_{\delta_v}\right) \\ dT_M/dt &= -T_M + u_{T_M} \end{aligned} \tag{3.3}$$

with smooth saturation function g

$$g(z) = \begin{cases} 40 - \exp(-x+39) & \text{if } x > 39 \\ z & \text{if } -39 \leq x \leq 39 \\ -40 + \exp(x+39) & \text{if } x < -39 \end{cases} \tag{3.4}$$

Finally the obtained model is of the seventh order

$$dx'/dt = f'(x',u') \tag{3.5}$$

with the augmented state $\mathbf{x}' = [\mathbf{x}^T, \mathbf{u}^T]^T$ and with the control variables being the demand signals to the actuators $\mathbf{u}' = [u_{\delta_h}, u_{T_M}, u_{\delta_v}]^T$. Constraints (3.2) are now defined for $\mathbf{u}'$, but because of the form of (3.3-3.4) will be also satisfied for actual control signals $\mathbf{u}$.

For the purpose of study of optimal control, equilibria of model (3.5) were investigated. Since in equilibrium $\mathbf{u} = \mathbf{u}'$, it is possible to omit three equations (3.3) and deal only with the fourth order system (3.1). Because thrust vectoring is usually applied only during maneuvers, δ_v in equilibrium is assumed to be zero. In such case the set of equilibria of (3.1) is parametrized by values of T_M and δ_h — it is a two-dimensional manifold in four-dimensional state space. Among all equilibria there are trim conditions, e.g., specific points in which $\alpha = \theta$. For each thrust magnitude T_M there is only one or two such trim conditions, and all other attainable equilibria of (3.1) correspond to ascending or descending flight. For higher T_M it is possible to trim the aircraft at higher α — for maximal thrust of 18,000 lbs maximal trimmed α is close to 35°. For angles of attack or pitch angles larger than 35° there are equilibria of (3.1) but with non-zero climbing angle.

3.2.2. Time-Optimal Control

The control problem is as follows: given initial state $\mathbf{x}^\circ$ and desired final state $\mathbf{x}^f$ minimize

$$J_{to} = \min\left\{t^f : x(t^f) = x^f\right\} \tag{3.6}$$

with respect to control signal $\mathbf{u}(t)$, $0 \leq t \leq t^f$. In what follows the plant considered is (3.5) even though primes are omitted to simplify notation. The minimal time problem is solved in hierarchical manner. The first step is the problem of reaching $\mathbf{x}^f$ from $\mathbf{x}^0$ in fixed time t^f. To solve this an auxiliary performance criterion J_{aux} is minimized with respect to control signals:

$$J_{aux}(t^f) = \sum_i \left[\rho_i \left(x_i(t^f) - x_i^f\right)^2\right] \tag{3.7}$$

Here ρ_i are appropriate weights playing the role of scaling coefficients. Also, setting some of ρ_i to zero allows us to specify the desired final set as a hyperplane rather than a point. This may be the case if values of only some of the state variables are actually of interest. If the desired state $\mathbf{x}^f$ (or, more generally the hyperplane specified by $\mathbf{x}^f$ and ρ) is reachable from $\mathbf{x}^0$ in time t^f then the minimum of (3.7) is $J_{aux}^{opt}(t^f) = 0$. Therefore the actual time optimal problem (3.6) can be reformulated as a search for:

$$t^{opt} = \min\left\{t^f : J_{aux}^{opt}(t^f) = 0\right\} \tag{3.8}$$

Minimization of (3.7) is performed using an iterative gradient scheme. The key element of the procedure is the calculation of the gradient of J_{aux} with respect to control signals. This involves solving at each step a system of adjoint equations

$$d\eta/dt = -(\partial \mathbf{f}(\mathbf{x}, \mathbf{u}/\partial \mathbf{x})^T \eta \tag{3.9}$$

with final conditions

$$\eta_i(t^f) = -2\rho_i\left(x_i(t^f) - x_{if}\right) \tag{3.10}$$

Then the gradient can be calculated according to:

$$(\partial J_{aux}/\partial \mathbf{u})(t) = \left((\partial \mathbf{f}/\partial \mathbf{u})^T \eta\right)(t) \tag{3.11}$$

For derivation of these sensitivity calculations see [3.7]. The gradient calculated according to (3.11) is used for determination of change direction in which minimum search is performed. In this study a conjugate gradient method (see e.g., [3.2]) is used for this purpose. Simplified flow of information during each iteration of minimization of (3.7) is depicted diagrammatically on Fig. 3.1. The most time-consuming element of each iteration is the directional search which consists of repeated simulation of the model with control signal $\mathbf{u}(t) + \gamma \mathbf{v}(t)$, where γ is the search step. Implementation issues concerning directional search, control discretization and incorporating constraints for control values are discussed in Section 3.2.4.

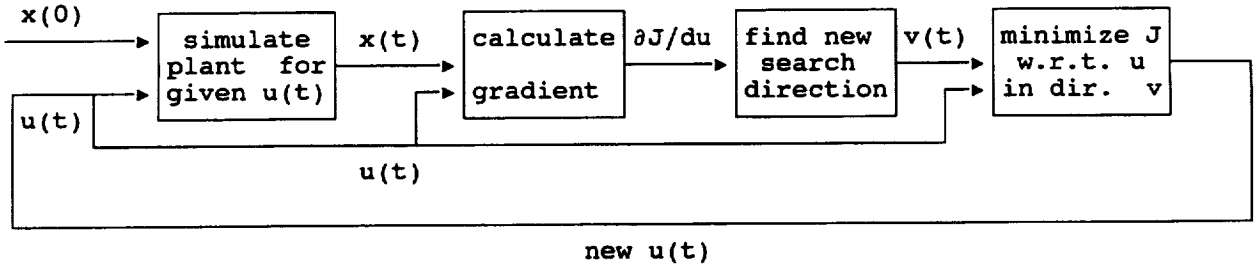

Figure 3.1. Flow of Information for Minimization of (3.7)

With the method of minimization of (3.7) available, determination of optimal time (3.8) is a simple one dimensional optimization problem. In this study it is solved using a bisection method which for our purposes proved to be effective enough.

An alternative, and often more numerically efficient, algorithm for minimization of (3.7) is the switching time variation method [3.3]. It seeks the solution in form of bang-bang controls with the independent variables being the switching times. If optimal control is indeed of bang-bang type with finitely many switchings then the resulting optimization problem is usually low-dimensional and converges much faster than optimization with respect to control values. If the time optimal control trajectory contains a singular arc (an interval with control values not on the constraints) the switching time variation method is still applicable, since for plants affine in control any control trajectory can be approximated arbitrarily closely with bang-bang control [3.1]. Technically (3.3) is not affine in control, but is strictly increasing and by trivial transformation may be made affine in a modified control signal with one-to-one correspondence to the actual control signal. Unfortunately, in a situation with a singular control arc, the method results in increasing number of switchings and quite slow convergence. On the other hand optimization with respect to control values, rather than switching times is more general and also suitable for integral quadratic performance criterion optimization. Therefore application of this method made it possible to use the same basic optimization module for different performance criteria.

3.2.3. Optimal Integral Performance Criterion Control

Control trajectories resulting from solution of the time-optimal problem often display large over-shoots which might be unacceptable from the designer's point of view. Also they include no information as to how to keep the final state. In many time-optimal control applications this issue is not relevant, as, e.g., in case of missile guidance. If, however, the control task is to change the angle of attack or pitch angle rapidly it is expected that the angle should be kept at the same level for at least some finite time. The problem with terminal end control is most apparent if only some of ρ_i are non-zero — i.e., if values of only some of the states are of interest. Then the time-optimal movement towards the target hyperplane

may result in such a final state for which no admissible control exists which would keep the state on the hyperplane. This difficulty can be overcome by using integral performance criterion:

$$J = \int_0^{t^f} f_0(x,x^f,t)\,dt \tag{3.12}$$

A typical choice of the integrand is a quadratic error function

$$f_0(x,x^f,t) = \sum_i \left[\rho_i\left(x_i(t) - x_i^f\right)^2\right] \tag{3.13}$$

If the final state x^f is an equilibrium corresponding to an admissible value of control then intuitively one may obtain the steady state control by minimization of (3.12-13) with $t^f \to \infty$. Even if x^f is not an equilibrium, still optimization with finite but large t^f yields a control which keeps the state close to the desired value. If the final set is not a point but a hyperplane (some of ρ_i are zero), minimization of (3.12-13) may result in controls keeping particular state coordinates exactly at desired values. This is the case for the control problems discussed in this study.

Criterion (3.12) is minimized in an iterative scheme, whose main elements are: calculation of current value of the criterion, calculation of its gradient with respect to the control signal, determination of the search direction and directional minimization. To find the gradient it is necessary to solve backwards in time the system of adjoint equations:

$$d\eta/dt = -(\partial f(x,u)/\partial x)^T \eta + (\partial f_0(x)/\partial x)^T \tag{3.14}$$

with final conditions

$$\eta_i(t^f) = 0\ . \tag{3.15}$$

Then the gradient of J with respect to control signal u is calculated according to formula (3.11). The rest of the optimization process is also similar to that discussed in Section 3.2.2 and depicted on Fig. 3.1.

3.2.4. Implementation

The actual numerical optimization of (3.7) and (3.12) in this study was performed in discrete time — with control signal piecewise constant on intervals with length Δ (except possibly for the last interval, which may be shorter if t^f is not commensurate with Δ). Discrete time approximation allows for utilization of all the powerful machinery of finite dimensional optimization. The infinite dimensional control signal u(t), $0 \le t \le t^f$ is replaced with finite dimensional vector $u = [u_1, u_2, \ldots, u_{Kf-1}]^T$

$0 \le k < K^f$, where K^f is the smallest integer such that $t^f \le K^f\Delta$. Consequently, the gradient of the performance criterion with respect to control signal is approximated by a finite dimensional vector $\mathbf{g}$ whose elements are calculated according to:

$$g_k = \partial J_{aux}/\partial u_k = \int_{k\Delta}^{(k+1)\Delta} \left((\partial \mathbf{f}/\partial u)^T \boldsymbol{\eta} \right) dt \tag{3.16}$$

Then the directional minimum search is performed in direction $\mathbf{v}$ determined by a conjugate gradient algorithm. Here a particular version of that algorithm is adopted from [3.5], which is robust with respect to inaccurate direction of search. This allows us to limit the number of calculations of the performance criterion (3.7) or (3.12) in each iteration.

A pure conjugate gradient algorithm is suitable only for unconstrained problems — in this case with no limits on control values. With constrained controls the minimum in direction $\mathbf{v}$ may be infeasible. This poses no difficulties in the directional search — in fact it is easier to find a minimum with a constrained search interval. However the resulting optimal step cannot be used for determination of the next search direction if the minimum lies on one of the interval's ends. This problem is solved as follows. After calculation of (3.11) the set of active constraints is calculated: the constraint is active if $g_k < 0$ and $u_k = u_{max}$ or if $g_k > 0$ and $u_k = u_{min}$. Then the whole minimization is done only with respect to controls with no active constraints — i.e., elements of $\mathbf{g}$ corresponding to active constraints are set to zero. If some of the active constraints become non-active or vice-versa, then the conjugate gradient algorithm is re-initialized with the steepest descent direction as the initial search direction. The same is done if in some iteration the search direction $\mathbf{v}$ becomes infeasible. As a result the conjugate gradient method works effectively as if no constraints were present and the formulae for determination of search direction are valid. Hitting or leaving any of the control constraints causes change of the space in which the minimization is performed. The method used may be viewed as a projection method ([3.2]) in which currently active constraints are treated as equality constraints and the others are ignored. Due to the extremely simple structure of constraints (3.2) the projection of the gradient amounts to putting some of the gradient elements to zero. Also, since the constraints are linear, they are satisfied for any control signal along the search line.

The directional minimization implemented in this study uses a combination of two-point gradient-based parabolic fit with three-point non-gradient parabolic fit. If the calculated vertex of the fitted parabola results in controls exceeding the constraints, a heuristic bisection-based search for minimum in the interval is performed. The number of criterion value calculations (i.e. simulations of the model) in each directional search was limited at cost of accuracy.

The preceding discussion, for sake of clarity, was limited to the scalar control case. Extension to more control signals (such as the case of aircraft control) is straightforward. The control vector, with respect to which the minimization is performed is now $\mathbf{u} = [u_1^{(1)},\ldots,u_1^{(M)},u_2,\ldots,u_2^{(M-1)},\ldots,u_{Kf-1}^{(1)},\ldots,u_{Kf-1}^{(M)}]^T$, where M is the number of control signals. The gradient of the performance criterion is composed of M vectors $\mathbf{g} = [\mathbf{g}^{(1)T},\ldots,\mathbf{g}^{(M)T}]^T$, each of which is calculated according to (3.16) with u being replaced by appropriate control $u^{(i)}$.

For the time-optimal problem the minimization of (3.7) is terminated when $J_{aux} \leq \epsilon$, where ϵ represents acceptable deviation from desired values, or, if for given t^f it is not possible to reach x^f, when the norm of gradient of J becomes small enough. For the integral-quality-criterion problem, only that second stop criterion was used.

3.3. Simulation

For the aircraft model a series of numerical optimization experiments was performed for both time-optimal and quadratic integral criterion problems with controlled variable being either angle of attack α or pitch angle θ. The original objective for the time-optimal problem was to calculate the minimum-time transition of the plant's state from one point (assuming it is an equilibrium of (3.1)) to some other specified point (preferably also an equilibrium). For the control of α (or θ) the procedure would be to find an equilibrium corresponding to a desired value of α (or θ) and then calculate the time-optimal trajectory. Unfortunately this turned out to be too difficult a problem with given control limits, and it was impossible to find appropriate controls moving the state to such a desired equilibrium in a reasonable time. Besides that, equilibria corresponding to high values of α are characterized by negative values of path angle, which is not exactly the desired state. Therefore a modified control problem is solved, in which the task is only to reach a given value of α (or θ) and $q = 0$. This corresponds to $\rho_3 = \rho_4 = 0$ (or $\rho_1 = \rho_4 = 0$) in (3.10) and to the target set being a two-dimensional hyperplane rather than a point in $\mathbf{R}^4$. This turned out to be easily solvable; however, specifying final values of three, instead of two, state variables caused serious problems with convergence of the minimization process due to a physical lack of aircraft controllability with present control signal constraints (particularly thrust).

Typical time-optimal trajectories are displayed on Figs. 3.2-3.6. The initial condition is the trimmed flight with T_m = 3,000 lbs at 0.3 mach and 15,000 ft. The corresponding pitch angle is close to 5°. The target is $q = 0$ and θ = 10°, 30°, 50°, 70°, so the simulated maneuver corresponds to aiming the nose of the aircraft in the desired direction. The dashed lines on control plots correspond to command signals fed to actuators while the solid lines are the actuators' outputs, i.e. the control signals proper. It may be observed that the optimal command signal fed to the actuators is not unique because

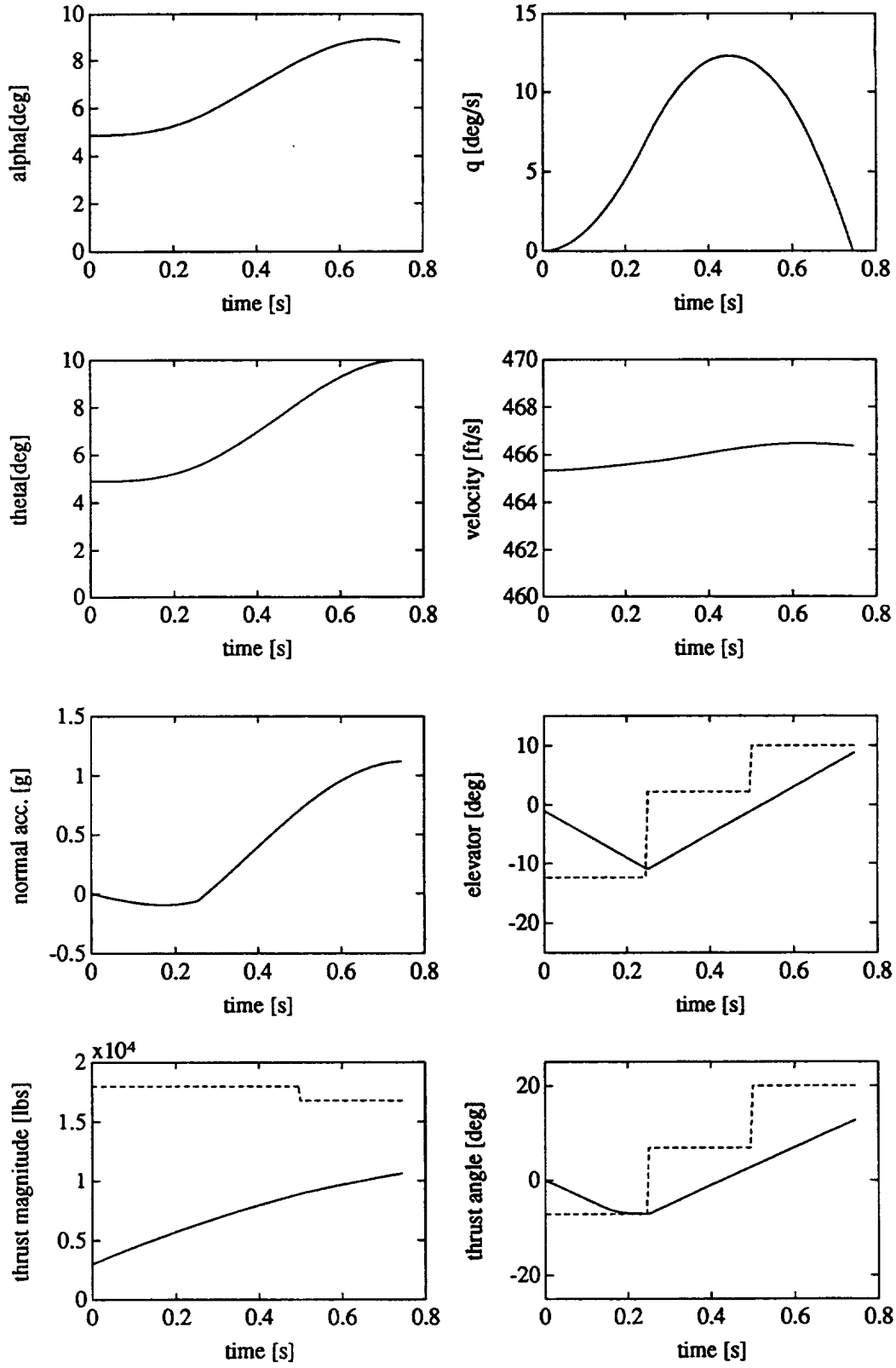

Figure 3.2. Time-optimal control to $\theta = 10°$ and $q = 0°/s$
Initial condition - trim corresponding to thrust 3,000

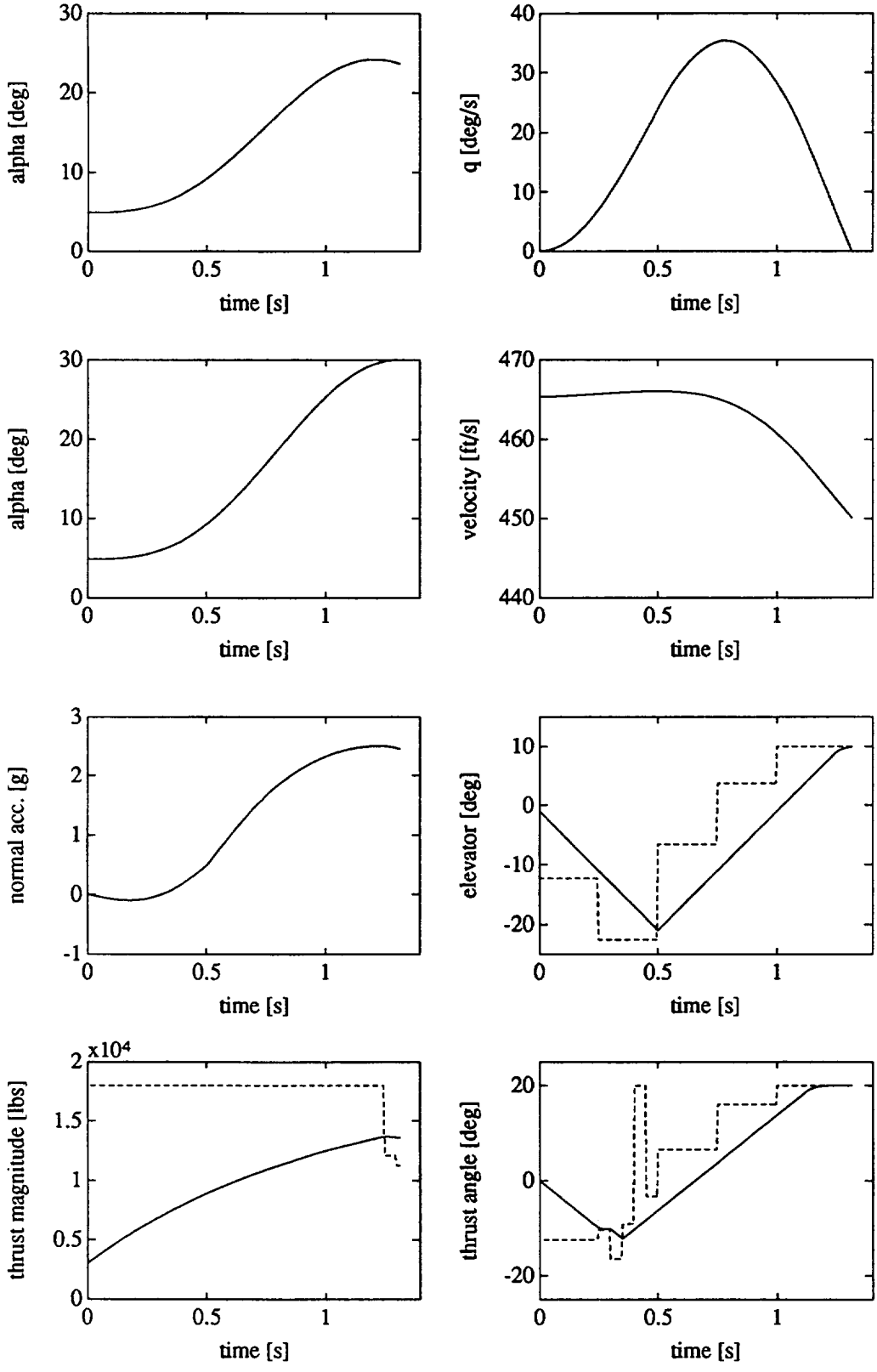

Figure 3.3. Time-optimal control to $\theta = 30°$ and $q = 0°/s$
Initial condition - trim corresponding to thrust 3,000

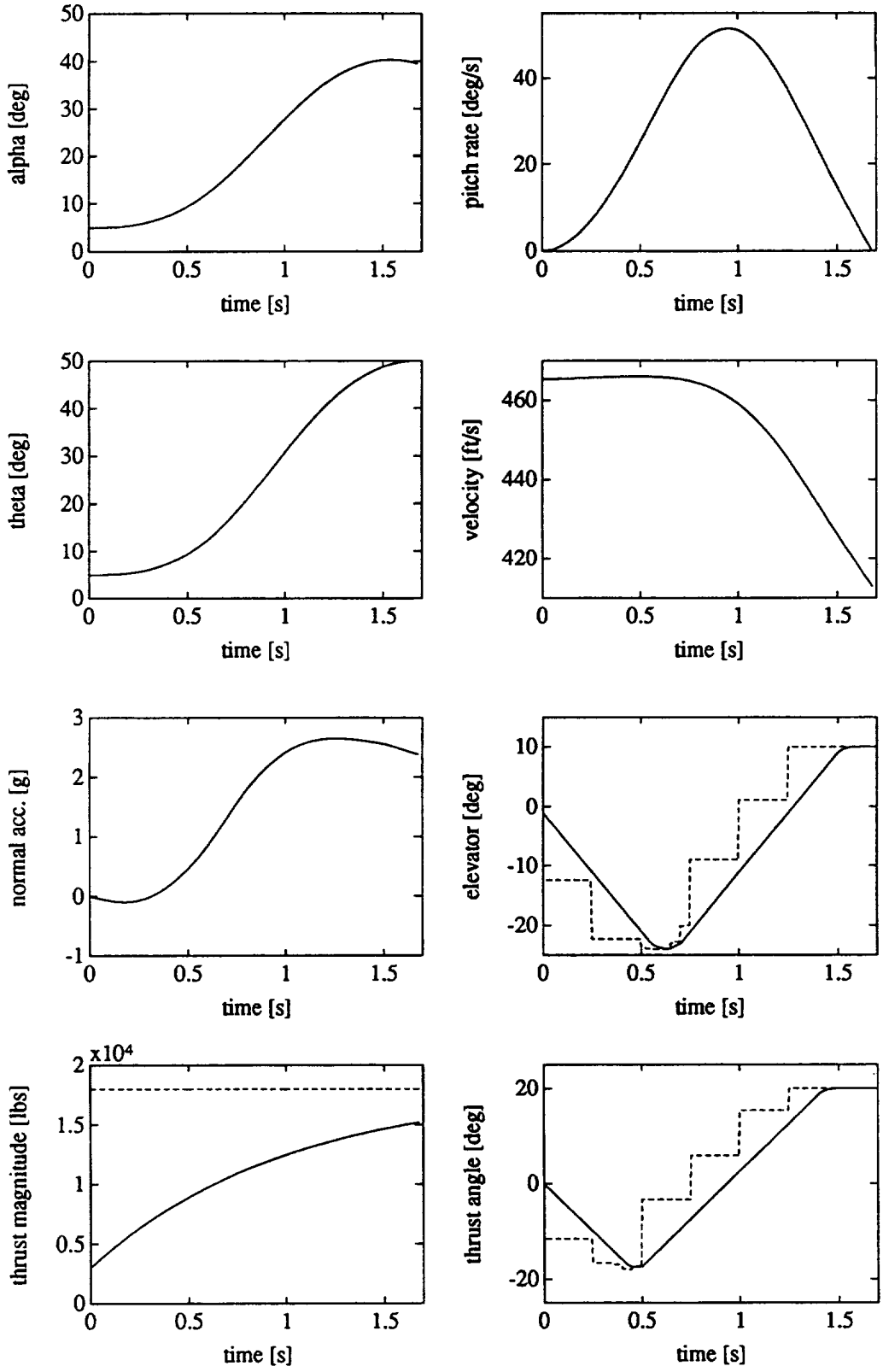

Figure 3.4. Time-optimal control to $\theta = 50°$ and $q = 0°/s$
Initial condition - trim corresponding to thrust 3,000

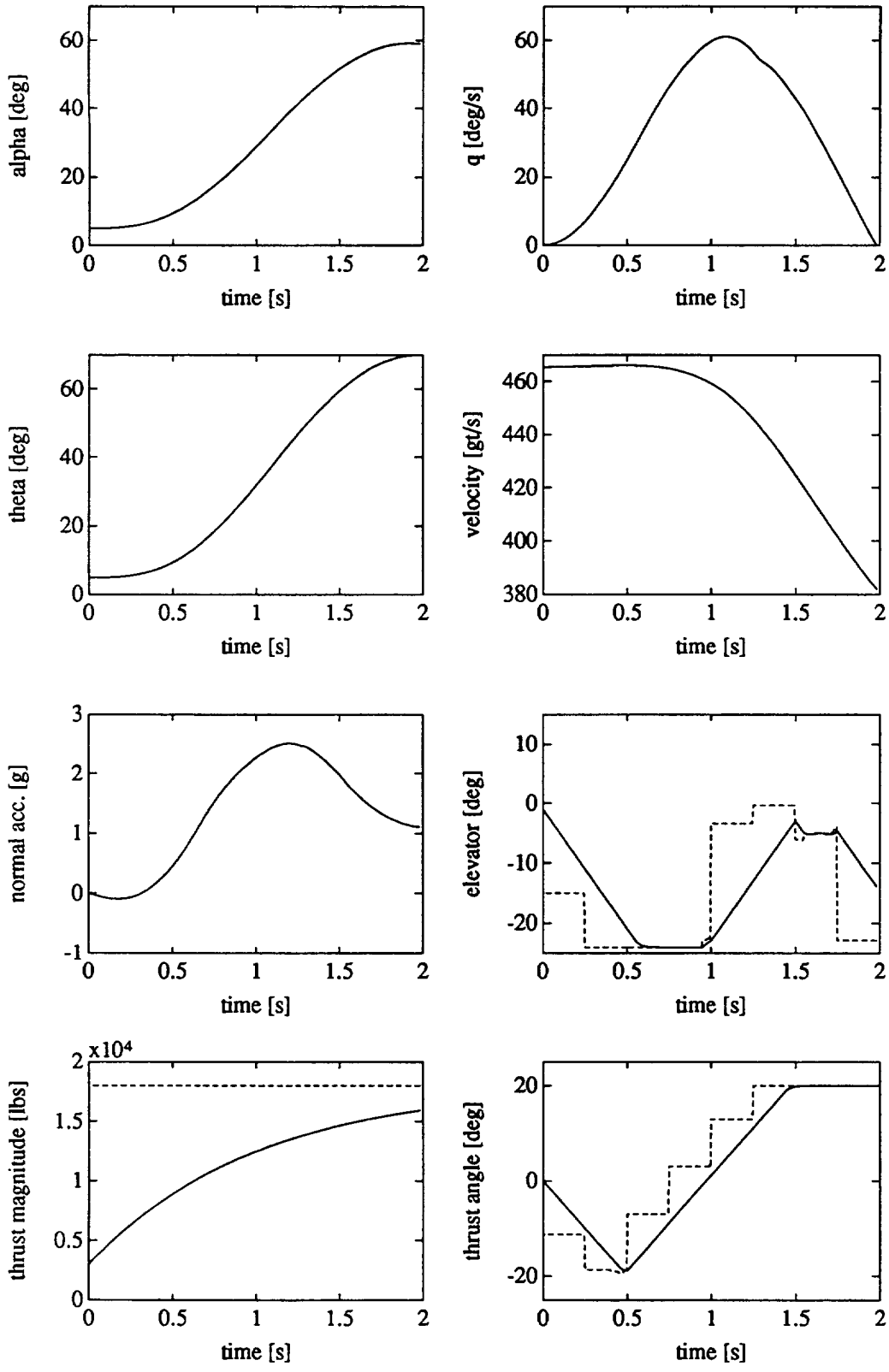

Figure 3.5. Time-optimal control to $\theta = 70°$ and $q = 0°/s$
Initial condition - trim corresponding to thrust 3,000

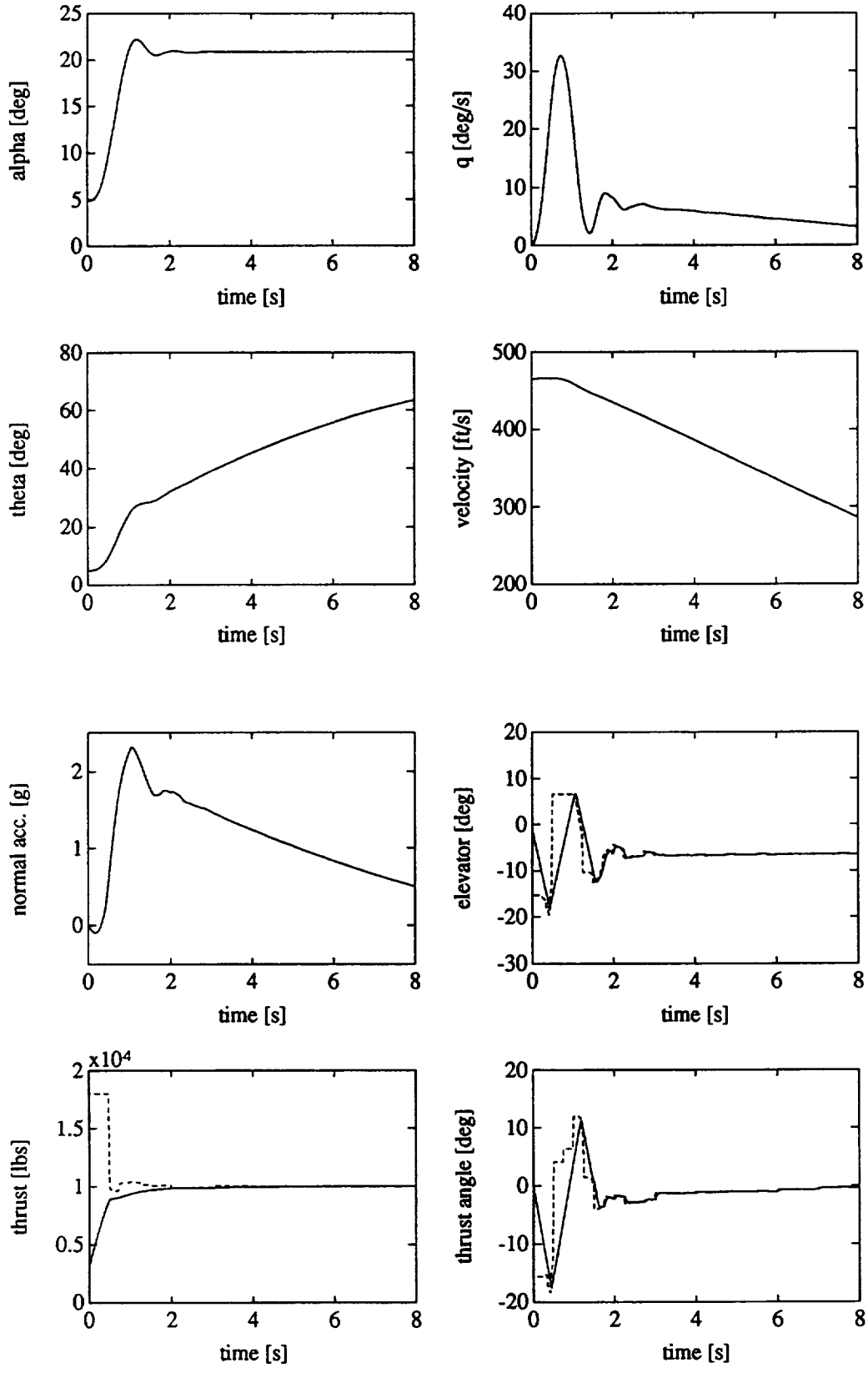

Figure 3.6. Quadratic-optimal control for target $\alpha = 20.8°$
Initial condition - trim corresponding to thrust 3,000

of the rate limitations on actuators' outputs. Theoretically the nonlinear saturation function g in (3.3) is monotone increasing, so bang-bang command signals are necessary to obtain the fastest changing control signals. However, from the practical point of view, g saturates so quickly, that any command signal differing from current actuator output by more than 2° results in the maximal rate of change. Results displayed on Figs. 3.2-3.5 show that indeed time-optimal change of pitch angle requires bang-bang control of all three actuators. This substantiates previous intuitive remarks about unsuitability of linear methods for high-performance control. Optimality requires utilizing the existing control capabilities fully to their limits, and increasing the speed of actuators is one of the ways to improve maneuverability. Time-optimal transition to $\theta = 70°$ reveals however an apparent singular control arc. This phenomenon has been generally observed for optimization of maneuvers with high values of angle of attack. Calculations performed so far suggest that in such situations time-optimal transition to high value of α or θ does not necessarily require bang-bang type of control, at least in the final part of the maneuver. Normal acceleration plots as well as pitch rate show that those maneuvers are within the desired range.

A series of optimizations of integral quadratic performance criterion (3.12) has also been executed in different variants. The controlled variable was either α or θ, which corresponds to either $\rho_2 = \rho_3 = \rho_4 = 0$ or $\rho_1 = \rho_2 = \rho_4 = 0$. Attempts to simultaneously regulate values of two or more states were not successful due to the control (particularly thrust) limitation. The simulations were performed with initial conditions corresponding to trim flight at T_M = 3,000, 10,000 and 18,000 pounds. In this case, unlike in time-optimal problem, only optimal stabilator/elevator and thrust direction command signals are calculated. The thrust magnitude is assumed to be increased (or decreased) by the pilot manually to the prescribed terminal trim. The control horizon is 8s — a value which, if significantly increased or decreased, does not affect the shape of optimal trajectories. Typical results for control of α are shown on Figs. 3.6-3.13 and for control of θ on Figs. 3.14-3.17. It is seen that the control is bang-bang in the initial segment of the trajectory but then smooths out and does not hit the bounds. The ripples on control trajectories are a result of finite discretization time Δ. In the numerical optimization variable Δ was used to speed-up calculations. If a decrease of Δ caused no significant decrease in the performance criterion, larger Δ was used. Even though the truly optimal control trajectories are much smoother than those obtained with discretized control, the resulting difference in state trajectories was almost unnoticeable. Since the controlled variable in all cases locks exactly on the desired value increasing the horizon in a very large range gives a picture of "semi infinite horizon control."

Figures 3.6-3.9 demonstrate results of quadratic-optimal regulation of α with initial trim state for $\alpha_0 = 4.9°$ (15,000 ft altitude and 0.3 mach), and desired value of α ranging over 20.8°, 50°, 60° and 70°. Rise time ranges from about 1s to about 1.8s with a maximum overshoot less than 10%, after

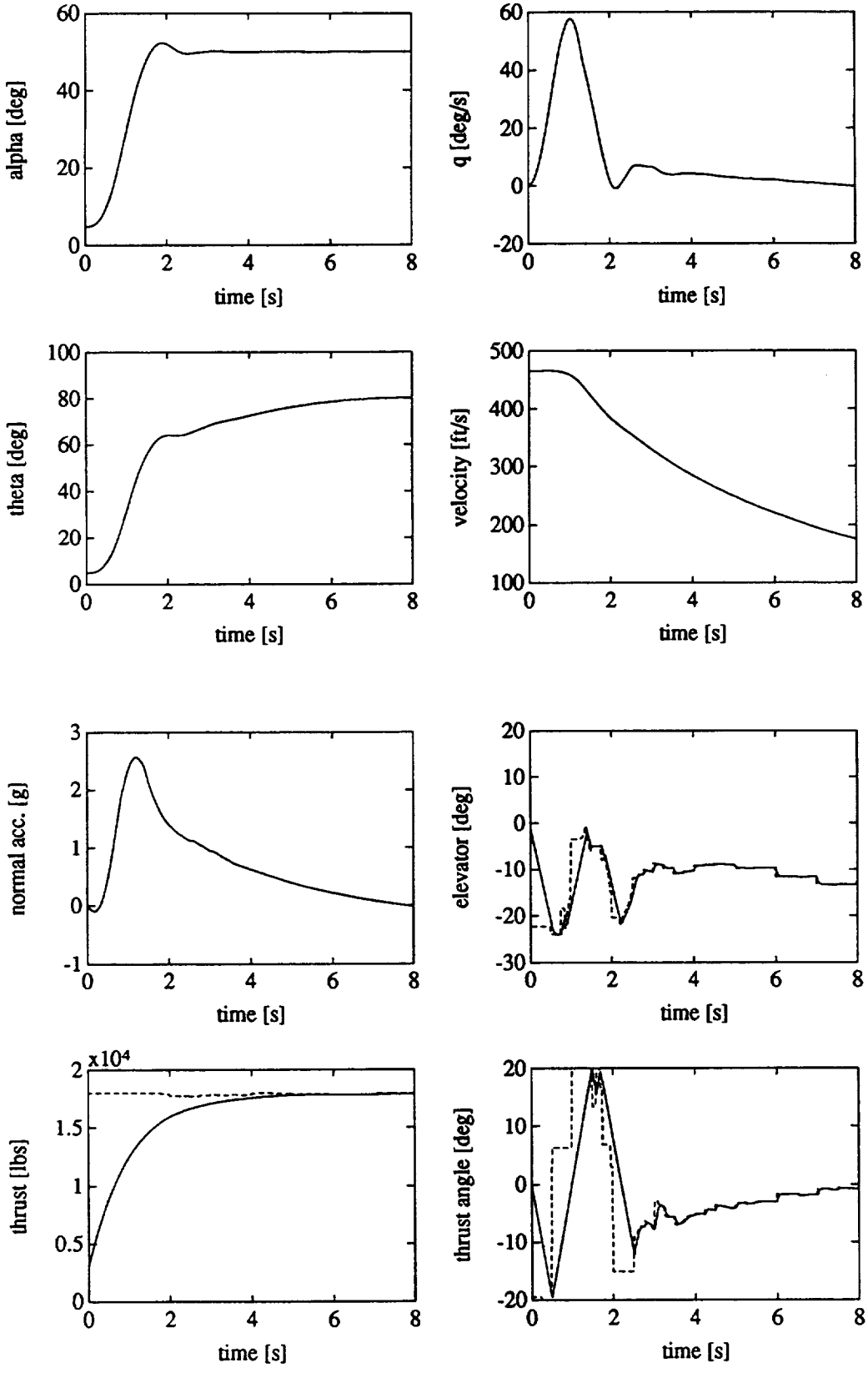

Figure 3.7. Quadratic-optimal control for target $\alpha = 50°$
Initial condition - trim corresponding to thrust 3,000

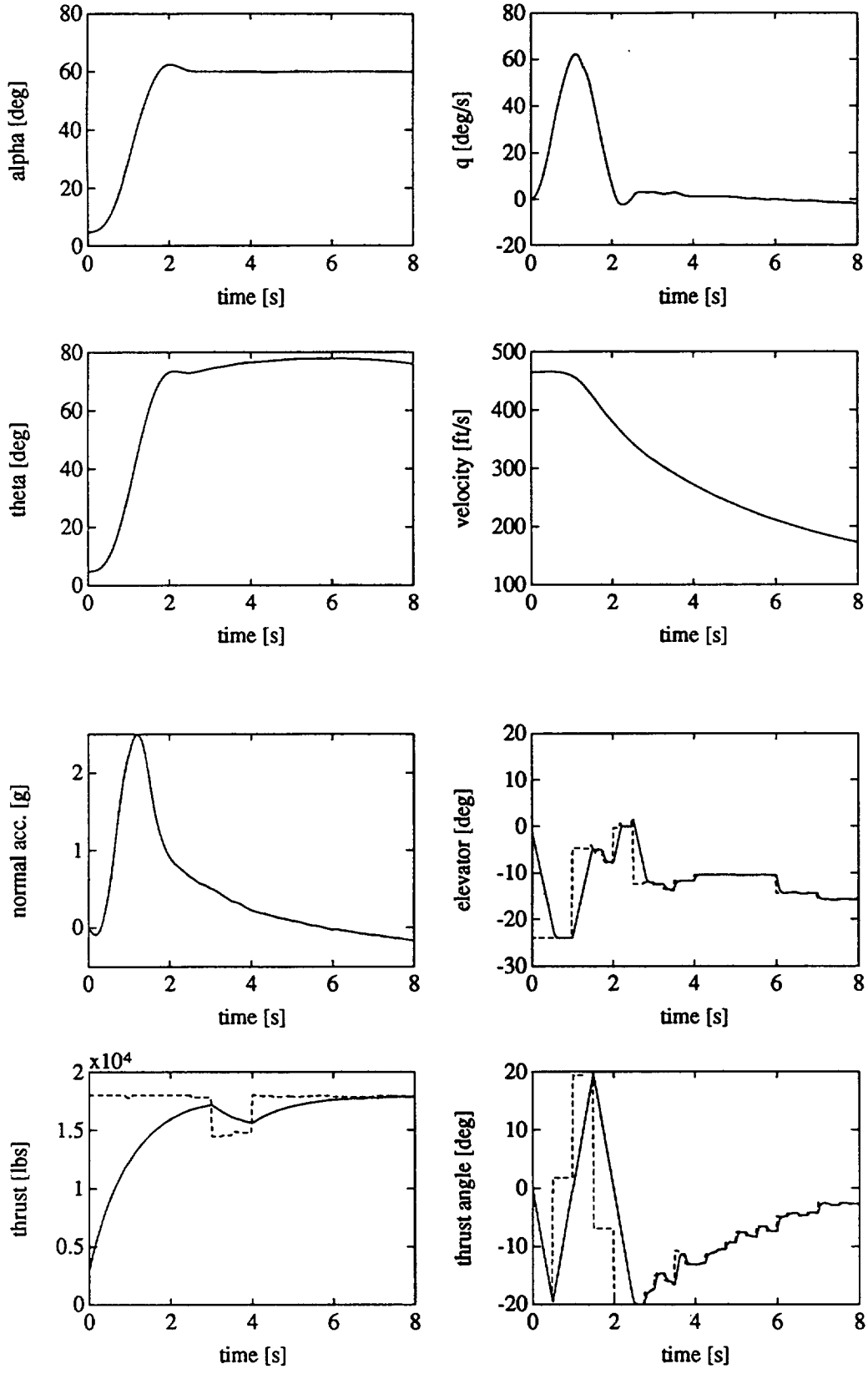

Figure 3.8. Quadratic-optimal control for target $\alpha = 60°$
Initial condition - trim corresponding to thrust 3,000

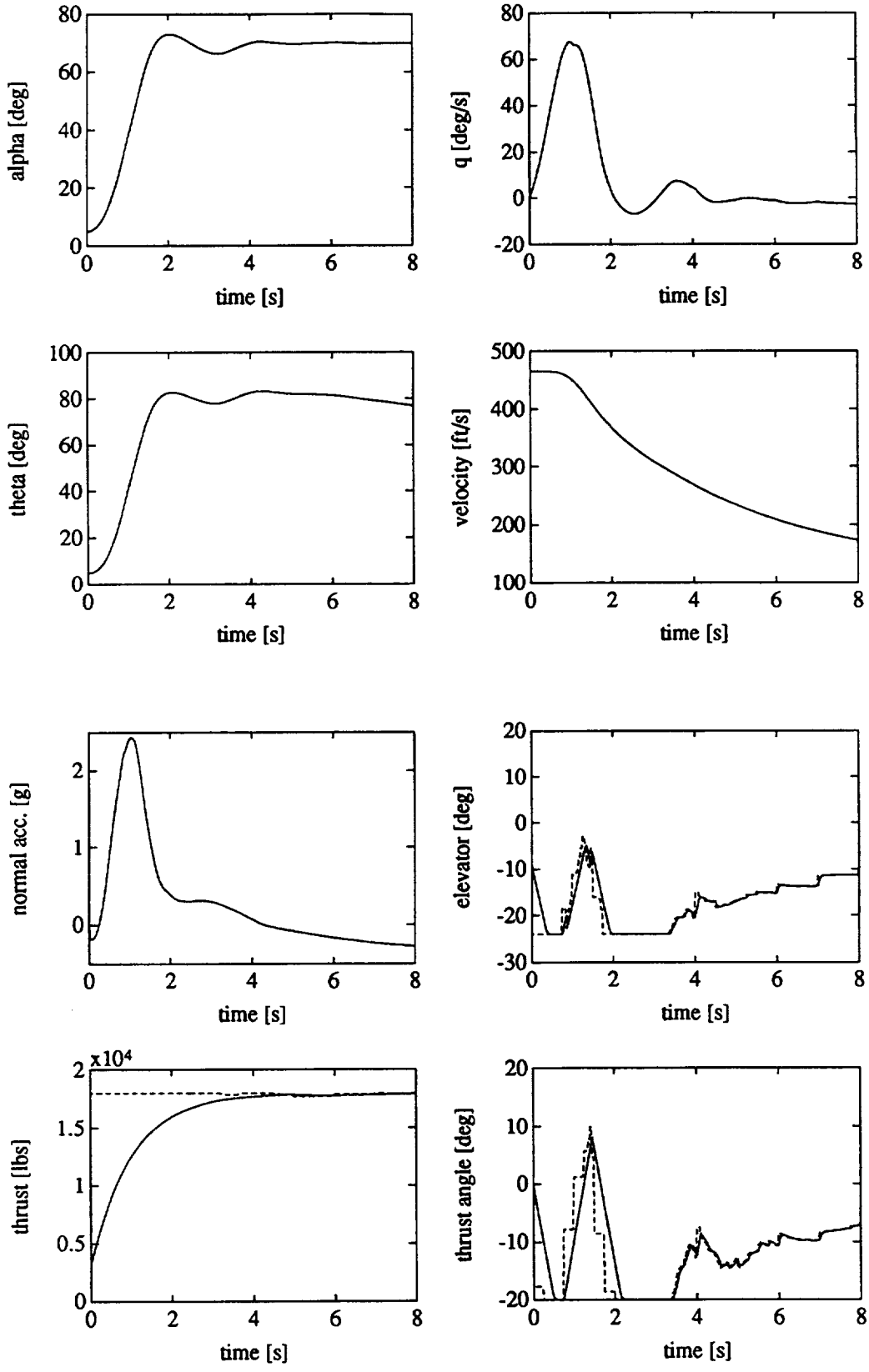

Figure 3.9. Quadratic-optimal control for target $\alpha = 70°$
Initial condition - trim corresponding to thrust 3,000

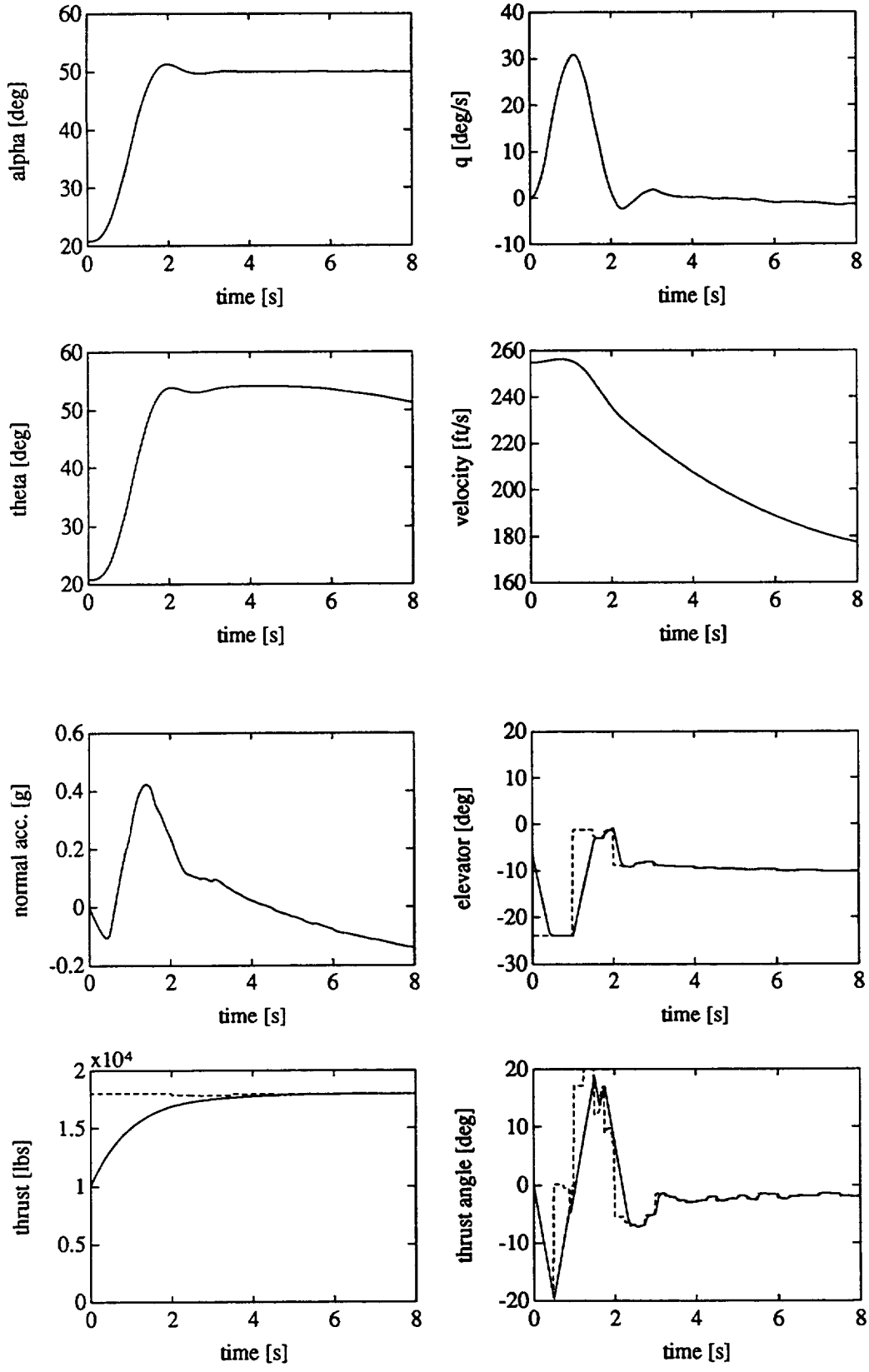

Figure 3.10. Quadratic-optimal control for target $\alpha = 50°$
Initial condition - trim corresponding to thrust 10,000

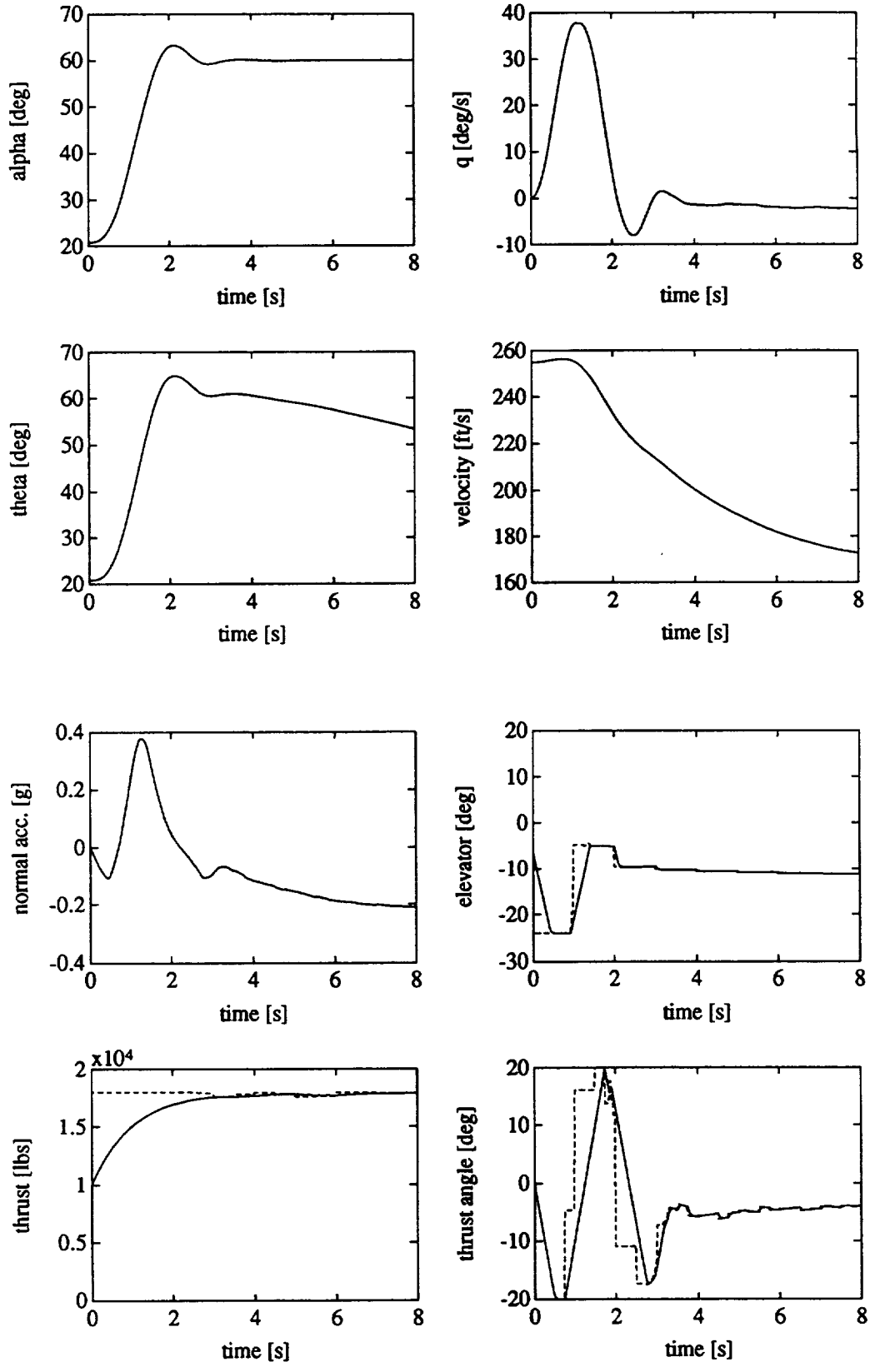

Figure 3.11. Quadratic-optimal control for target $\alpha = 60°$
Initial condition - trim corresponding to thrust 18,000

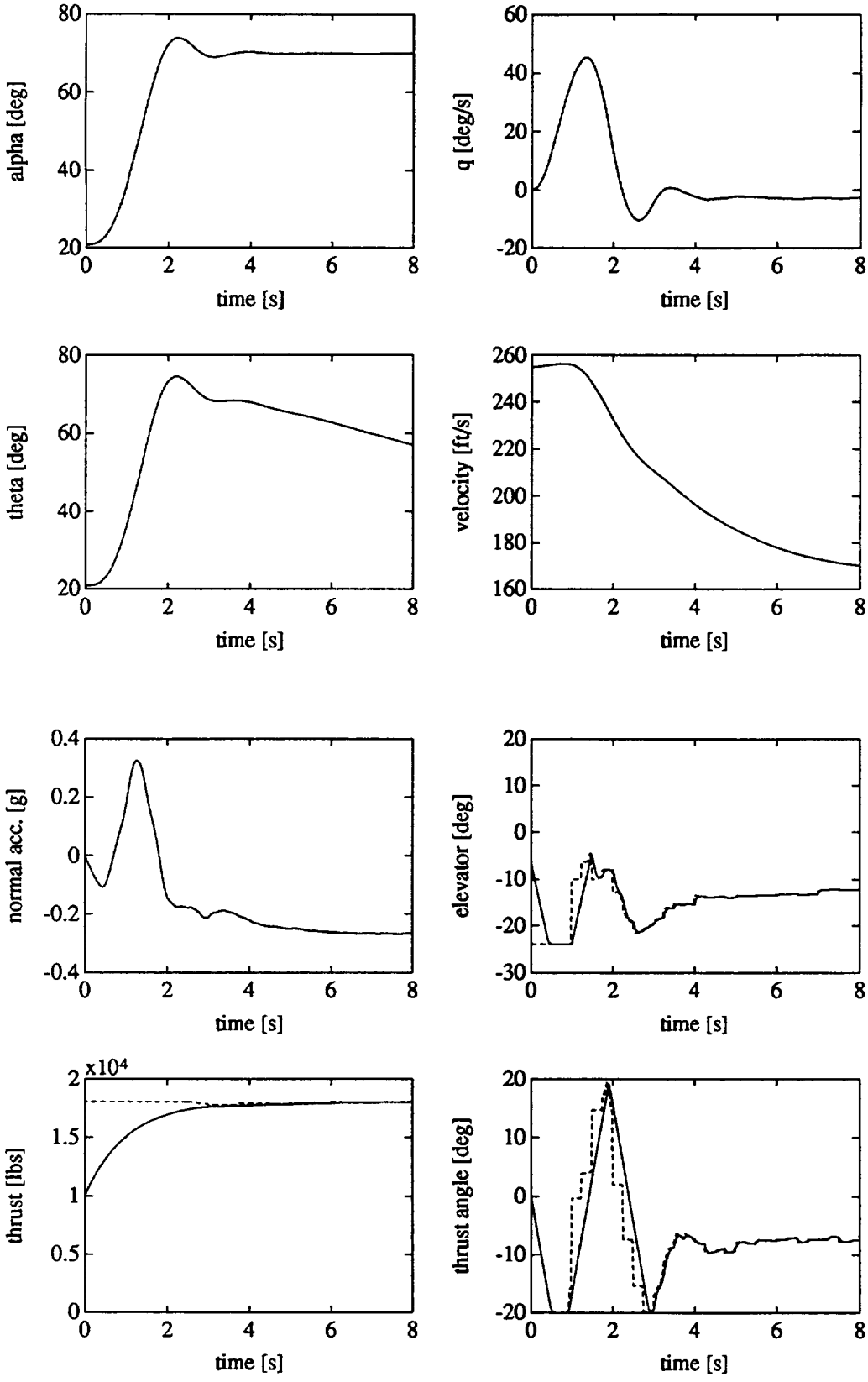

Figure 3.12. Quadratic-optimal control for target $\alpha = 70°$
Initial condition - trim corresponding to thrust 10,000

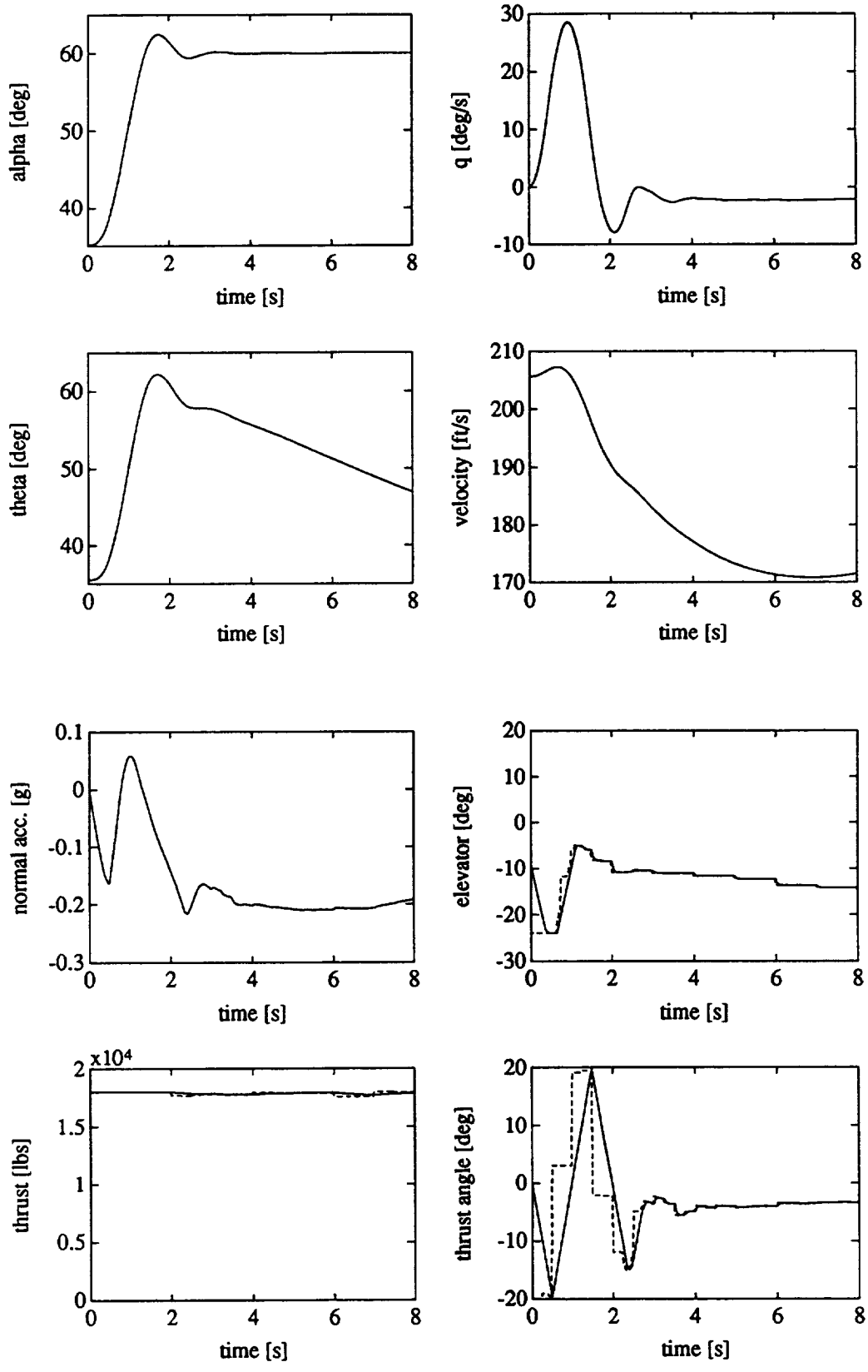

Figure 3.13. Quadratic-optimal control for target $\alpha = 60°$
Initial condition - trim corresponding to thrust 18,000

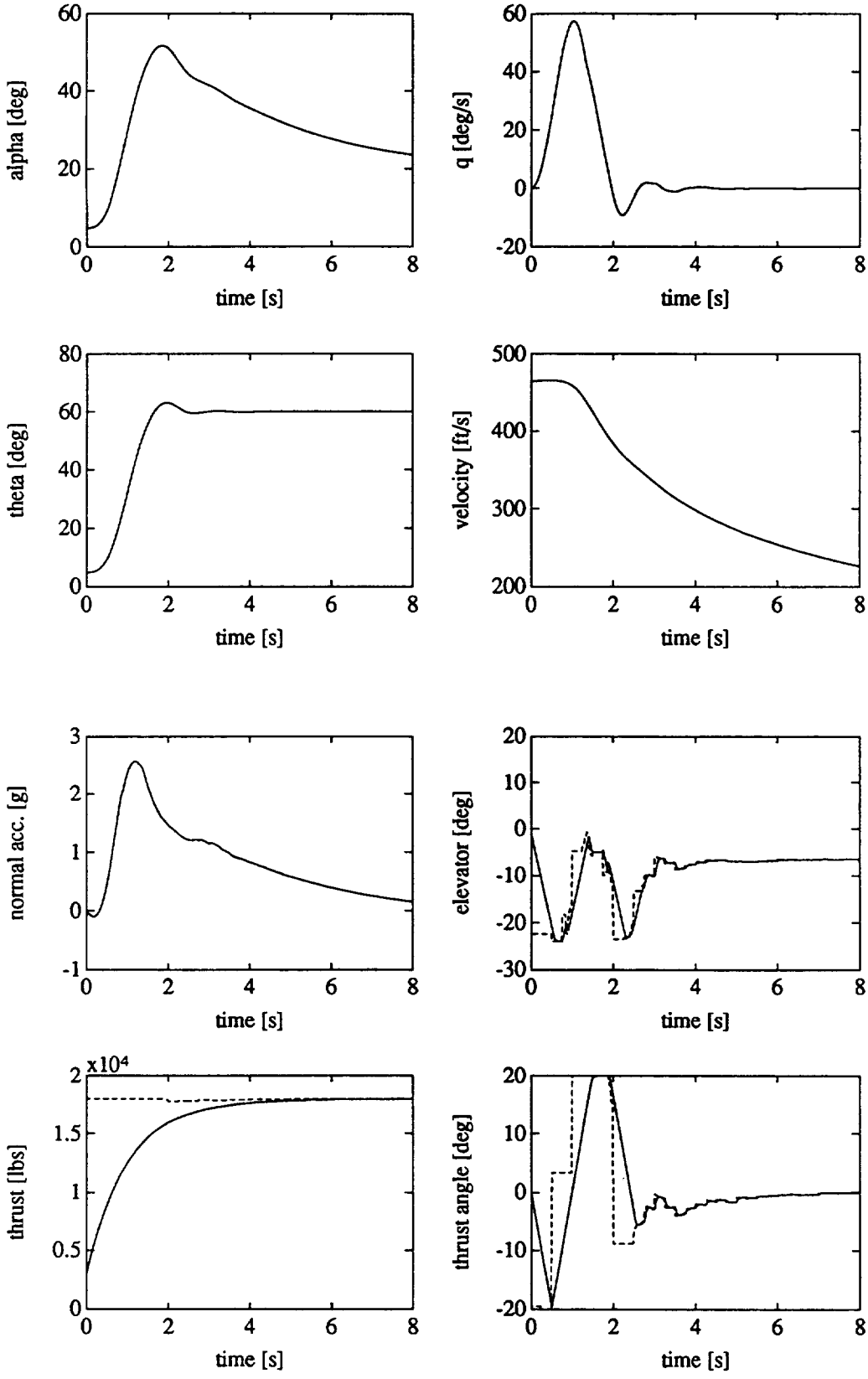

Figure 3.14. Quadratic-optimal control for target $\theta = 60°$
Initial condition - trim corresponding to thrust 3,000

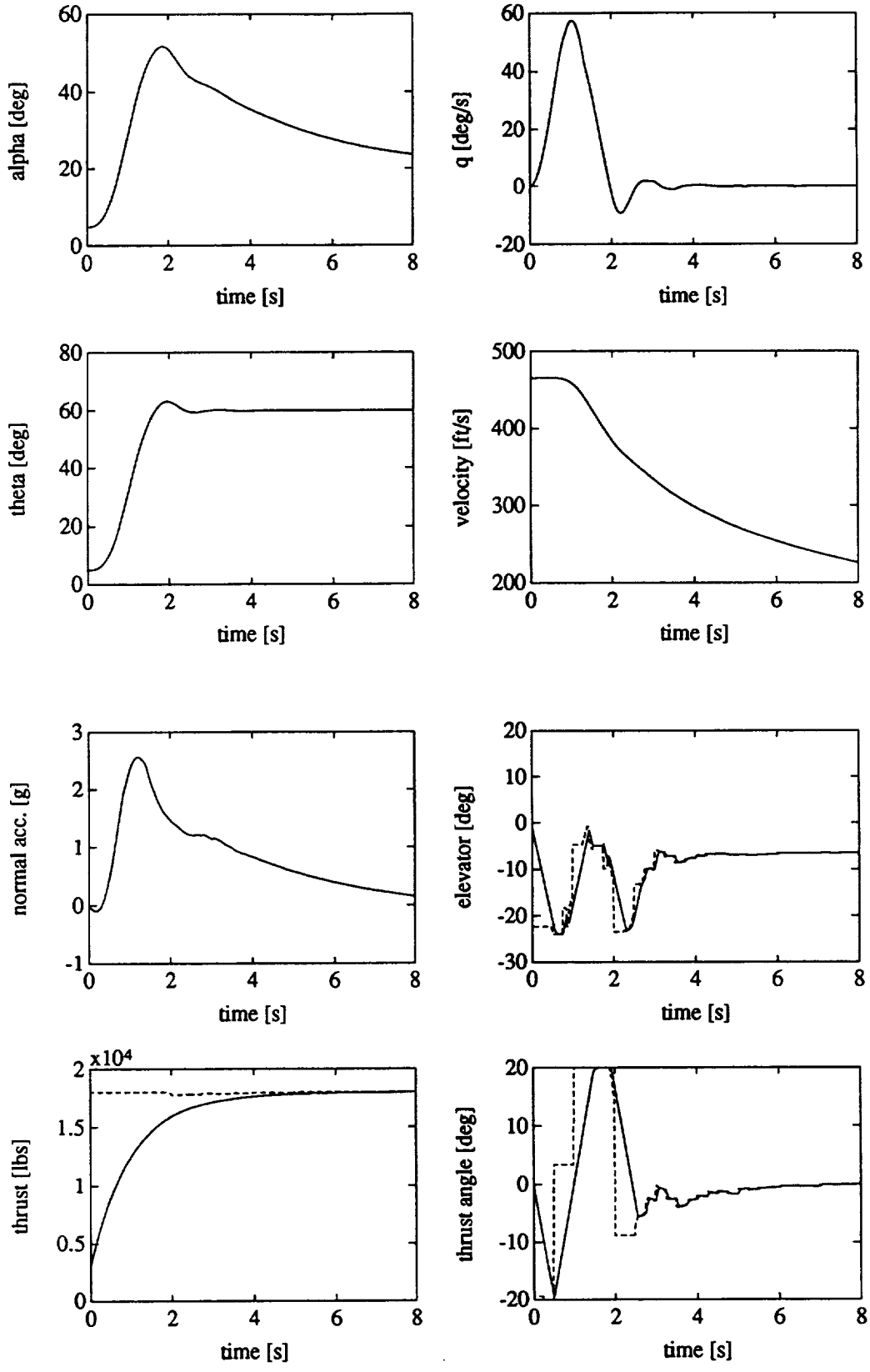

Figure 3.15. Quadratic-optimal control for target $\theta = 60°$
Initial condition - trim corresponding to thrust 10,000

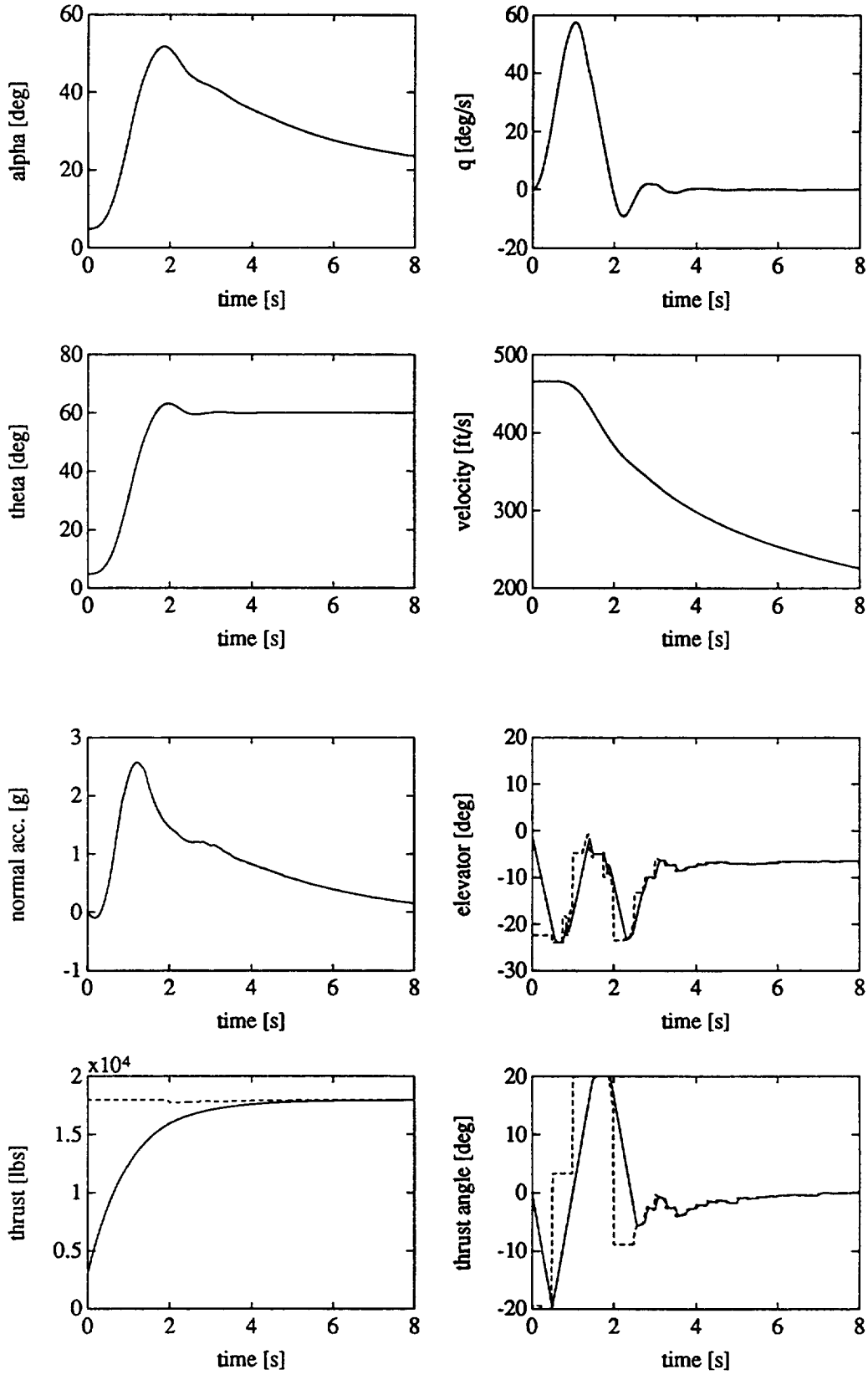

Figure 3.16. Quadratic-optimal control for target $\theta = 80°$
Initial condition - trim corresponding to thrust 10,000

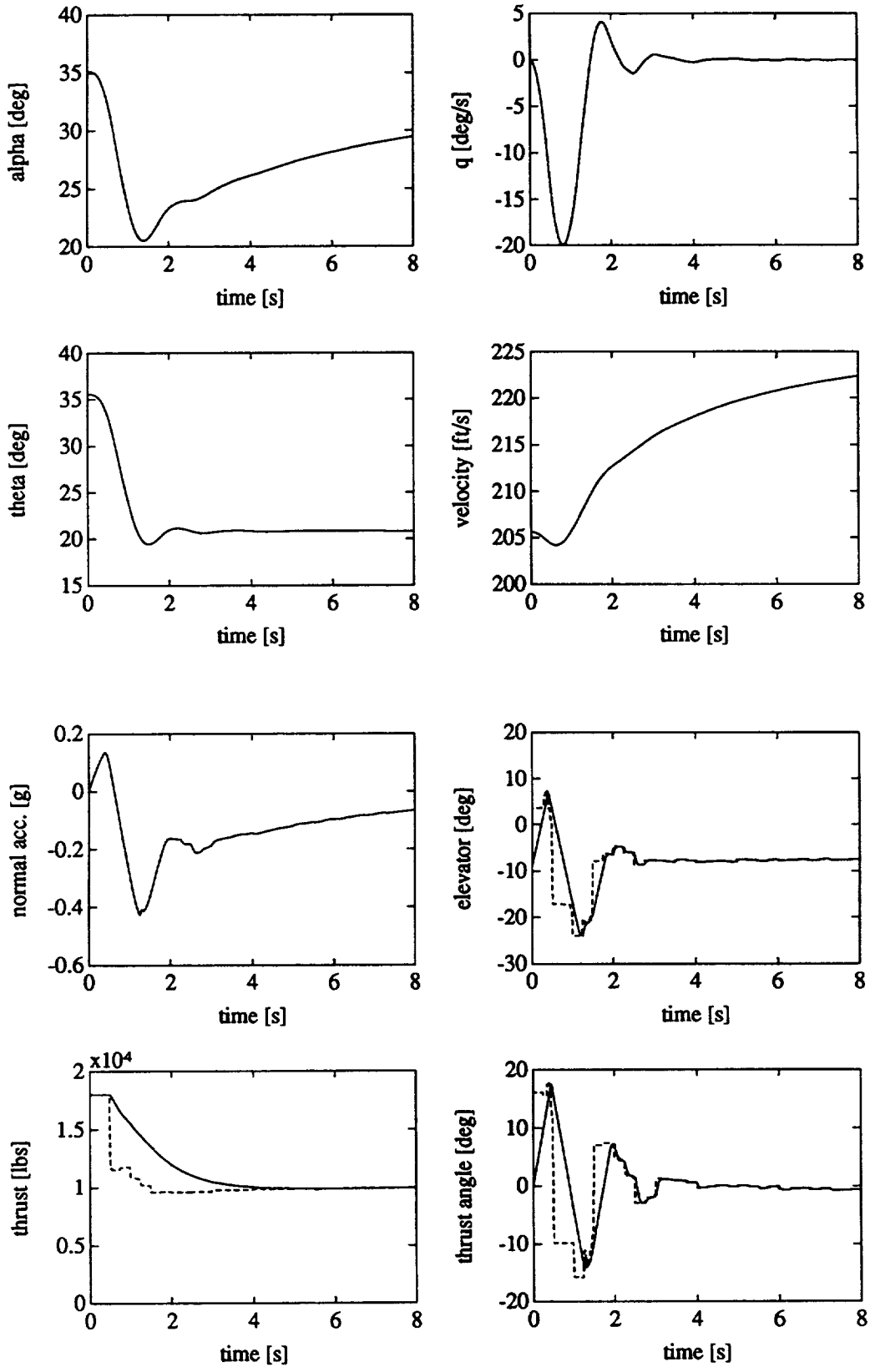

Figure 3.17. Quadratic-optimal control for target $\theta = 20.8°$
Initial condition - trim corresponding to thrust 18,000

which the control holds α exactly at its desired value. The maximum normal acceleration peaks at about 2.5g for the most demanding case ($\alpha^f = 70°$) with pitch rate peaking at less than 70°/s in about 1s. Figures 3.10-3.13 demonstrate typical optimal maneuvers for initial conditions corresponding to thrusts of 10,000 and 18,000 lbs (with angle of attack at trim equal to 20.8° and 35.2°, respectively) with different values of target α. Since they start with larger thrust value, consequently the time needed to reach the desired output level is shorter.

Optimization results for pitch angle regulation were quite similar. Again initial portions of optimal trajectories are of bang-bang type, and closely resemble the time-optimal case. Figures 3.14-3.16 demonstrate typical results for target $\theta^f = 60°$ and $\theta^f = 80°$. Also an example of optimal descent from $\theta = 35.2°$ to $\theta = 20.8°$ is shown on Fig. 3.17.

Both the time-optimal and quadratic-criterion-optimal trajectories display certain similarities between optimal stabilator/elevator angle and thrust angle command signals, lending some credibility to current practice of scheduling the thrust angle proportionally to elevator angle deflection. This is particularly true for low angle of attack values. However, for $\alpha \geq 50°$ these similarities begin to disappear. Careful examination, e.g., of Figs. 3.8 or 3.11 reveals that for truly high performance regulation of α at high values both control signals have to be determined independently. The same was found true for regulation of θ. Also in the time-optimal case Fig. 3.5 shows that both angles should be controlled separately.

3.4. Practical Considerations and Conclusions

Performed numerical optimizations provide a useful set of benchmark tests for rapid changes of angle of attack of pitch angle of the plane in question. Several characteristic features of optimal trajectories are revealed: bang-bang type command signals for actuators are required most of the time, with possible singular arcs for large angles of attack, even in the time-optimal case. This finding motivates a search for nonlinear control algorithms for rapid maneuvers, as linear controllers cannot successfully provide bang-bang signals. Also optimal trajectories suggest that ***separate control of elevator angle and thrust angle is advisable rather than scheduling of the latter after the former.***

For the calculations of this section a computer package was developed for solution of optimal control problems discussed in Section 3.2. The program was developed for the particular aircraft model, but due to its modular nature it is possible to substitute any plant model and any performance criterion of the type (3.12). Written in standard C language the package is essentially portable to any computer system with a C language compiler supporting ANSI standard. ***It is proposed that existing version of the program, still requiring the author's intervention to change the plant's model, is developed into a***

universal program allowing easy numerical solutions of optimal control problems for any plant, provided its model is supplied in form of appropriate C language functions.

3.5. References

[3.1] H. Hermes and J.P La Salle, *Functional Analysis and Time Optimal Control*, New York: Academic Press, 1969.

[3.2] D.G. Luenberger, *Optimization by Vector Space Methods*, New York:Wiley, 1969.

[3.3] R.R. Mohler, *Nonlinear Systems Vol.2*, Englewood Cliffs:Prentice Hall, 1991.

[3.4] A.J. Ostroff, "High Alpha Application of Variable-Gain Output Feedback Control," *J. Guidance, Control & Dyn.*, Vol. 15, 491-497, 1992.

[3.5] D.F. Shanno, "Conjugate Gradient Methods with Inexact Searches," *Mathematics of Operations Research*, Vol. 3, 244-256, 1978.

[3.6] H.J. Sussmann, "Optimal Control," H. Nijmeijer and J.M. Schumacher eds., *Three Decades of Mathematical System Theory*, Berlin:Springer Verlag, 1989, pp. 409-425.

[3.7] A.P. Wierzbicki, *Models and Sensitivity of Control Systems*, Amsterdam:Elsevier, 1984.

4. NEURAL NETWORK CONTROL

4.1. General Concept

The great potential of feedforward artificial neural networks in identification, estimation and control of dynamical systems have long been recognized, and a multitude of applications have been proposed [4.4-4.6]. It is generally agreed that, although neural networks cannot be viewed as a universal panaceum for all design problems, they provide numerous advantages absent in other modeling techniques. These include automatic learning with no unnecessary assumptions about model structure, smooth behavior with good interpolation and extrapolation properties, and possibly very fast parallel hardware implementations due to simple modular structures of the networks.

Most of the applications of feedforward networks are based on their universal approximating abilities. Generally, for any finite-dimensional continuous mapping there exists a multilayer feedforward network, with suitable size and neurons' parameters, that approximates the given mapping arbitrarily closely. In particular, for control of dynamical systems, any finite dimensional feedback controller can be implemented by means of neural approximations. This may be advantageous if the form of the controller is conceptually known, but is not explicitly available in closed form. If only examples of the desired control actions are available, a neural network may be utilized to learn the unknown underlying principle from the examples. In particular, it has been suggested in [4.10] that this idea be used for approximation of optimal feedback using optimal trajectories calculated in open-loop mode.

As remarked in the previous chapter, truly high-performance control calls for some kind of optimality. Unfortunately, optimal control theory offers mostly tools for calculation of open-loop controls. While closed loop solutions exist for special cases of linear systems, the design of optimal feedback controllers in the general nonlinear case is most often untractable. In fact, even the very existence of optimal feedback mapping is far from being obvious for a nonlinear plant [4.5,4.8]. The approach used here is to train a neural network on a set of optimal trajectories derived numerically from the model of the system, under the tacit assumption that the plant is regular enough for the closed-loop synthesis to be indeed possible. The method from [4.10] is extended here in the sense that a number of optimal trajectories is calculated not only for different initial conditions, but also for different target values of the controlled output variable. The numerically obtained optimal trajectories contain information on how the control signal depends on state variables and on the desired final state. An artificial neural network is trained to extract this information from the optimal trajectories and then used in a feedback scheme to generate a sub-optimal policy. The whole synthesis is done off-line and, therefore, problems with slow learning of large neural networks are not so critical here.

4.2. Methodology

The neural network controller was trained to approximate quadratic-optimal regulation of angle-of-attack of the fourth order model of longitudinal dynamics of the modified F18 (HARV) and with all actuators' dynamics and control constraints. The following subsections give detailed descriptions of the algorithms used.

4.2.1. Feedforward Neural Networks

The basic element of a multilayered perceptron, or a feedforword neural network, is a multi-input, single output static processing element, called an artificial neuron. It performs a nonlinear transformation:

$$x \to y(x) = \sigma\left(\sum_i w_i x_i + \theta\right) \tag{4.1}$$

where w_i are the neuron's input weights, θ is the activation threshold, and σ is the activation function. By extending the input vector x with a fictitious element always equal to 1, it is possible to treat the threshold θ as a weight associated with a constant input, therefore both w_i and θ are often denoted as the neuron's weights. The activation function is usually a sigmoid, i.e. is smooth, monotone increasing and bounded, with a typical example being $\sigma(x) = 1/(1+e^{-x})$.

A network consists of neurons arranged in two or more "layers," with each neuron of the next layer having outputs of all neurons of the previous layer as its inputs. The neurons in each layer have the same number of inputs and outputs. Customarily all the layers besides the output one are called the hidden layers. The numbers of the neurons in each layer may be different and determine the properties of the network. The general structure of a network with two hidden layers is depicted on Fig. 4.1.

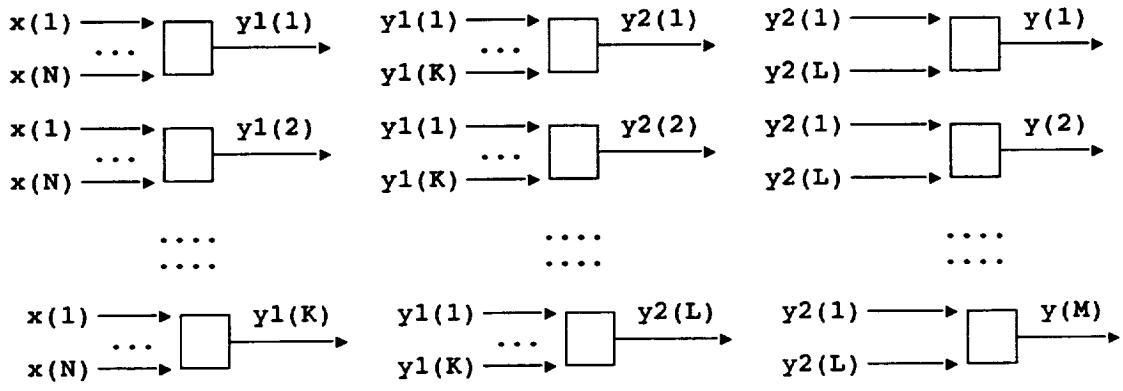

Figure 4.1. Structure of a network with two hidden layers.

A feedforward multilayer network with N inputs, M outputs, K layers and with l_i neurons in the l-th hidden layer can be thought of as a nonlinear function $f:\mathbf{R}^N \rightarrow \mathbf{R}^M$, with its i-th output equal

$$y_i = \sigma_i^{(K)} \left[\theta_{i,j}^{(K)} + \sum_j w_{ij}^{(K)} \sigma_j^{(K-1)} \left(\dots \theta_m^{(l)} + \sum_n w_{m,n}^{(l)} x_n \dots \right) \right] . \tag{4.2}$$

The properties of this mapping are determined by the weight vector

$$w = \left[w_{1,1}^{(1)}, \dots, w_{l1,N}^{(1)}, \dots, w_{1,1}^{(K)}, \dots, w_{M,lK-1}^{(K)}, \theta_1^{(1)}, \dots, \theta_M^{(K)} \right]^T \tag{4.3}$$

which contains all neurons' weights and thresholds.

4.2.2. Neural Network Approximation of Nonlinear Functions

Most of the applications of feedforward artificial neural networks are based on the approximation result, which may be stated as follows. Consider a compact subset of $\mathbf{R}^n$, **U** and a continuous function $\mathbf{f}: \mathbf{D} \rightarrow \mathbf{R}^m$. The network architecture considered here is a single hidden layer network with activation function σ of the hidden layer nonconstant and bounded (which is satisfied by sigmoidal functions), and the activation function of the output layer linear. Then for any $\epsilon > 0$, there exists a (sufficiently large) network, such that the mapping (4.2) realized by the network approximates the function **f** in the uniform sense with error smaller than ϵ, i.e.

$$\sup_{x \epsilon U} \left| f^{net}(x) - f(x) \right| < \epsilon . \tag{4.4}$$

This result is stated and proven in [4.2]. The result also holds with the output activation function monotone increasing and bounded with range (0,1) if the range of approximated function is contained in m-dimensional rectangle $[0,1]^m$. Since a continuous function is always bounded over a compact set, this means that a continuous function can also be approximated by a network with sigmoidal outputs if only proper scaling is used. Similar result holds for approximation in $\mathcal{L}^p$ sense — i.e., for $1 \leq p < \infty$ and $\epsilon > 0$ if $\mathbf{f} \epsilon \mathcal{L}^p(\mathbf{U},\mathbf{R}^m)$ then there exists a network such that

$$\left[\int_U \left| \left(f(x) - f^{net}(x) \right) \right|^p dx \right]^{1/p} < \epsilon . \tag{4.5}$$

Several extensions to this have been introduced. For example approximations in Sobolev spaces were also considered. If the function to be approximated is m times differentiable over **U** - $f \epsilon C^m(U)$, and if the activation function of the hidden layer has bounded derivatives of order up to m, then for $\epsilon > 0$

it is possible to find a (sufficiently large) neural network approximating not only the function but also all its derivatives of order up to m with error smaller than ϵ, i.e.

$$\left[\sum_{|\alpha|<m} \int_U | D^\alpha \left(f(x) - f^{net}(x)\right) |^p dx\right]^{1/p} < \epsilon \qquad \text{if } p < \infty \tag{4.6}$$

or

$$\max_{|\alpha|<m} \sup_{x\epsilon U} \left| D^\alpha (f(x) - f_{net}(x)) \right| < \epsilon \qquad \text{if } p = \infty \ . \tag{4.7}$$

The assumption of compact set **U** can be replaced for $p < \infty$ if the integration is done with respect to some finite measure μ.

Approximation results reviewed above are, unfortunately, of purely existential nature, and give no constructive procedure to find a required approximating network. In particular, size of the network required to obtain desired accuracy is unknown. Also the way to determine appropriate values of the network's parameters (the weights of the neurons) is not addressed. Selection of the size of the network is usually based upon experience or trial and error procedure, although systematic procedures for treating this problem have been also developed [4.9]. Calculation of appropriate values of the network's weights, often called training of the network, is discussed in some detail in Subsection 4.2.4.

The approximation capabilities of feedforward networks facilitate their application whenever an analytically unknown function has to approximated. In that sense neural networks are in fact just one of many possible methods of nonlinear function fitting, together with polynomials, splines, Walsh functions, Fourier series, etc. What sets apart neural networks from all those methods is their specific structure — with many simultaneously operating, identical processing elements, each of which carries only a small portion of the responsibility for the overall result. As a consequence, they are particularly well suited for parallel, fast acting, fault resistant hardware implementations. Also, the approximating properties of neural network approximations are quite advantageous when compared, e.g., with polynomials. Our previous studies suggest that quality of interpolation by neural networks is very good if the size of the network is judiciously chosen. The nature of the sigmoid function allows also for extrapolation much more sensible than in other approximation methods.

4.2.3. Neural Network Sub-Optimal Feedback Synthesis

Since a suitably large feedforward neural network can approximate any continuous function, in particular it can be used for implementation of a nonlinear control law. A typical situation is when the control algorithm, which is known to exist, is not given explicitly, but only in form of desired input-

output behavior of the plant, or as a set of examples of "correct" control actions. In an iterative process of "learning" the weights of the neurons are adjusted so that some performance criterion is minimized. A wealth of examples of such applications may be found in a survey paper [4.3]. In this study a particular control application of neural networks is taken from [4.10].

Consider a finite-dimensional time-invariant dynamical system of the form

$$\mathbf{dx/dt} = \mathbf{f(x(t),u(}t\mathbf{)}) \tag{4.8}$$

with control signal constrained by

$$\mathbf{u}_{min} \leq \mathbf{u}(t) \leq \mathbf{u}_{max} \, . \tag{4.9}$$

Let the control objective be either time-optimal transfer of the plants state from some initial condition $\mathbf{x}_0$ to a desired terminal state $\mathbf{x}_f$, or minimization of infinite horizon quadratic error criterion:

$$J = \int_0^\infty \sum_i \rho_i (x_i - x_{if})^2 \, dt \tag{4.10}$$

For the time-optimal control to be well posed $\mathbf{x}_f$ must be attainable from $\mathbf{x}_0$ in finite time by some control satisfying (4.9). Then the sufficient conditions for the time-optimal control to exist can be found in [4.1]. For the quadratic criterion (4.10) minimization to be well posed, $\mathbf{x}_f$ should be an equilibrium of (4.8). In both cases, if the solution exists, it is time-invariant, i.e., if the starting time is shifted but the initial condition is the same, the optimal control signal is identical modulo time shift. Now consider a family of such optimal control problems with fixed desired state $\mathbf{x}_f$ and initial condition varying within some neighborhood of x_f. This may correspond to the problem of time-optimal or quadratic optimal rejection of random state disturbance with fixed desired steady state value. Intuition based on the principle of optimality suggests that the value of optimal control signal should be expressible as a function of the state, hopefully with some smoothness properties. Unfortunately this does not have to be the case. Discussion of difficulties arising in this problem and further references may be found in [4.4] or in survey paper [4.8]. In this study it is assumed that indeed in the region of interest the optimal control signal for fixed desired state may be expressed as

$$\mathbf{u}^{opt}(t) = \mathbf{g(x(t))} \tag{4.11}$$

which is unique up to a set of measure zero (e.g., a switching hypersurface). In extension to the work of [4.10] we furthermore consider a family of such feedback synthesis problems, parametrized by desired

final state x_f. We introduce the command or target signal x_f as additional input to the controller and look for a feedback law of the form:

$$u^{opt}(t) = g(x(t), x_f) \ . \tag{4.12}$$

The approach is to teach a neural network to approximate this finite-dimensional static mapping from off-line generated optimal trajectories corresponding to different initial conditions and different target points. The previously mentioned approximation theorem guarantees uniform approximation of a continuous function, whereas optimal controls are often bang-bang — both in time-optimal and quadratic optimal cases (see previous section). However, continuous functions over a compact set are dense in $\mathcal{L}^2$, so it is possible to approximate (4.12) by a neural network arbitrarily closely.

4.2.4. Training of Neural Network Controller

The process of finding the proper weights for the neurons is called training. It is an iterative gradient-based procedure, during which the quadratic error is minimized:

$$J = \sum_i \left\| y_i - y^{net}(z_i) \right\|^2 \tag{4.13}$$

where the sum is calculated over the training set consisting of pairs $\{z_i, y_i\}$, with z and y being the input and desired output of the network, respectively, and y^{net} is the mapping realized by the network. In case of quadratic regulation of angle of attack, investigated in Section 4.3, the input consists of the state of the aircraft, and of desired value of α: $z = [\alpha, q, \theta, v, \alpha_f]^T$, and the network output is the aircraft control vector $y = [\delta_h, T_M, \delta_T]^T$. The values of y_i and z_i in this case come from sampling of desired input-output trajectories. It has to be noted that criterion (4.13) is a discretized version of integral criterion (4.5) with $p = 2$, and this introduces yet another level of approximation. For the resulting network to approximate the optimal feedback mapping closely, not only has the minimum of (4.13) be achieved (which in itself may be a difficult and time-consuming problem), but also the training set has to be constructed judiciously. An obvious conflict here is between quality of the controller and effort required for its parameter identification (training).

For the minimization of (4.13) the gradient of J with respect to the network's weights is calculated through a chain rule, whose particular application to neural networks is nicknamed "backpropagation" (see [4.3]). After the gradient $\partial J/\partial w$ is calculated the search direction δw (in the weight space) is determined and the minimum of J with respect to the step size γ in the direction δw is

found, which includes calculation of J for several values of γ. Finally the modified values of the weights are set according to:

$$w^{new} = w^{old} + \Delta w = w^{old} + \gamma^{opt} \delta w \tag{4.14}$$

The flow of information during the training process is shown on Fig. 4.2.

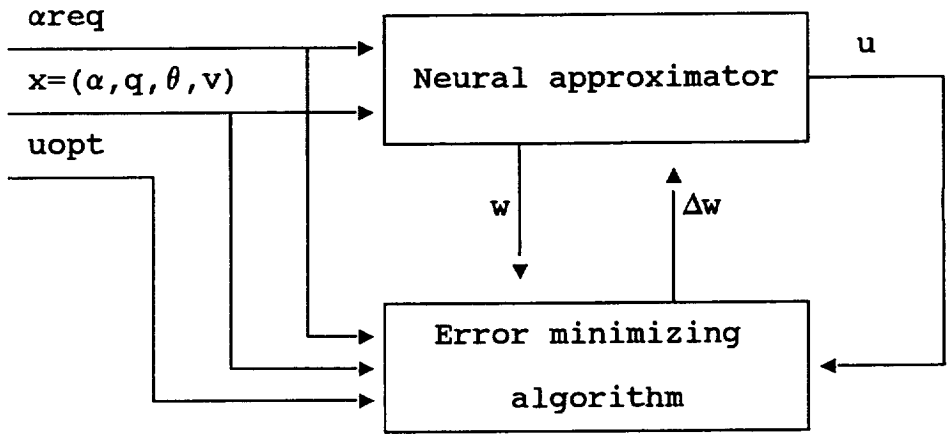

Figure 4.2. Training of neural suboptimal controller.

In this study a version of conjugate gradient algorithm from [4.7] is used for determination of the search direction. The line search is performed using a combined two-point gradient-based and three-point non-gradient parabolic fit.

4.3. Simulations

A neural network approximation of the optimal control was developed for the aircraft model discussed in Section 3.2.1. The control problem considered was minimization of quadratic performance index (3.12-3.13) with $\rho_2 = \rho_3 = \rho_4 = 0$, $\rho_1 = 1$ — i.e, with the angle of attack being the regulated output variable. A family of solutions to this problem is discussed in Section 3.3. The training data for the neural network was obtained by sampling 15 numerically found trajectories — with initial conditions trimmed with angle of attack approximately equal 5°, 20° and 35°, and with target values of α equal 5°, 20°, 35°, 50°, 60° and 70°. The trajectories were sampled every 0.1s, which with 8s horizon resulted in 1200 training points necessary for a single evaluation of performance criterion. The network's inputs are taken to be four states α, q, θ, v and the desired value α^{req} and the outputs are $u_{\delta h}$, u_{TM}, $u_{\delta T}$.

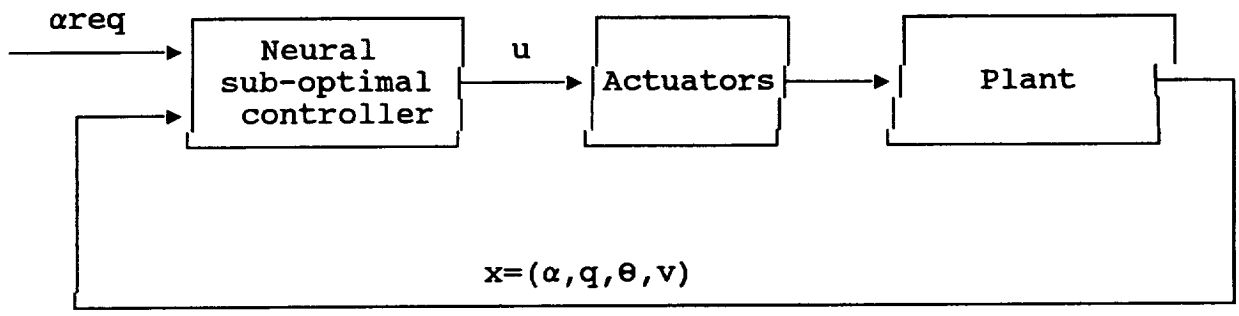

Figure 4.3. Neural controller configuration

A number of single hidden layer networks was trained on this training data in configuration from Fig. 4.2. The networks used had one hidden layer and the neuron's activation function used was standard sigmoid. Then the resulting neural network controllers were tested in feedback configuration depicted on Figs. 4.3. A typical performance of a simulated neural network controller is shown on Figs. 4.4-4.7. Here the same initial conditions and target values were used for two neural controllers — with 30 (A) and 15 (B) hidden neurons. The initial transition to the vicinity of required value is of very good quality. Then however a "steady state" error occurs. This is may be due to the fact that the network actually wants to perform the plant's dynamics inversion which obviously is not 100% correct. There is no explicit dynamic error feedback and as a result a small error will always occur. Also the network was trained as a static mapping, and the approximation error minimized during training does not correspond to the regulation error. A much better approach would be to train the networks in the feedback loop with the aircraft model, accounting for different sensitivities of the output with respect to control actions in different state-space regions. This is proposed for our future research.

An interesting test of the capabilities of neural controller is depicted on Fig. 4.8. Here the desired value of the output is set to 80° — a value that is outside the range covered by the training data. A quite satisfactory output trajectory adds credence to the claims about good extrapolation properties of neural networks.

4.4. Conclusions and Practical Considerations

The neural network based controller presented in the previous subsection demonstrates how the results of optimal control theory may be applied to the synthesis of feedback controllers. Results are promising, but at least a few shortcomings are apparent. First of all the simulations reveal problems with terminal state accuracy. These result from inaccurate inversion of the plant dynamics obtained through the training process. This indicates a need for incorporating the idea of dynamic error feedback into the

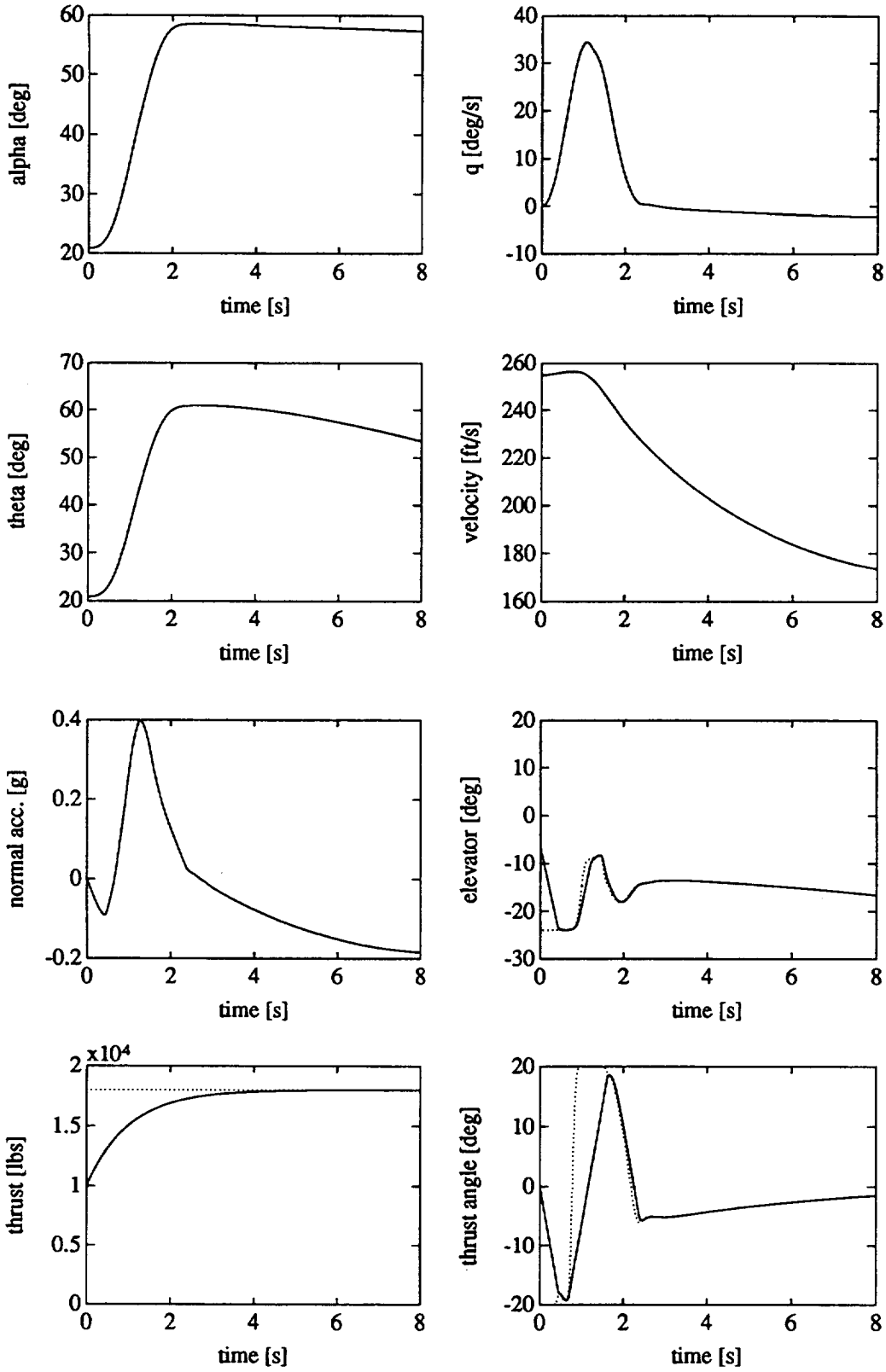

Figure 4.4 Sub-optimal neural control (net A) with target $\alpha = 60°$
Initial condition - trim corresponding to thrust 10,000

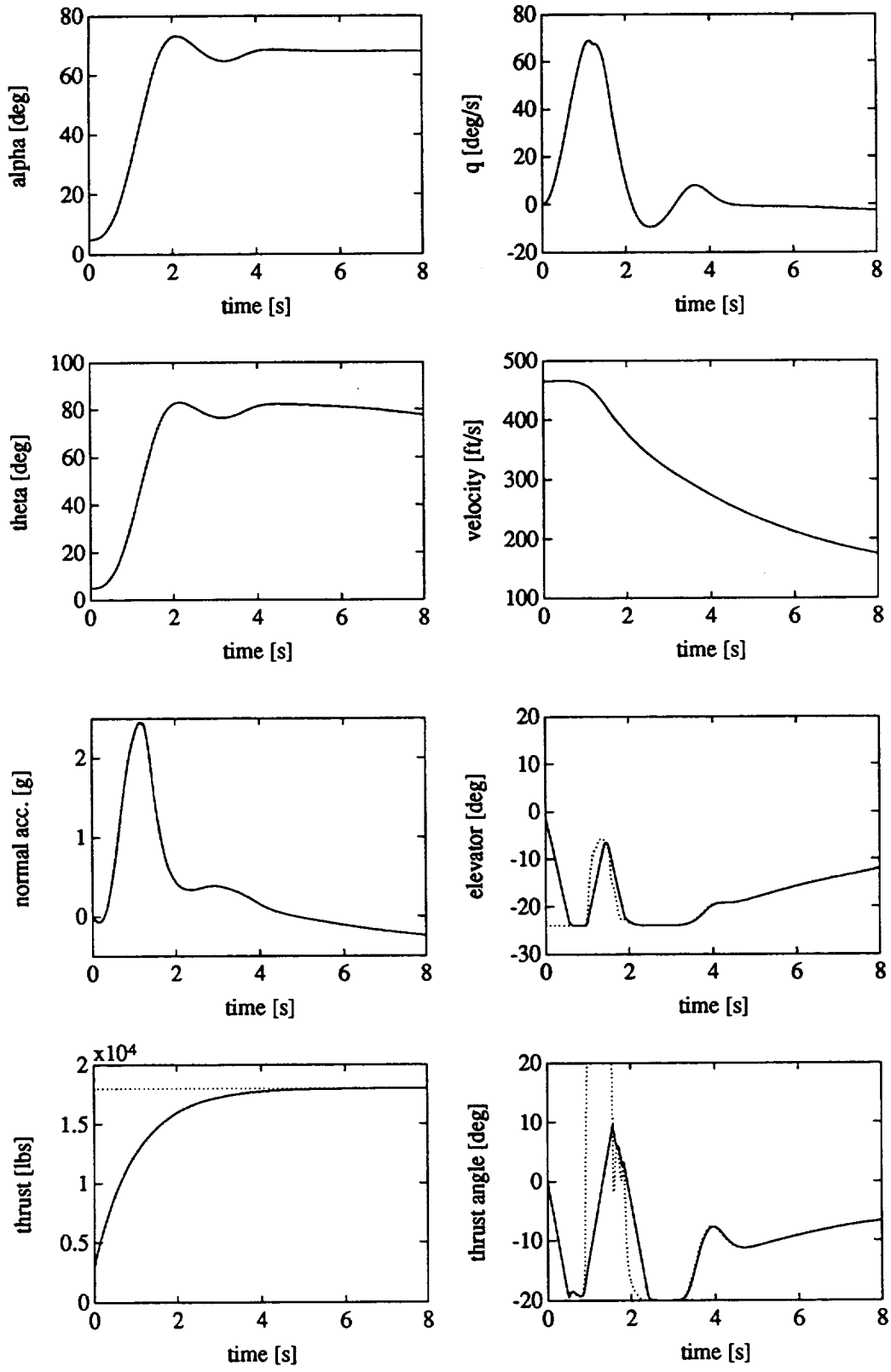

Figure 4.5 Sub-optimal neural control (net A) with target $\alpha = 70°$
Initial condition - trim corresponding to thrust 3,000

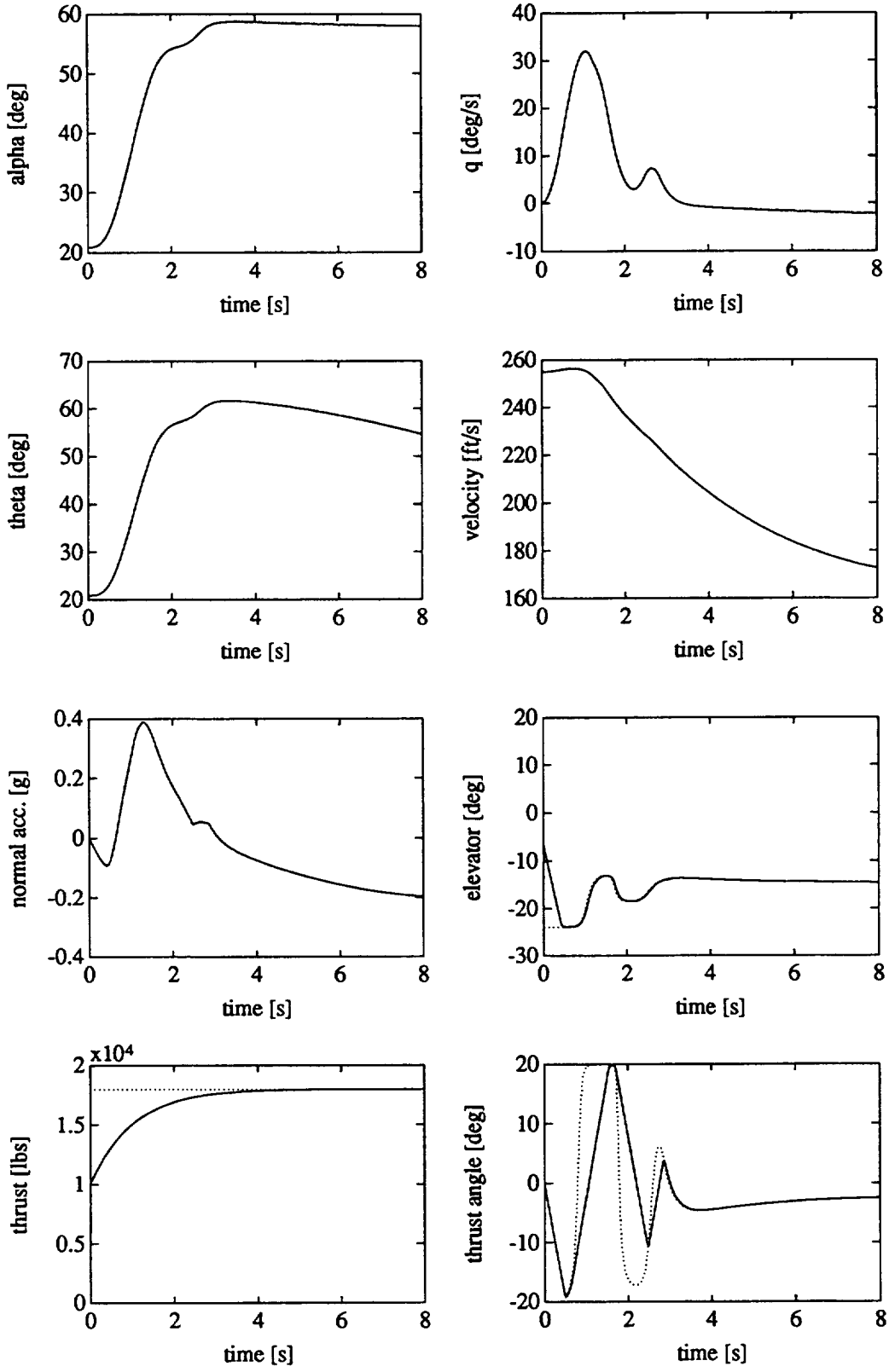

Figure 4.6 Sub-optimal neural control (net B) with target $\alpha = 60°$
Initial condition - trim corresponding to thrust 10,000

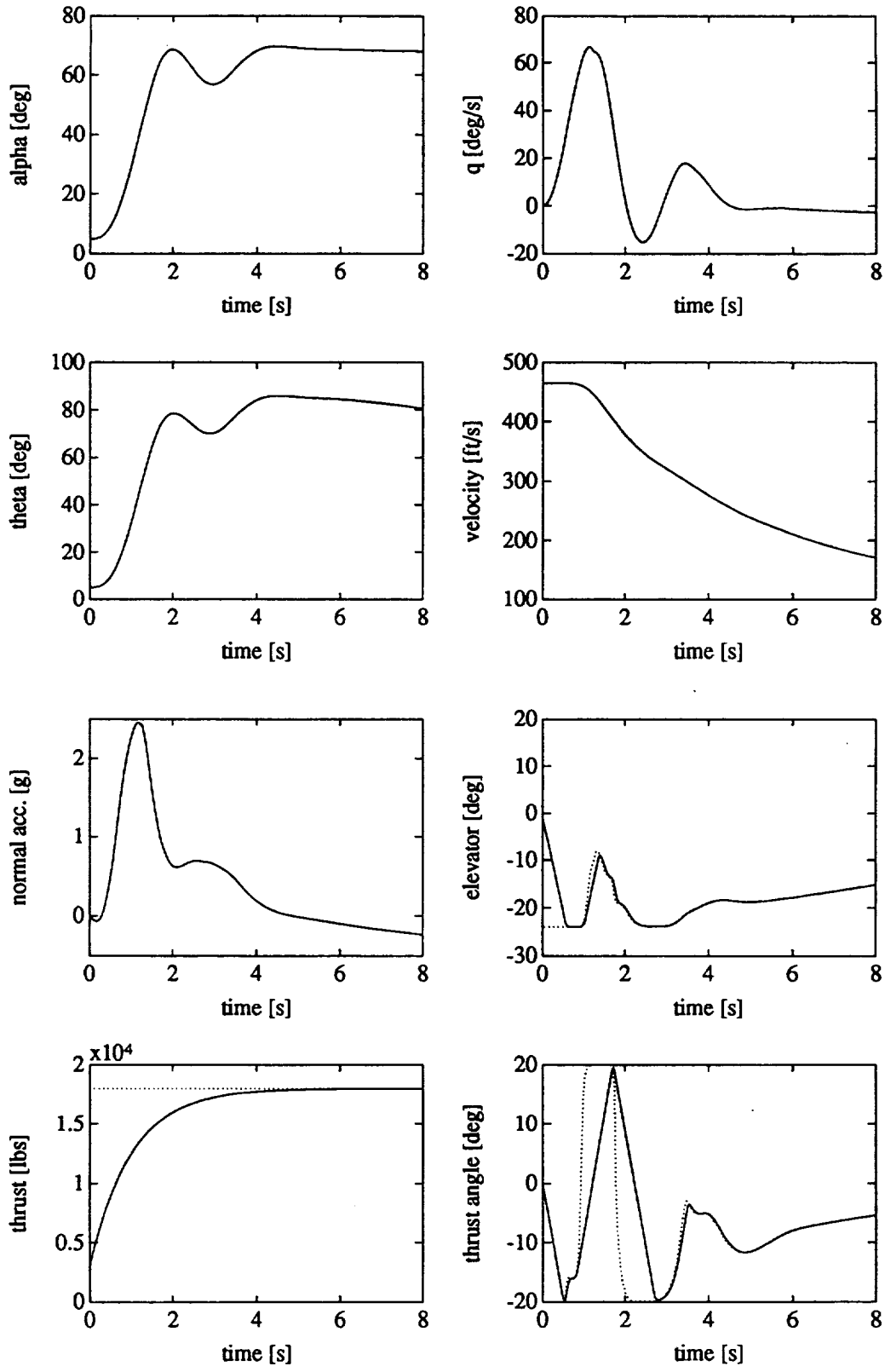

Figure 4.7 Sub-optimal neural control (net B) with target $\alpha = 70°$
Initial condition - trim corresponding to thrust 3,000

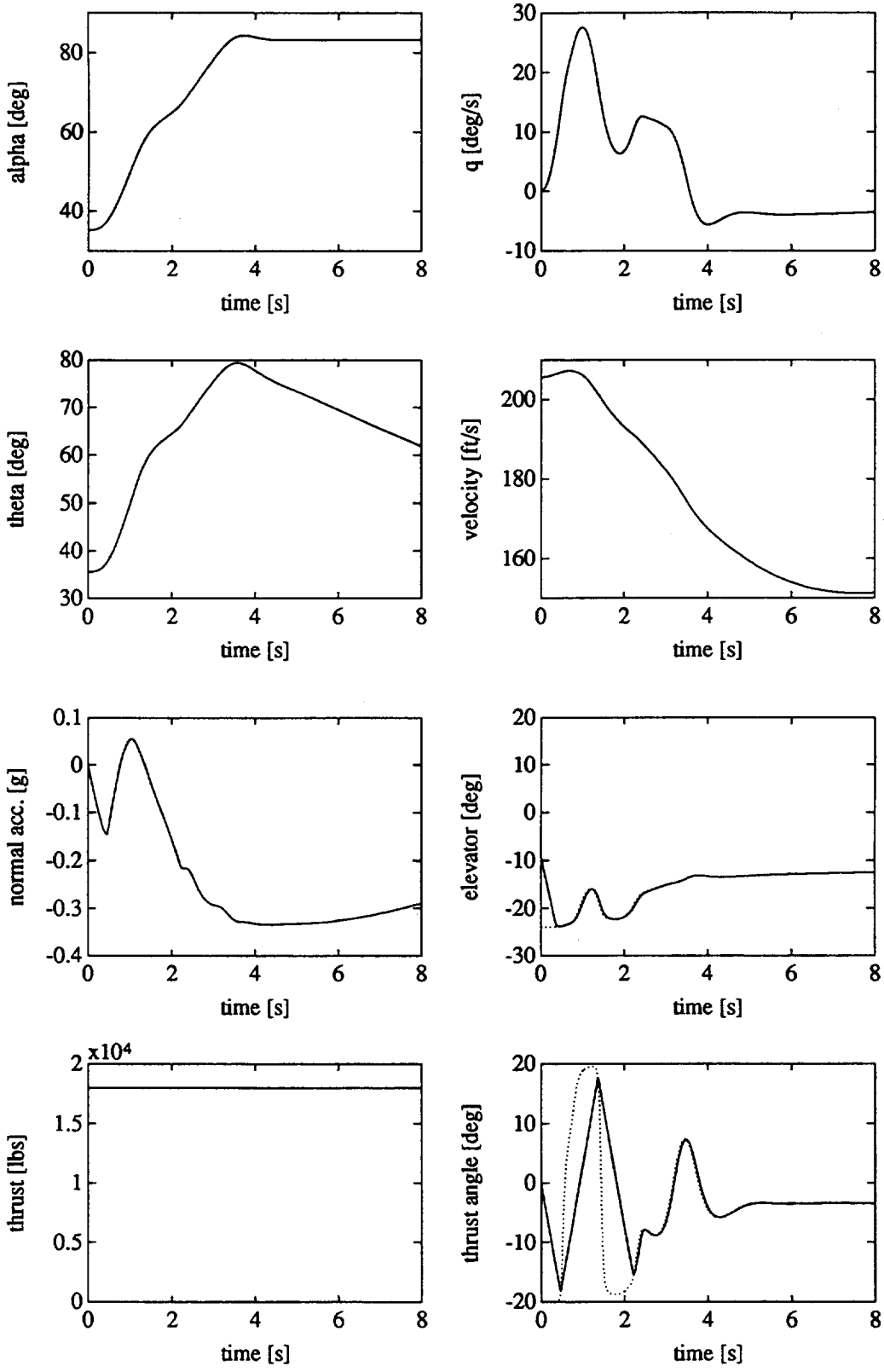

Figure 4.8 Sub-optimal neural control (net B) with target $\alpha = 80°$
Initial condition - trim corresponding to thrust 18,000

neural controller design. One possibility is to allow a second parallelly acting regulator, possibly a linear one, activated in the neighborhood of the desired value. Such additional controller would provide corrective action to eliminate the error. Another possibility is to establish an outer loop controller regulating the α^{req} value fed to the network in order to get true desired value as output. This possible controller configuration is depicted on Fig. 4.9. In both cases the established linear control techniques may be used for design of the local controller, since it is not intended to work with large variations of α.

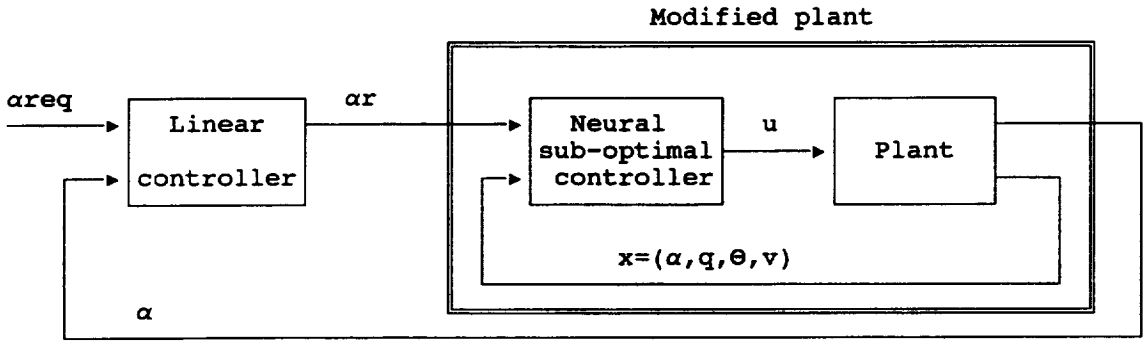

Figure 4.9. Proposed configuration with an additional controller

The more general problem involves robustness with respect to model inaccuracy. The optimal trajectories, used as source of training data for the network, were generated using an exact model of the plant. Discrepancies between the plant and the model are sure to cause serious problems in terms of the controller performance. For small modelling errors the previously discussed concept of additional linear feedback might provide a satisfactory solution. For larger uncertainties the approaches introduced in Sections 5 and 6 and in [4.11] may be more useful. The latter suggests a number of controllers designed for different nominal models of the plant and with a hierarchical classifying network interpolating between the nominal controllers. Work on applying that method to control of an aircraft is currently under way and proposed for continuation.

The neural networks used here were merely simulations implemented on a serial computer. This necessarily is an impediment for the processing speed, particularly if the learning phase is concerned. However recent advent of hardware implementations of neural networks makes practical application much more realistic. Faster future computing power may make on-line training with the actual airplane maneuver more feasible and thus alleviate some of the problems associated with simulation training.

4.5. References

[4.1] H. Hermes and J. P. Lasalle, *Functional Analysis and Time Optimal Control*, New York: Academic Press, 1969.

[4.2] K. Hornik, "Approximation Capabilities of Multilayer Feedforward Networks," *Neural Networks*, Vol. 4, 251-257, 1991.

[4.3] K.J. Hunt, D. Sbarbaro, R. Żbikowski and P. J. Gawthrop, "Neural Networks for Control Systems — A Survey," *Automatica*, Vol. 28, 1083-1112, 1992.

[4.4] S. Łojasiewicz, Jr. and W. Szpunar, "Optimal Feedback," E.O. Roxin, ed., *Modern Optimal Control*, New York: Marcel Dekker, 1989, pp. 289-299.

[4.5] W.T. Miller, R.S. Sutton and P.J. Werbos, eds., *Neural Networks for Control*, Cambridge: MIT Press, 1990.

[4.6] K.S. Narendra and K. Parthasarathy, "Identification and Control of Dynamical Systems Using Neural Networks," *IEEE Trans. Neural Networks*, Vol. 1, 4-27, 1990.

[4.7] D.F. Shanno, "Conjugate Gradient Methods with Inexact Searches," *Mathematics of Operations Research*, Vol. 3, 244-256, 1978.

[4.8] H.J. Sussmann, "Optimal Control," H. Nijmeijer and J.M. Schumacher, eds., *Three Decades of Mathematical System Theory*, Berlin: Springer Verlag, 1989, pp. 409-425.

[4.9] H. White, "Connectionist Nonparametric Regression, Multilayer Feedforward Networks Can Learn Arbitrary Mappings," *Neural Networks*, Vol. 3, 535-549, 1990.

[4.10] R.R. Zakrzewski and R.R. Mohler, "On Time-Sub-Optimal Control Using Artificial Neural Networks," *Proc. 31st IEEE Conf. Decision Contr.*, Tucson, 1992, pp. 895-896.

[4.11] R.R. Zakrzewski, R.R. Mohler and W.J. Kolodziej, "Hierarchical Intelligent Controller with Flexible AC Transmission Systems Application," *Proc. 12th World Congress of IFAC*, 1993.

5. NONLINEAR ADAPTIVE CONTROL

5.1. General Concept

This section discusses results of studies of a control approach based on input-output model of the control plant. The majority of practically used control algorithms utilize, either explicitly or implicitly, some model of the plant dynamics. One of the possible forms of such a model is an input-output model, relating applied control action to resulting observed behavior of the system. The main reason to use input-output, rather than state space models, is that they employ only measured quantities subsequently used by the controller, and therefore are more natural in control system setting. Also, very often the model of the plant is not given prior to the controller synthesis, and has to be identified, either off-line or on-line, using the available input-output data. In such a case the input-output modelling approach is more effective, since it has simpler model structure and results in fewer parameters to be identified. Furthermore, for a given plant and given input and output signals, the state space model is not unique, while the input-output model is — although, of course, both may be practically realized by various approximate modelling techniques. Obviously, the input-output modelling approach also has its disadvantages. The main one is that it is basically a black-box-type technique, in which the phenomena "inside" the plant are of no interest, as long as its response to the input is modelled correctly. If the dynamics of the plant is easily available from physical considerations the state space model usually can be constructed with no difficulties and its parameters have well understood interpretations. On the other hand parameters, of input-output models usually have no immediate physical interpretation.

There are several standard input-output modelling techniques for nonlinear systems in both discrete and continuous time settings. They include Volterra series, Wiener series, nonlinear time series, neural networks, etc. — a detailed survey may be found in [5.4]. In this work the time series approach is used. This technique is a natural extension of discrete time modelling of linear systems, known in the stochastic setting as auto-regressive moving average (ARMA) models. Therefore, an often used acronym is NARMA — for nonlinear ARMA [5.2]. The nonlinear time series expresses future values of outputs as a nonlinear function of a finite number of past values of output and of control. For the purpose of system identification this unknown nonlinear function is usually decomposed into a sum of nonlinear functions with parameters to be identified appearing linearly. This allows for easy application of parameter identification techniques from linear systems theory, although their convergence in an on-line identification setting in a feedback loop is a far more complicated question than in the linear case. If the time-series model is to be used for calculation of control action, it is also desirable that it should be easily solved for current value of control. Therefore, most often control appears in the model either linearly (or more correctly in an affine fashion) or as some strictly monotone function.

In the aircraft problem, the physical model of the dynamics is well known and is easily expressible in state space form. Nevertheless, there are significant reasons to look at input-output black-box-type modelling as an alternative approach. The main problem arises from the aerodynamic stability derivatives. They are complex nonlinear functions of angle of attack, Mach number and altitude. If these relations are entered into the state space model it appears so complicated that its usefulness for on-line control generation becomes quite doubtful. Furthermore, the exact form of the dependencies of stability derivatives on state variables is not known — even for fixed angle of attack, Mach number and altitude their measurement accuracy may be as low as 50% in extreme cases. Therefore, an overly complicated nonlinear state space model would not seem to be very useful for on-line control calculations. A much better choice is a simple input-output model capturing the essential dynamics of the aircraft. In this work the time series model used includes polynomial nonlinearities in angle of attack.

The control algorithm used here is an adaptive, or self-tuning, non-linear model reference technique. The time-series input-output model is identified on-line using a recursive least squares (RLS) method, and one step ahead error between the predicted and reference output is minimized.

The following sections describe in some detail identification and control algorithms used, provide simulations and discuss conclusions for future research and practical implementations.

5.2. Methodology

5.2.1. Nonlinear Time Series Model

The nonlinear time series model considered here has general form:

$$y^{mod}(k+1) = f(y(k), y(k-1), \ldots, y(k-n), u(k), u(k-1), \ldots, u(k-m)) \tag{5.1}$$

Where f is a nonlinear function. To facilitate easy identification of the model the form assumed in most practical applications is:

$$y^{mod}(k+p) = P^T \phi(k) \tag{5.2}$$

where P is the parameter matrix, and $\phi(k) = \phi(y(k),y(k-1),\ldots,y(k-n),u(k-1),u(k-2),\ldots,u(k-r))$ is a nonlinear function of current and past values of input and output. Linear dependence of the future output on unknown parameters allows one to use one of the linear regression methods for identification [5.1].

The plant studied here is a fourth-order nonlinear model of the longitudinal dynamics of the aircraft. The same model was used in studies described in Sections 3 and 4, and is discussed in detail in Appendix B. The difference here is that only one control signal is used — the stabilator/elevator angle, while thrust is assumed to point parallel to body axis and to be of constant magnitude all the time. Thus,

the simulated plant has four states — α, q, θ and v, and one control δ_h. For the purpose of the control system synthesis, however, measurements of only two outputs are assumed — α and q. Thus in the identification model we have

$$\begin{aligned} y &= [\alpha, q]^T \\ P &= [p_\alpha, p_q] \ . \end{aligned} \tag{5.3}$$

The choice of elements of the regressors' vector ϕ is motivated by the fact that nonlinearities in the short period dynamics are associated with angle of attack. Also it is recognized that due to the highly nonlinear nature of the aircraft dynamics it is probably impossible to fit a "black-box" model describing the plant's dynamics accurately in the whole range of flight condition. Instead it is more practical to fit a simple local approximate model, and allow its rapid adaptation according to the change of operating conditions. Therefore, the regressor form is chosen as:

$$\phi_k = \left[\alpha, \sigma^2, \alpha^3, q, q\alpha, q\alpha^2, q\alpha^3, u, u\alpha, u\alpha^2, u\alpha^3, 1\right]^T (k) \ . \tag{5.4}$$

This results in a second-order model corresponding to a currently dominant short-period behavior, but including nonlinearities in α, particularly significant at large values of angle of attack.

5.2.2. Identification Algorithm

For the on-line identification of the unknown parameters of the model (5.2)-(5.4), a recursive least squares (RLS) algorithm was implemented. The basic update formula for parameter estimates at moment k is

$$p(k) = (Q(k-2)\,\phi(k-1)) \Big/ \left(\lambda(k-1) + \phi(k-1)^T Q(k-2)\,\phi(k-1)\right) \tag{5.5}$$

with covariance matrix Q being updated according to:

$$Q(k-1) = (1/\lambda(k-1)) \left[Q(k-2) - \left(Q(k-2)\,\phi(k-1)\,\phi(k-1)^T Q(k-2)\right) \Big/ \left(\lambda(k-1) + \phi(k-1)^T Q(k-2)\,\phi(k-1)\right) \right] \tag{5.6}$$

Since two parameter vectors p_α and p_q are estimated, two covariance matrices Q_α and Q_q are also calculated. Due to the approximate nature of model (5.2)-(5.4) the currently fitted parameters are expected to change together with operating conditions. To allow for such changes the forgetting factor

λ is introduced. As a precaution against unlimited growth of the covariance matrix Q at the steady state, which is a consequence of $\lambda < 1$ when the input is not persistently exciting, a policy with variable forgetting factor is adopted. The formula for $\lambda(k)$, taken from [5.3], is:

$$\lambda(k) = 1 - \epsilon\left(e(k)^2 / \bar{e}(k)^2\right) \tag{5.7}$$

where e(k) is current prediction error of the model:

$$e(k-1) = y(k-1) - y^{mod}(k-1) = y(k-1) - p(k-1)^T \phi(k-1) \tag{5.8}$$

and $\bar{e}(k)$ is an average of e(k) over a few last samples. For two identification processes going on for p_α and p_q two values of forgetting factor λ_α and λ_q are determined with y in (5.8) denoting either α or q. As an additional precaution against uncontrolled growth of matrix Q, its trace is monitored and Q is reset to a diagonal matrix whenever the threshold value for the trace is exceeded.

5.2.3. Adaptive Control Algorithm

The control methodology is based on model algorithmic control (MAC) [5.5]. The basic formula of the algorithm is:

$$y^{ref}(k+1) = y^{mod}(k+1) + \left(y(k) - y^{mod}(k)\right) \tag{5.9}$$

where y^{ref} is required (reference) output, generated using the command signal (in the aircraft case from the pilot), y is the actual output and y^{mod} is the output value predicted by the model:

$$y^{mod}(k+1) = p^T \phi(k) \ . \tag{5.10}$$

Since regressors' vector $\phi(k)$ depends on control value u(k), the equation (5.9) can be solved for u(k) resulting in required output in moment k+1. In the case of the aircraft control problem, the output is assumed to be the angle of attack α, and the model is (5.2)-(5.4). The value of control necessary to get the required output value is calculated as:

$$u(k) = \left(\alpha^r - p_{1\alpha}\alpha - p_{2\alpha}\alpha^2 - p_{3\alpha}\alpha^3 - p_{4\alpha}q - p_{5\alpha}\alpha - p_{6\alpha}q\alpha^2 - p_{7\alpha}q\alpha^3 - p_{12\alpha}\right) / \left(p_{8\alpha} + p_{9\alpha}\alpha + p_{10\alpha}\alpha^2 + p_{11\alpha}\alpha^3\right) \tag{5.11}$$

with

$$\alpha^r = \alpha^{ref}(k+1) - \left(\alpha(k) - \alpha^{mod}(k)\right) . \tag{5.12}$$

If the computed control exceeds the bounds for δ_h its set equal to the maximal (or minimal) allowed value. If the processing time of the on-board computer needed to calculate (5.10)-(5.12) is small enough in comparison with the sampling time used, then the above formula may be used in the controller. If, however, the calculation time cannot be neglected, only information sampled at moment k-1 can be used for calculation of control at time k. Therefore, the correction term in (5.9) is replaced with prediction error at moment k-1 and the equation becomes:

$$\alpha^{ref}(k-1) = \hat{\alpha}^{mod}(k+1) + \left(\alpha(k-1) - \alpha^{mod}(k-1)\right) \tag{5.13}$$

with $\hat{\alpha}^{mod}(k+1)$ being calculated using the estimated values of angle of attack and pitch rate at moment k, instead of yet unavailable actual values:

$$\begin{aligned} \hat{\alpha}^{mod}(k+1) &= p_\alpha^T \hat{\phi}(k) \\ \hat{\phi}(k) &= \left[\hat{\alpha}, \hat{\alpha}^2, \hat{\alpha}^3, \hat{q}, \hat{q}\hat{\alpha}, \hat{q}\hat{\alpha}^2, \hat{q}\hat{\alpha}^3, u, u\hat{\alpha}, u\hat{\alpha}^2, u\hat{\alpha}^3, 1\right]^T (k) . \end{aligned} \tag{5.14}$$

Estimated current values of measured outputs are calculated taking into account previous prediction errors:

$$\begin{aligned} \hat{\alpha}(k) &= p_\alpha^T \phi(k-1) + \left(\alpha(k-1) - \alpha^{mod}(k-1)\right) \\ \hat{q}(k) &= p_q^T \phi(k-1) + \left(q(k-1) - q^{mod}(k-1)\right) . \end{aligned} \tag{5.15}$$

Also in equation (5.11), which is used for the calculation of control value, $\hat{\alpha}$ and $\hat{q}$ are used instead of α and q, and (5.12) is replaced with

$$\hat{\alpha}^r = \alpha^{ref}(k+1) - \left(\alpha(k-1) - \alpha^{mod}(k-1)\right) . \tag{5.16}$$

The algorithm is made adaptive, or self-tuning ([5.6]), by including the identification mechanism described in Section 5.2.2 for parameters p_α and p_q. Thus the design is a certainty-equivalence one, and its validity depends upon the assumption that indeed the identification and calculation of control can be

performed separately. Here we tacitly assume legitimacy of such method for the problem being solved, but it has to be pointed out that this is a heuristic method justified mostly by simulation experiments.

The generation of reference trajectory α^{ref} is performed using the command signal and current output value α. The reason to include output feedback in calculation of α^{ref} is to avoid unrealistic values of reference signal, leading to control values outside the region of local validity of identified model. If in the previous step the reference value was not attained, then the reference in the next step is less demanding, so that it can be attained. In this study a second-order algorithm is used for calculation of α^{ref}:

$$y^{ref}(k+1) = a_1\alpha(k) + a_2\alpha(k-1) + \alpha^{cmd} . \tag{5.17}$$

The overall flow of information in the algorithm is schematically depicted on Fig. 5.1

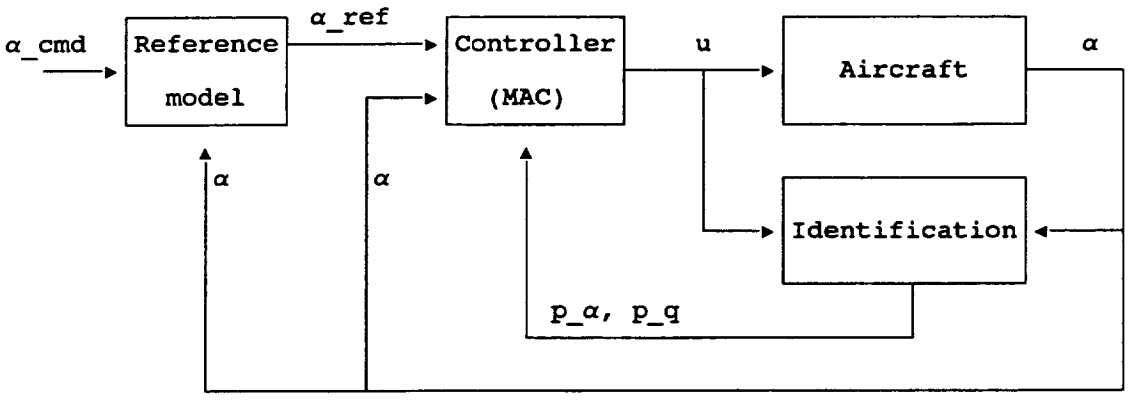

Figure 5.1. Flow of information in adaptive control algorithm

Attempts of the control algorithm to solve (5.9) exactly may result in control signal changing very abruptly and often oscillating, while trying to track the reference trajectory. Therefore a modified one step ahead design was introduced aimed at smoother control trajectories. Instead of solving (5.9) the following cost function is minimized with respect to current control value:

$$J = \left(\hat{\alpha}^{mod}(k+1) - \hat{\alpha}^{r}(k+1)\right)^2 + \rho(u(k) - u(k-1))^2 \tag{5.18}$$

with $\hat{\alpha}^{mod}$, $\hat{\alpha}^{r}$ as before. Minimization of (5.18) results in

$$u(k) = \left(\left(\hat{\alpha}^{r} - a\right)b + \rho u(k-1)\right) \Big/ \left(b^2 + \rho\right) \tag{5.19}$$

with

$$a = p_{1\alpha}\hat{\alpha} + p_{2\alpha}\hat{\alpha}^2 + p_{3\alpha}\hat{\alpha}^3 + p_{4\alpha}\hat{q} + p_{5\alpha}\hat{\alpha} + p_{6\alpha}\hat{q}\hat{\alpha}^2 + p_{7\alpha}\hat{q}\hat{\alpha}^3 + p_{12\alpha}$$

$$b = p_{8\alpha} + p_{9\alpha}\hat{\alpha} + p_{10\alpha}\hat{\alpha}^2 + p_{11\alpha}\hat{\alpha}^3 \ .$$

Obviously, for $\rho = 0$ (5.19) reduces to (5.16), whereas for $\rho \to \infty$ we obtain u(k) = u(k-1) = const. As before, if (5.19) results in a value outside the allowed range, the closest feasible value is used instead.

5.3. Simulations

The adaptive control algorithm described in Section 5.2 was simulated on the complex fourth-order nonlinear model of longitudinal dynamics of the HARV aircraft. Only one control signal, the elevator/stabilator angle, is used with both thrust magnitude and thrust direction assumed to be constant. The maneuvers presented here were simulated at 15,000 feet and 0.3 Mach. Initial estimates of parameters p_α and p_q are set to zero, and the simulation is initiated at trim condition corresponding to $\alpha = 5°$. Then the adaptive controller is simulated with $\alpha^{cmd} = 5°$ for 5 seconds, during which the controller learns current dynamics of the aircraft. This corresponds to a practical situation, when the control and identification is performed continuously and before any maneuver the parameter estimates will never be zero. The variable forgetting factor (5.7)-(5.8) is calculated with $\epsilon = 0.01$ and the past prediction errors are averaged over last 10 samples.

Figure 5.2 displays the result of simulation of nonlinear adaptive algorithm for command signal first jumping to 60° and then decreasing to 30° and 5°. The output trajectory is showed together with reference signal, which is displayed in dotted line. For contrast, Fig. 5.3 shows simulation of the same algorithm, but with linear identification model used. It is observed that controller utilizing the nonlinear model performs much better. As seen on the figures both these results were done on a simulation model that did not account for saturation of change rate of the elevator angle. If this phenomenon is included in the plant's dynamics both controllers sustain undesirable oscillation. This was probably caused by lower maneuverability with rate saturation and by inadequate modelling of saturation with the model (5.2)-(5.4) which includes only terms linear in control. A possible remedy is to take into consideration the rate limitations in calculation of control value. Also for higher maneuverability both thrust magnitude and thrust direction ought to be included as control signals. This will require a little more involved

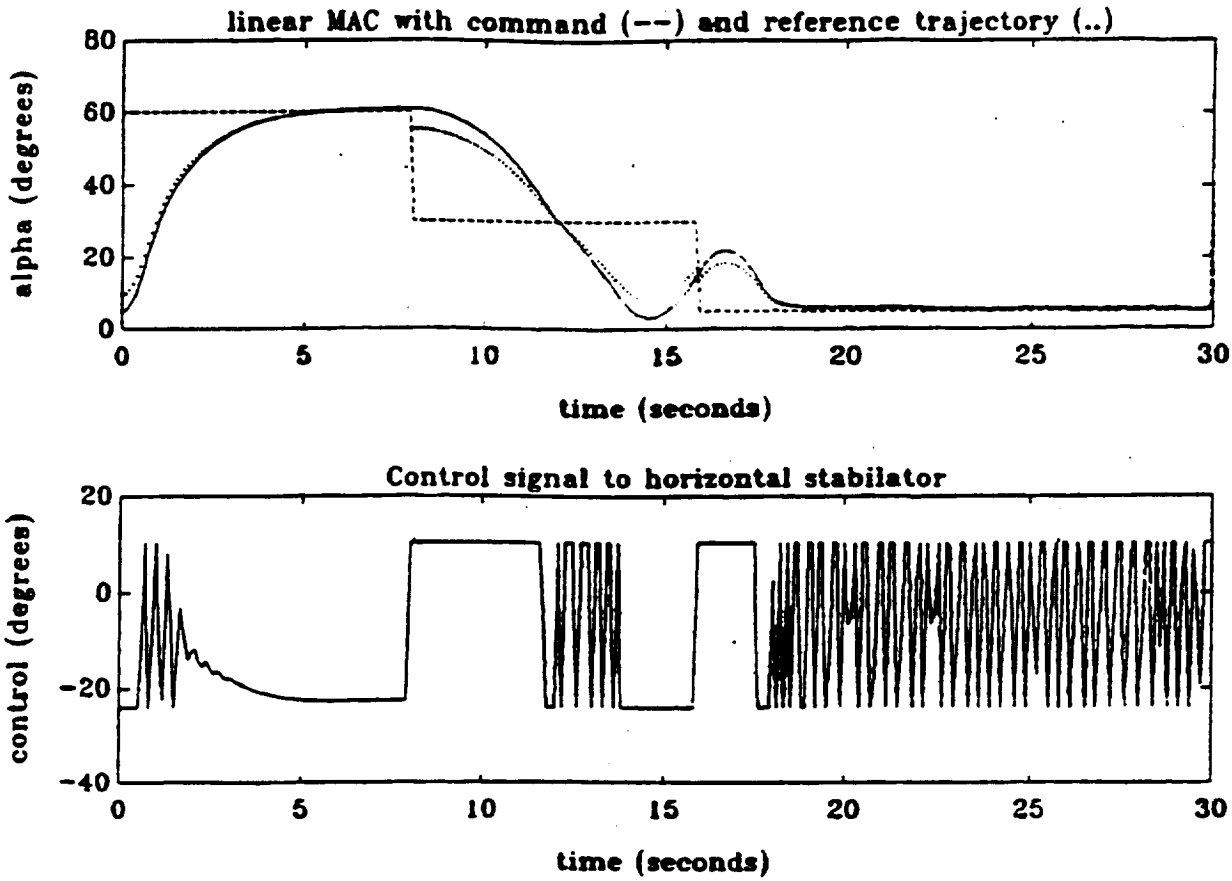

Figure 1. Response for Linear MAC

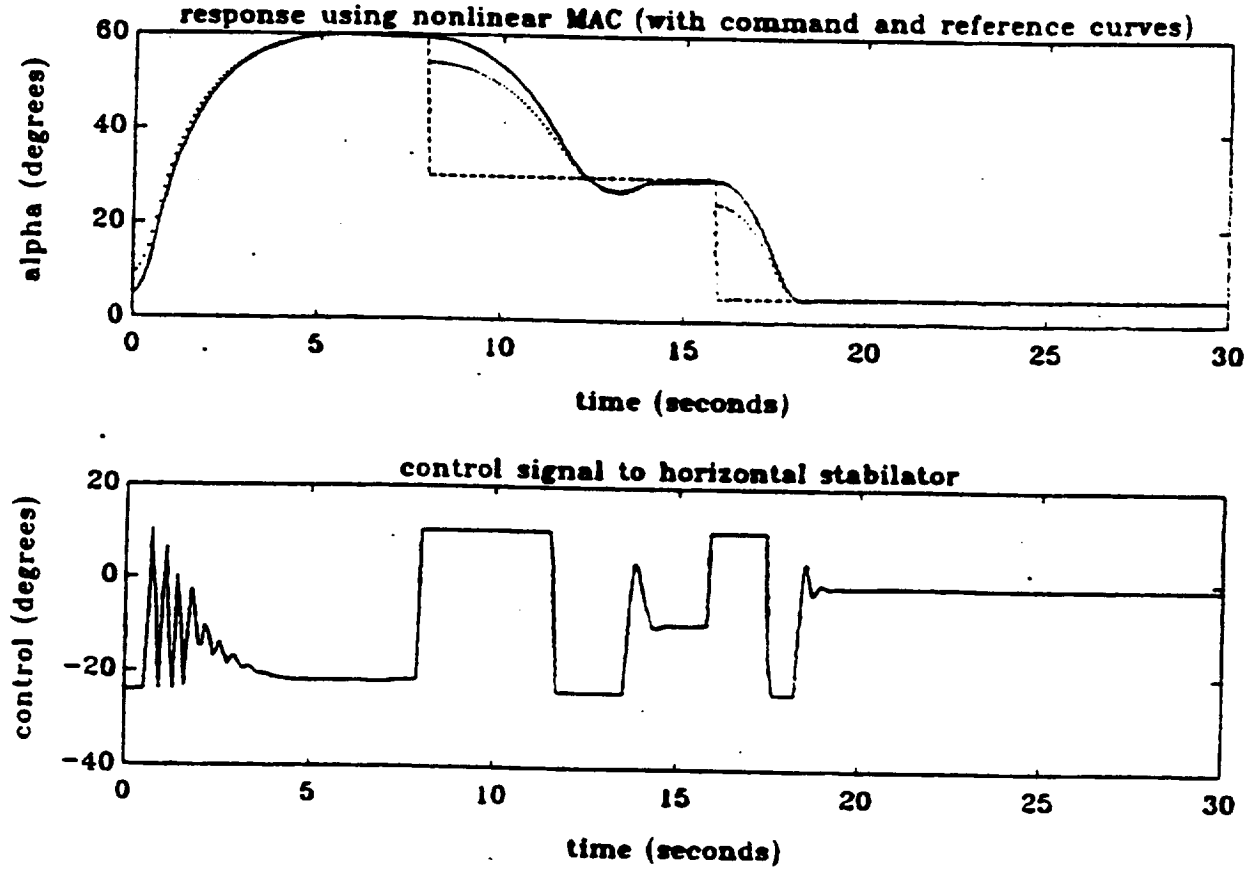

Figure 2. Response for Nonlinear MAC

calculations for minimization of (5.18), which will become a three-dimensional optimization problem with constraints. These problems are addressed in Sections 3, 4, 6, and 7.

5.4. References

[5.1] S.A. Billings and W.S.F. Voon, "Least Squares Parameter Estimation Algorithms for Non-Linear Systems," *Int. J. Systems Sci.*, Vol. 15, 601-615, 1984.

[5.2] S. Chen and S.A. Billings, "Representations of Non-Linear Systems — The NARMAX Model," *Int. J. Control*, Vol. 49, 1013-1032, 1989.

[5.3] G.C. Goodwin and K.S. Sin, *Adaptive Filtering, Prediction and Control*, Englewood Cliffs: Prentice Hall, 1984.

[5.4] R. Haber and H. Unbehauen, "Structure Identification of Nonlinear Dynamic Systems — A Survey of Input/Output Approaches," *Automatica*, Vol. 26, 651-677, 1990.

[5.5] K. Harris, "Properties of Nonlinear Model Algorithmic Control," *Proc. 24th IEEE Conf. Decision Contr.*, 1985, pp. 663-665.

[5.6] K.R. Sales and S.A. Billings, "Self-Tuning Control of Non-Linear ARMAX Models," *Int. J. Control*, Vol. 51, 753-769, 1990.

6. BILINEAR AND LINEAR ADAPTIVE CONTROL

6.1 Concept

This section describes the design of an adaptive controller for a high performance highly maneuverable aircraft over flight regimes including very high angles of attack. The purpose for adaptive control is to provide a mechanism to account for unknown changes in the system dynamics that is to be controlled. The goal of traditional adaptive control is to use concepts from linear theory to control an aircraft over a highly nonlinear flight regime. Adaptive control for a small class of nonlinear and time varying system is investigated in [6.14,6.15,6.30,6.37]. Model reference adaptive control usually includes system identification. Also, a model system may generate a desired reference trajectory. Then, a controller uses this information to calculate a command signal such that the output of the system follows the reference trajectory. A block diagram of such model reference adaptive controller is shown in Figure 6.1. Two important elements have to be developed for an effective adaptation routine. Here, a class of prediction models is selected first. The prediction model approximates the dynamics of the system, and it has parameters that can be modified by an estimator. The estimator is the second part of the adaptation. It estimates the values of the parameters to improve the prediction model. The simplest class of prediction models are those that are linear in parameters. In this project, each model of linear, bilinear, and nonlinear prediction models were checked for control performance. The most common estimation algorithm for such models is the recursive least squares algorithm to choose parameters to minimize the mean-square difference between the prediction model and actual system. The purpose of making the algorithm recursive is to allow for on-line identification of parameters.

The input reference model [6.8] is an intermediate step that allows the system to follow the command signal while meeting a variety of design criteria (for instance, rise time, overshoot, settling time, etc.). The control is calculated such that the system follows the reference trajectory, and such that the control signal remains within its constraints. Each block of the adaptive controller is described in the sections that follow.

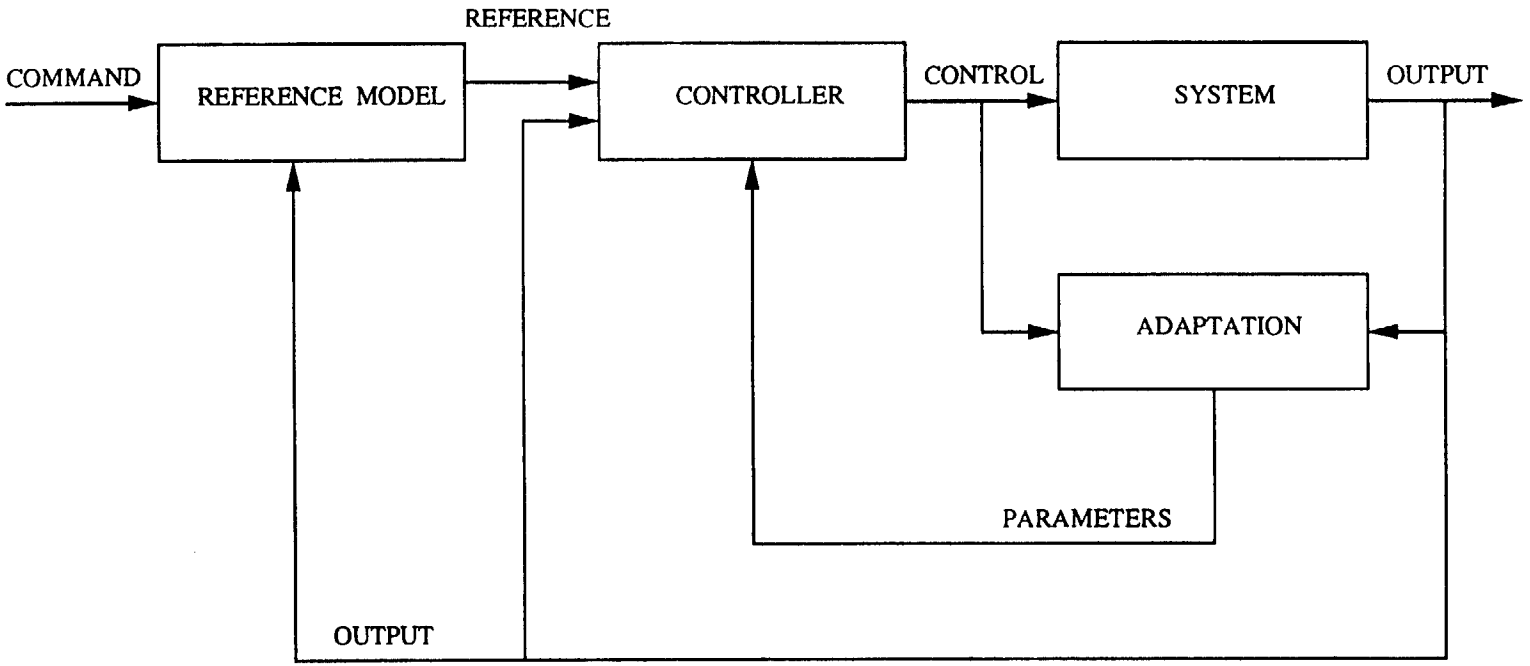

Figure 6.1 Block Diagram of Adaptive Control.

6.2 System Dynamics

The supermaneuverable aircraft dynamics described in this section is based on a modified version (HARV) of the F-18 aircraft. The controllers consist of the stabilator and thrust vectoring. The stabilator angle, an aerodynamic control input to the aircraft dynamics, is useful at normal flight conditions. The thrust vectoring is useful at high angle of attack, low dynamic pressure operating conditions, where the aerodynamic control effectiveness is inadequate. The aerodynamic coefficients are considered to be functions of the stabilator deflection as well as the angle of attack, Mach number, altitude, and pitch rate. The effects of leading edge flap, trailing edge flap, speed brake, landing gear, etc, are not considered. It is assumed that all simulations were to occur at a nominal constant altitude of 15000 feet. The longitudinal equations of motion are given in Appendix B.

The input dynamics were described by three states — thrust magnitude (T), thrust vectoring angle (δ_v), and stabilator angle (δ_h). The stabilator and the thrust vectoring dynamics include a velocity limiter of 40° per second for the stabilator angle, and 80° per second for the thrust vectoring angle [6.2]. The differential equations are stated below.

Stabilator Angle Dynamics:

$$\dot{\delta}_h = \begin{bmatrix} -40 & \left(\delta_{h_{cmd}} - \delta_h\right) < \frac{-4}{3} \\ 30\left(\delta_{h_{cmd}} - \delta_h\right) & \frac{-4}{3} \le \left(\delta_{h_{cmd}} - \delta_h\right) \le \frac{4}{3} \\ 40 & \left(\delta_{h_{cmd}} - \delta_h\right) > \frac{4}{3} \end{bmatrix} \tag{6.1}$$

The magnitude of the stabilator angle is limited according to the following equation.

$$-24.0° \le \delta_h \le 10.5° \tag{6.2}$$

Thrust Vectoring Dynamics:

$$\dot{\delta}_v = \begin{cases} -80 & \left(\delta_{v_{cmd}} - \delta_v\right) < \frac{-8}{3} \\ 30\left(\delta_{v_{cmd}} - \delta_v\right) & \frac{-8}{3} \le \left(\delta_{v_{cmd}} - \delta_v\right) \le \frac{8}{3} \\ 80 & \left(\delta_{v_{cmd}} - \delta_v\right) > \frac{8}{3} \end{cases} \tag{6.3}$$

The magnitude of the thrust vectoring angle is limited according to the following equation.

$$-20° \le \delta_v \le 20° \tag{6.4}$$

Thrust Magnitude Dynamics:

$$\dot{T} = \left(T_{cmd} - T\right) \tag{6.5}$$

where T_{cmd} is command signal of the magnitude of thrust. The magnitude of thrust is limited according to the following equation.

$$0 \le T \le 18000 \text{ lbs} . \tag{6.6}$$

6.3 Prediction Model

Here we are interested in simply approximating the real system in order to synthesize an effective adaptive control in real time. Modeling is important since the choice of model is often the first step toward the prediction or control of a process. An appropriately chosen model structure can greatly simplify the parameter estimation procedure and facilitate the design of prediction and control algorithms for the process.

6.3.1 Class of Models

System models can be developed by two distinct methods. Analytical modeling consists of a systematic application of basic physical laws to system components and the interconnection of these components. Experimental modeling, or modeling by synthesis, is the selection of mathematical relationships which seem to fit observed input-output data. Experimental modeling is emphasized in this section.

Experimental models can be described by state-space, difference-operators, autoregressive moving average models [6.15], etc. In this section, we discuss the difference-operator representation among several approaches. Generally, state-space models can be generated as a set of first-order difference equations. An alternative description is to use a high-order difference equation with an appropriate difference-operator representation. In order to describe these models in a succinct manner, we introduce the forward and backward shift operator q and q^{-1}. If y(t) denotes the value of the sequence {y(t)} at time t, where $t \in \{0,1,...\}$, then qy(t) denotes the value of the sequence at time (t+1), and q^{-1} y(t) denotes the value of the sequence at time (t-1). That is,

$$qy(t) = y(t+1) \quad \text{for } t \geq 0 \tag{6.7}$$

$$q^{-1}(t) = y(t-1) \quad \text{for } t \geq 1 \; ; \qquad q^{-1}y(0) = 0 \tag{6.8}$$

and consequently,

$$q^{i}y(t) = y(t+i) \quad \text{for } t \geq 0 \tag{6.9}$$

$$q^{-i}y(t) = y(t-i) \quad \text{for } t \geq i \; ; \qquad q^{-i}y(0) = 0 \quad \text{for } 0 \leq t < i \tag{6.10}$$

The first approach is to simply assume that the model can be adequately described by a linear time-varying system.

A linear time varying system can be described by the equation

$$A(q^{-1},t)\,y(t) = B(q^{-1},t)\,u(t) \tag{6.11}$$

where $A(q^{-1},t)$ and $B(q^{-1},t)$ are time varying polynomials of q^{-1}. $A(q^{-1},t)$, without loss of generality, is assumed to be monic. Thus, $A(q^{-1},t)$ could be described by the equation below.

$$A(q^{-1},t) = 1 + a_1(t)\,q^{-1} + a_2(t)\,q^{-2} + a_3(t)\,q^{-3} + \ldots + a_n(t)\,q^{-n} \tag{6.12}$$

This leads to a simple prediction model with the following form:

$$\hat{y}(t) = \Phi(t)^T\,\hat{\theta}(t) \tag{6.13}$$

$$\Phi(t)^T = [y(t-1), y(t-2), \ldots, y(t-n), u(t-1), u(t-2), \ldots, u(t-m)] \tag{6.14}$$

$$\hat{\theta}(t)^T = [-a_1(t), -a_2(t), \ldots, a_n(t), b_1(t), b_2(t), \ldots, b_m(t)] \tag{6.15}$$

The second approach is to simply assume that the model can be adequately described by a bilinear time-varying system.

A bilinear time-varying system can be described by the equation below [6-7,6-29],

$$y(t) = \sum_{i=1}^{m_y} a_i\,y(t-i) + \sum_{i=1}^{m_z} b_i\,u(t-i) + \sum_{i=1}^{m_y}\sum_{j=1}^{m_z} c_{ij}\,y(t-i)\,u(t-j) \tag{6.16}$$

where m_y, m_z, are the orders of the output and input.

This leads to a simple prediction model with the following form:

$$\hat{y}(t) = \Phi(t)^T\,\hat{\theta}(t) \tag{6.17}$$

$$\begin{aligned}\Phi(t)^T = \big[&y(t-1), y(t-2), \ldots, y(t-m_y), u(t-1), u(t-2), \ldots, u(t-m_z),\\ &y(t-1)\,u(t-1), y(t-2)\,u(t-1), \ldots, y(t-m_y)\,u(t-m_z)\big]\end{aligned} \tag{6.18}$$

The third approach is to simply assume that the model can be adequately described by a nonlinear time-varying system.

Input-output descriptions that expand the current output in terms of past inputs and outputs provide models that represent a broad class of nonlinear systems.

A nonlinear time varying system can be described by the equation below [6.6],

$$y(t) = F_G\left(y(t-1), y(t-2), \ldots, y(t-n_y), u(t-1), u(t-2), \ldots, u(t-n_z)\right) \tag{6.19}$$

where $F_G(\cdot)$ is some nonlinear function, is about as far as one can go in terms of specifying a general finite nonlinear system. Model (6.19) is referred to as a NARMAX (nonlinear ARMAX) model.

6.3.2 Aircraft Prediction Model

As can be seen from Section 6.3.1, several different approaches exist to formulate a prediction model for a nonlinear system.

First, a linear aircraft prediction model for aircraft is considered as follows:

$$\hat{\alpha}(t+1) = \Phi(t)^T \hat{\theta}(t-1) \tag{6.20}$$

$$\begin{aligned}\Phi(t)^T = \big[&\alpha(t-1), q(t-1), \alpha(t-2), q(t-2), \alpha(t-3), q(t-3), \delta_h(t), \\ &\delta_v(t), \delta_h(t-1), \delta_v(t-1), \delta_h(t-2), \delta_v(t-2)\big]\end{aligned} \tag{6.21}$$

Second, a bilinear aircraft prediction model for aircraft is given by

$$\hat{\alpha} = \Phi(t)^T \hat{\theta}(t-1) \tag{6.22}$$

$$\begin{aligned}\Phi(t)^T = \big[&\alpha(t-1), q(t-1), \alpha(t-2), q(t-2), \alpha(t-3), q(t-3), \delta_h(t), \\ &\delta_v(t), \delta_h(t-1), \delta_v(t-1), \delta_h(t-2), \delta_v(t-2), \\ &\alpha(t-1)\,\delta_h(t), \alpha(t-2)\,\delta_h(t-1), \alpha(t-3)\,\delta_h(t-2), \alpha(t-1)\,\delta_v(t)\big]\end{aligned} \tag{6.23}$$

Third, a nonlinear aircraft prediction model is considered as follows:

$$\hat{\alpha} = \Phi(t)^T \hat{\theta}(t-1) \tag{6.24}$$

$$\begin{aligned}\Phi(t)^T = [&\alpha(t-2),\ q(t-2),\ \alpha(t-3),\ q(t-3),\ \alpha(t-4),\ q(t-4),\ \delta_h(t-1),\\ &\delta_v(t-1),\ \delta_h(t-2),\ \delta_v(t-2),\ \delta_h(t-3),\delta_v(t-3),\ \alpha(t-2)\,\delta_h(t-1),\\ &\alpha(t-3)\,\delta_h(t-2),\ \alpha(t-2)\,q(t-2),\ \alpha(t-2)\,q(t-2),\ \delta_v(t-1)\,\alpha(t-2),\\ &\delta_v(t-2)\,\alpha(t-3),\ \alpha^2(t-2),\ \alpha^2(t-3),\ \alpha^3(t-2),\ \alpha^2(t-2)\,q(t-2),\\ &\alpha^2(t-2)\,\delta_h(t-1),\ \delta_v(t-1)\,\alpha^2(t-2)]\end{aligned} \tag{6.25}$$

6.3.3 Parameter Estimation

Overview of the Recursive Least Squares Algorithm

The recursive-least-squares (RLS) algorithm is the most popular on-line parameter estimation algorithm which is the minimization of

$$J_N = \frac{1}{N}\sum_{t=1}^{N} \lambda^{N-t}\left[y(t) - \hat{\theta}^T\phi(t)\right]^2 \tag{6.26}$$

The problem is to obtain model parameter estimates which,in a least squares sense, minimize the difference between the actual output, y(t), and its value predicted by the model. The vector contains past input and output values and its dimension depends on the order of the model to be estimated. This leads to the recursive least squares algorithm with a variable forgetting factor. The parameter vector update law is given by

$$\hat{\theta}(t) = \hat{\theta}(t-1) + K(t)\left[y(t) - \hat{\theta}(t-1)^T\,\phi(t)\right] \tag{6.27}$$

and the gain update by

$$K(t) = \frac{P(t-1)\,\phi(t)}{\lambda + \phi(t)^T P(t-1)\,\phi(t)} \tag{6.28}$$

Covariance matrix update:

$$P(t) = \frac{1}{\lambda}\left[P(t-1) - \frac{P(t-1)\,\phi(t)\,\phi(t)^T P(t-1)}{\lambda + \phi(t)^T P(t-1)\,\phi(t)}\right] . \tag{6.29}$$

The basic RLS algorithm with $\lambda = 1$ has several important properties. First the least squares algorithm has a fast convergence rate (exponentially fast for a linear time invariant system with proper excitation). Also, the stability of the RLS algorithm combined with direct and indirect adaptive control is well understood and many proofs have been published in this area [6.5,6.15,6.20].

The main disadvantage with basic RLS is that the covariance matrix gradually decays to a small value and therefore the algorithm does not retain its adaptivity to adequately track time-varying systems. The covariance matrix in the RLS algorithm tends towards zero which causes the adaptation to turn off. This is undesirable in the case where the parameters are time varying. Several modifications have been made to the RLS algorithm to correct this problem. A variety of modifications are proposed in the literature to keep the algorithm awake. The modifications in general are of two different types. The first idea is the inclusion of the forgetting factor. The second type of modifications that have been proposed is to manipulate the covariance matrix directly. Modification of the covariance matrix approach is considered in the following section.

Constant Covariance

An approach proposed by Goodwin in [6.15], is to maintain a constant covariance by the addition of a properly scaled identity matrix. This leads to the following algorithm.

$$P'(t) = \left[I - K(t)\,\phi(t)^T\right]\frac{P(t-1)}{\lambda(t)} \tag{6.30}$$

Let τ = trace $(P'(t))$, and C_0, C_1 denote two positive constants such that $C_1 > C_0$.

IF $\tau > C_0$

$$P(t) = P'(t) + \frac{C_1 - \tau}{n} I \tag{6.31}$$

IF $\tau \leq C_0$

$$P(t) = \frac{C_0}{\tau} P'(t) + \frac{C_1 - C_0}{m} I \tag{6.32}$$

The algorithm ensures a constant trace of C_1, and the following bounds are placed of the eigenvalues of P(t).

$$\frac{C_1 - C_0}{m} \leq \lambda[P(t)] \leq C_1 \tag{6.33}$$

Covariance Regularization

The basic idea of updating is a combination of a covariance resetting feature and a guarantee of lower and upper bounds on the covariance matrix. This algorithm replaces equation (6.29) by:

$$P'(t) = \left[I - K(t)\,\phi(t)^T\right] \frac{P(t-1)}{\lambda(t)} \tag{6.34}$$

$$P(t) = \left[1 - \frac{C_0}{C_1}\right] P'(t) + C_0 I \tag{6.35}$$

where C_0, C_1 denote two strictly positive constants such that $C_1 > C_0$.

This modification maintains the following bound on the eigenvalues of the covariance.

$$C_0 \leq \lambda[P(t)] \leq C_1 \tag{6.36}$$

Its performance was reasonable, but the best results were obtained by combining the matrix regularization with the constant covariance. This resulted in the following algorithm.

Let τ = trace (P'(t)), C_0, C_1 denote two positive constants such that $C_1 > C_0$, and $0 < C_2 < 1$

IF $\tau > C_0$

$$P(t) = C_2 P'(t) + \frac{C_1 - C_2 \tau}{n} I \tag{6.37}$$

IF $\tau \leq C_0$

$$P(t) = \frac{C_0}{\tau} \tau P'(t) + \frac{C_1 - C_0}{m} I \tag{6.38}$$

One way to interpret this algorithm is that it is a combination of the constant covariance and the covariance resetting.

6.4 Control Calculation

The controller was designed to perform or meet several goals. First and most importantly the control values are calculated such that the angle of attack of the aircraft follows the reference model. The control values were also calculated such that the thrust vectoring would return to zero if it were no longer needed, and a certain amount of smoothness was desired for the control signals. The following cost function was minimized at each step.

$$\begin{aligned} J = {} & \frac{1}{2}\rho_1\left[\alpha_{ref}(t+1) - \hat{\alpha}(t+1)\right]^2 + \frac{1}{2}\rho_2\left[\delta_{h_{cmd}}(t) - \delta_{h_{cmd}}(t-1)\right]^2 \\ & + \frac{1}{2}\rho_3\left[\delta_{v_{cmd}}(t) - \delta_{v_{cmd}}(t-1)\right]^2 + \frac{1}{2}\rho_4\left[\delta_{v_{cmd}}(t)\right]^2 \end{aligned} \tag{6.39}$$

6.4.1 One Step Ahead Predictor Controller

Let the prediction model in equation (6.13) be described by,

$$\hat{\alpha}(t+1) = a\,\delta_{h_{cmd}}(t) + b\,\delta_{v_{cmd}}(t) + \bar{\phi}(t)^T \bar{\theta}(t-1) \tag{6.40}$$

$$\phi(t) = \left[\delta_{h_{cmd}} \quad \delta_{v_{cmd}} \quad \bar{\phi}(t)\right] \tag{6.41}$$

$$\theta(t-1)^T = \left[a(t-1)\ b(t-1)\ \bar{\theta}(t-1)^T\right] \tag{6.42}$$

Taking the derivative of J with respect to the control gives

$$\begin{aligned}
\frac{dJ}{d\,\delta_{h_{cmd}}} &= \rho_1\left[\alpha_{ref}(t+1) - \hat{\alpha}(t+1)\right](-a) + \rho_2\left[\delta_{h_{cmd}}(t) - \delta_{h_{cmd}}(t-1)\right] \\
\frac{dJ}{d\,\delta_{v_{cmd}}} &= \rho_1\left[\alpha_{ref}(t+1) - \hat{\alpha}(t+1)\right](-b) + \rho_3\left[\delta_{v_{cmd}}(t) - \delta_{v_{cmd}}(t-1)\right] \\
&\quad + \rho_4\left[\delta_{v_{cmd}}(t)\right]
\end{aligned} \tag{6.43}$$

This control yields the following:

$$\begin{bmatrix} \delta_{h_{cmd}}(t) \\ \delta_{v_{cmd}}(t) \end{bmatrix} = \begin{bmatrix} \rho_1 a^2 + \rho_2 & \rho_1 a b \\ \rho_1 a b & \rho_1 b^2 + \rho_3 + \rho_4 \end{bmatrix}^{-1} \begin{bmatrix} \rho_1 a \eta + \rho_2 \delta_{h_{cmd}}(t-1) \\ \rho_1 b \eta + \rho_3 \delta_{v_{cmd}}(t-1) \end{bmatrix} \tag{6.44}$$

where

$$\eta = \alpha_{ref} - \bar{\phi}(t)^T \bar{\theta}(t-1) \tag{6.45}$$

To include the velocity and magnitude limits in the control calculation two extra conditions are added. The first condition requires that $\delta_{v_{cmd}}(t)$ be recalculated if $\delta_{h_{cmd}}(t)$ has reached the magnitude limit. The second condition requires that $\delta_{v_{cmd}}(t)$ be recalculated if $\delta_{h_{cmd}}(t)$ is a value requiring 80° per second. $\delta_{v_{cmd}}(t)$ is recalculated as follows:

$$\delta_{v_{cmd}}(t) = \frac{\eta - a\,\delta_{h_{cmd}}(t)}{b} \tag{6.46}$$

After the control values have been calculated they are limited by 40° per second for $\delta_{h_{cmd}}(t)$ and by 80° per second for $\delta_{v_{cmd}}(t)$.

6.5 COMPUTATION

6.5.1 Models

In design of real systems, there exist some restrictions to be considered because of physical properties. For example, the input dynamics are described by three states-thrust magnitude, thrust vectoring angle, and stabilator angle. All of these have the limitations noted in Section 6.2.2.

The linear prediction model is rewritten as follows:

$$\hat{\alpha}(t+1) = b_0(t-1)\,\delta_{h_{cmd}}(t) + b_1(t-1)\,\delta_{v_{cmd}}(t) + \bar{\Phi}(t)^T\,\bar{\theta}(t-1) \tag{6.47}$$

$$\begin{aligned}\bar{\Phi}(t)^T = \big[&\alpha(t-1),\, q(t-1),\, \alpha(t-2),\, q(t-2),\, \alpha(t-3),\, q(t-3),\\ &\delta_{h_{cmd}}(t-1),\, \delta_{v_{cmd}}(t-1),\, \delta_{h_{cmd}}(t-2),\, \delta_{v_{cmd}}(t-2)\big]\end{aligned} \tag{6.48}$$

$$\theta(t-1)^T = \left[b_0(t-1)\;\; b_1(t-1)\;\; \bar{\theta}(t-1)^T\right] \tag{6.49}$$

$$\phi(t)^T = \left[\delta_{h_{cmd}}(t)\;\; \delta_{v_{cmd}}(t)\;\; \bar{\Phi}(t)^T\right] \tag{6.50}$$

The bilinear prediction model becomes

$$\begin{aligned}\hat{\alpha}(t+1) = {} & b_{11}(t-1)\,\delta_{h_{cmd}}(t) + b_{12}(t-1)\,\delta_{h_{cmd}}(t)\,\alpha(t-1) + b_{13}(t-1)\,\delta_{v_{cmd}}(t)\\ & + b_{14}(t-1)\,\delta_{v_{cmd}}(t)\,\alpha(t-1) + \bar{\Phi}(t)^T\,\bar{\theta}(t-1)\end{aligned} \tag{6.51}$$

$$\bar{\Phi}(t)^T = [\alpha(t-1),\ q(t-1),\ \alpha(t-2),\ q(t-2),\ \alpha(t-3),\ q(t-3),$$
$$\delta_{h_{cmd}}(t-1),\ \delta_{v_{cmd}}(t-1),\ \delta_{h_{cmd}}(t-2),\ \delta_{v_{cmd}}(t-2),$$
$$\alpha(t-2)\,\delta_{h_{cmd}}(t-1),\ \alpha(t-3)\,\delta_{h_{cmd}}(t-2)] \tag{6.52}$$

$$\hat{\theta}(t-1)^T = \left[b_{11}(t-1)\ b_{12}(t-1)\ b_{13}(t-1)\ b_{14}(t-1)\ \bar{\theta}(t-1)^T\right] \tag{6.53}$$

$$\phi(t)^T = \left[\delta_{h_{cmd}}(t)\ \delta_{h_{cmd}}(t)\,\alpha(t-1)\ \delta_{v_{cmd}}(t)\ \delta_{v_{cmd}}(t)\,\alpha(t-1)\ \bar{\Phi}(t)^T\right] \tag{6.54}$$

The nonlinear prediction model becomes

$$\hat{\alpha}(t+1) = c_{11}(t-1)\,\delta_{h_{cmd}}(t) + c_{12}(t-1)\,\delta_{h_{cmd}}(t)\,\alpha(t-1) + c_{13}(t-1)\,\delta_{h_{cmd}}(t)\,\alpha^2(t-1)$$
$$c_{14}(t-1)\,\delta_{v_{cmd}}(t) + c_{15}(t-1)\,\delta_{v_{cmd}}(t)\,\alpha(t-1) + c_{16}(t-1)\,\delta_{v_{cmd}}(t)\,\alpha^2(t-1)\,\bar{\Phi}(t)^T\,\bar{\theta}(t-1) \tag{6.55}$$

$$\bar{\Phi}(t)^T = [\alpha(t-1),\ q(t-1),\ \alpha(t-2),\ q(t-2),\ \alpha(t-3),\ q(t-3),\ \delta_h(t-1),$$
$$\delta_v(t-1),\ \delta_h(t-2),\ \delta_v(t-2),\ \alpha(t-1)\,\delta_h(t-1),\ \alpha(t-2)\,\delta_h(t-1),$$
$$\alpha(t-1)\,q(t-1),\ \alpha(t-2)\,q(t-2),\ \delta_v(t-1)\,\alpha(t-2)$$
$$\delta_v(t-2)\,\alpha(t-3),\ \alpha^2(t-2),\ \alpha^2(t-3),\ \alpha^3(t-2),\ \alpha^2(t-2)\,q(t-2)] \tag{6.56}$$

$$\hat{\theta}(t-1)^T = \left[c_{11}(t-1)\ c_{12}(t-1)\ c_{13}(t-1)\ c_{14}(t-1)\ c_{15}(t-1)\ c_{16}(t-1)\ \bar{\theta}(t-1)^T\right] \tag{6.57}$$

$$\phi(t)^T = \left[\delta_{h_{cmd}}(t)\ \delta_{h_{cmd}}(t)\,\alpha(t-1)\ \delta_{h_{cmd}}\,\alpha^2(t-1)\ \delta_{v_{cmd}}(t)\ \delta_{v_{cmd}}(t)\,\alpha(t-1)\ \delta_{v_{cmd}}\,\alpha^2(t-1)\ \bar{\Phi}(t)^T\right] \tag{6.58}$$

6.5.2 Identification and Control

This adaptation was performed using the modified RLS described in Section 6.2.3.3. The controller is calculated to minimize the cost function in equation (6.39) by

$$\begin{bmatrix} \delta_{h_{cmd}}(t) \\ \delta_{v_{cmd}}(t) \end{bmatrix} = \begin{bmatrix} \rho_1 a^2 + \rho_2 & \rho_1 a b \\ \rho_1 a b & \rho_1 b^2 + \rho_3 + \rho_4 \end{bmatrix}^{-1} \begin{bmatrix} \rho_1 a \eta + \rho_2 \delta_{h_{cmdt}} - 1 \\ \rho_1 b \eta + \rho_3 \delta_{v_{cmd}}(t-1) \end{bmatrix} \tag{6.59}$$

This leads to the following control law calculation:

$$\delta_{h_{cmd}}(t) = \frac{\delta_{h_{cmd}}(t-1)\left(b^2\rho_1\rho_2 + \rho_2\rho_3 + \rho_2\rho_4\right) + \left(a\eta - ab\delta_{v_{cmd}}(t-1)\rho_1\rho_3 + a\eta\rho_1\rho_4\right.}{b^2\rho_1\rho_2 + a^2\rho_1(\rho_3 + \rho_4) + \rho_2(\rho_3 + \rho_4)} \tag{6.60}$$

$$\delta_{v_{cmd}}(t) = \frac{\delta_{v_{cmd}}(t-1)\left(b^2\rho_1\rho_3 + \rho_2\rho_3\right) + \left(b\eta - ab\,\delta_{h_{cmd}}(t-1)\,\rho_1\rho_2\right.}{b^2\rho_1\rho_2 + a^2\rho_1(\rho_3 + \rho_4) + \rho_2(\rho_3 + \rho_4)} \tag{6.61}$$

where

$$\eta = \alpha_{ref} - \bar{\phi}(t)^T \bar{\theta}(t-1) \tag{6.62}$$

6.6 Simulation

Several different simulations were used to evaluate the model performance. Two cases of the results are described below. The first maneuver corresponds to the maneuver presented by Ostroff in [6.32]. The angle of attack is changed from 5°, to 60°, 35°, and back to 5° in 8 second intervals. In the second maneuver the angle of attack is changed rapidly from 5° to 85° for an extended period of time.

6.6.1 Simulation Data

In the case of the linear prediction model, the controlled maneuvers use $C_0 = 600$, $C_1 = 1200$, $C_2 = 0.98$, $\rho_1 = 100$, $\rho_2 = 0.001$, $\rho_3 = 0.001$, $\rho_4 = 0.001$.

In the bilinear prediction model, the first maneuver starts with $C_0 = 800$, $C_1 = 1600$, $C_2 = 0.98$, $\rho_1 = 92$, $\rho_2 = 0.0001$, $\rho_3 = 0.0099$, $\rho_4 = 0.0$.

For the second maneuver, the bilinear prediction model starts with $C_0 = 800$, $C_1 = 1600$, $C_2 = 0.98$, $\rho_1 = 89$, $\rho_2 = 0.07$, $\rho_3 = 0.00001$, $\rho_4 = 0.00044$.

In the nonlinear prediction model, both maneuvers start with $C_0 = 1200$, $C_1 = 2400$, $C_2 = 0.98$, $\rho_1 = 95$, $\rho_2 = 0.0001$, $\rho_3 = 0.01$, $\rho_4 = 0.0$.

6.7 Conclusions

The character of the response for the first maneuver in the linear prediction model, the bilinear prediction model, and the nonlinear prediction model is similar to the response reported by Ostroff in [6.32]. However, the adaptive controller provided a somewhat faster response. The angle of attack reached 55° in approximately 2.0 seconds while the variable gain approach in [6.31,6.32] reached 55° in just under 3.5 seconds. The time optimal control (with a limitation of 40° per second on the thrust vectoring) reached 55° in about 1.8 seconds [6.24]. In the case of maneuvers one and two, comparing the bilinear adaptive controller with the linear controller, we see that the response of the bilinear adaptive controller is slightly faster for given desired trajectories (60°, 35°, and 5°) and has a smaller oscillation at the terminal end. For the second maneuver, the bilinear controller held the angle of attack at 85° as the aircraft approached steady state.

6.8 REFERENCES

[6.1] J. Cao, F. Arret, E. Hoffman, and H. Stalford, "Analytical Aerodynamic Model of A High Alpha Research Vehicle Wind-Tunnel Model," NASA CR-187469, September, 1990.

[6.2] "Simulation Model Description of a Twin-Trail High Performance Airplane," NASA Langley Research Center.

[6.3] K.J. Astrom and B. Wittenmark, *Adaptive Control*, Addison Wesley, 1989.

[6.4] S. Bittanti, P. Bolzern, and M. Campi, "Adaptive Identification via Prediction-Error Directional-Forgetting Factor: Convergence Analysis," *Int. J. Control*, Vol. 50, 2407-2421, 1989.

[6.5] M.J. Chen and J.P. Norton, "Estimation Technique for Tracking Rapid Parameter Changes," *Int. J. Control*, Vol. 45, 1387-1398, 1987.

[6.6] S. Chen and S.A. Billings, "Representations of Nonlinear Systems: The NARMAX Model," *Int. J. Control*, Vol. 49, 1013-1032, 1989.

[6.7] S. Chen and S.A. Billings, "Recursive Prediction Error Parameter Estimator for Nonlinear Models," *Int. J. Control*, Vol. 49, 569-594, 1989.

[6.8] D.A. Collins, "Adaptive Model Reference Control of Highly Maneuverable High Performance Aircraft," M.S. Thesis, Oregon State University, 1993.

[6.9] G. Daviddov, A. Shavit, and T. Koren, "Estimation of Dynamical Varying Parameters by the Internal Model Principle," *IEEE Trans. Automat. Contr.*, Vol. 37, 498-503, 1991.

[6.10] I. Derese and E. Noldus, "Design of Linear Feedback Laws for Bilinear Systems," *Int. J. Control*, Vol. 31, 219-237, 1980.

[6.11] B. Etkin, *Dynamic of Atmospheric Flight*, John Wiley & Sons, 1972.

[6.12] E.B. Feng, J.S. Yu, and W.S. Jiang, "New Method for Predictive Controller Design for Bilinear System," *Int. J. Control*, Vol. 53, 97-111, 1991.

[6.13] W. Garrard, D. Enns, and S.A. Snell, "Nonlinear Feedback Control of Highly Maneuverable Aircraft," *Int. J. Control*, Vol. 56, 799-812, 1992.

[6.14] G.C. Gooddwin and E.K. Teoh, "Adaptive Control of a Class of Linear Time Varying Systems," *IFAC Adaptive System in Control and Signal Processing*, San Francisco, USA, 1-6, 1983.

[6.15] G.C. Goodwin and K.S. Sin, *Adaptive Filtering Prediction and Control*, Prentice Hall, 1984.

[6.16] P.O. Gutman, "Stabilizing Controllers for Bilinear Systems," *IEEE Trans. Automat. Contr.*, Vol. 26, 917-922, 1981.

[6.17] R. Haber and H. Unbehauen, "Structure Identification of Nonlinear Dynamic System — A Survey on Input/Output Approaches," *Automatica*, Vol. 26, 651-677, 1990.

[6.18] H. Kang, G. Vachtsevanos, and F.L. Lewis, "Lyapunov Redesign for Structural Convergence Improvement in Adaptive Control," *IEEE Trans. Trans. Automat. Contr.*, Vol. 35, 250-253, 1990.

[6.19] I.J. Leontaritis and S. Billings, "Input-Output Parametric Models for Nonlinear System, Part I: Deterministic Nonlinear Systems," *Int. J. Control*, Vol. 41, 303-328, 1985.

[6.20] L. Ljung, *System Identification: Theory for the User*, Prentice Hall, 1987.

[6.21] R. Longchamp, "Stable Feedback Control of Bilinear Systems," *IEEE Trans. Automat. Contr.*, Vol. 25, 302-305, 1980.

[6.22] R.R. Mohler, S. Cho, C.S. Koo, and R.R. Zakrzewski, Semi-Annual Report on "Nonlinear Stability and Control Study of Highly Maneuverable High Performance Aircraft," OSU-ECE Report NASA 9102, Corvallis, OR, August 1991.

[6.23] R.R. Mohler, S. Cho, C.S. Koo, and R.R. Zakrzewski, Semi-Annual Report on "Nonlinear Stability and Control Study of Highly Maneuverable High Performance Aircraft," OSU-ECE Report NASA 9202, Corvallis, OR, August 1992.

[6.24] R.R. Mohler, S. Cho, C.S. Koo, and R.R. Zakrzewski, Semi-Annual Report on "Nonlinear Stability and Control Study of Highly Maneuverable High Performance Aircraft," OSU-ECE Report NASA 9301, Corvallis, OR, February 1993.

[6.25] R.R. Mohler, S. Cho, C.S. Koo, and R.R. Zakrzewski, Semi-Annual Report on "Nonlinear Stability and Control Study of Highly Maneuverable High Performance Aircraft," OSU-ECE Report NASA 9302, Corvallis, OR, July 1993.

[6.26] R.R. Mohler, S. Cho, C.S. Koo, and R.R. Zakrzewski, Semi-Annual Report on "Nonlinear Stability and Control Study of Highly Maneuverable High Performance Aircraft," OSU-ECE Report NASA 9101, Corvallis, OR, February 1991.

[6.27] R.R. Mohler, *Bilinear Control Process*, Academic Press, 1973.

[6.28] R.R. Mohler, *Nonlinear Systems: V. 1, Dynamic and Control*, Prentice Hall, 1991.

[6.29] R.R. Mohler, *Nonlinear Systems: V. 2, Applications to Bilinear Control*, Prentice Hall, 1991.

[6.30] K.G. Nam and A. Arapostathis, "A Model Reference Adaptive Control Scheme for Pure-Feedback Nonlinear System," *IEEE Trans. Automat. Contr.*, Vol. 33, 803-811, 1988.

[6.31] A.J. Ostroff, "Superagility Application of Variable Gain Output Feedback Control Design Methodology," *NASA High Angle of Attack Technology Conference*, Hampton, VA, 1990.

[6.32] A.J. Ostroff, "Application of Variable-Gain Output Feedback for High Alpha Control," ASAA Paper No. 89-3576, *Guidance, Navigation and Control Con.*, Boston, 1989.

[6.33] A.J. Ostroff, "High-Alpha Application of Variable-Gain Output Feedback Control," *Journal of Guidance, Control, and Dynamics*, Vol. 15, 491-491, 1992.

[6.34] A.J. Ostroff, "Longitudinal-Control Design Approach for High-Angle-of-Attack Aircraft," NASA Technical Paper 3302, 1993.

[6.35] J.J.E. Slotine and W. Li, *Applied Nonlinear Control*, Prentice Hall, 1991.

[6.36] N.R. Sripada and D. Grant Fisher, "Improved Least Squares Identification," *Int. J. Control*, Vol. 46, 1889-1913, 1987.

[6.37] C. Wen and D.J. Hill, "Adaptive Linear Control of Nonlinear System," *IEEE Trans. Automat. Contr.*, Vol. 35, 1253-1257, 1990.

[6.38] B.E. Ydstie and R.W.H. Sargent, "Convergence and Stability Properties of an Adaptive Regulator with Variable Forgetting Factor," *Automatica*, Vol. 22, 749-751, 1986.

7. SLIDING MODE CONTROL

7.1 Concepts

Sliding-mode control (SMC) appeared in the Russian literature as early as 1930s and was further developed independently in Russia and the U.S.A. along with variable structure control (VSC) systems in the early sixties (e.g., [7-30,7-49]). VSC systems is a part of nonlinear control systems where the structure is not fixed but is varied as part of the control process, for example, by switching control-gain between two values according to some law.

The SMC typically uses a high-speed switching control law to make the state trajectory of the system approach a switching ("discontinuous") surface which is called the sliding surface and to remain on this sliding surface once the state trajectory intersects the surface, or at least for some desired period of time such as in handling state constraints.

Design of SMC consists of at least two main parts. One is the reaching mode, in which the state trajectory starting from anywhere on the state plane, is directed toward the sliding surface. The other part is the sliding-mode with the state trajectory on the sliding surface. For these two modes, we have to design the switching surface and control law for reachability and existence of a sliding-mode.

In general, discontinuous control is used and it is switched between two values near the sliding surface to satisfy the reachability condition. In the ideal case, the switching time of a sliding-mode is zero, but in reality fast switching of the control input causes the state trajectory to chatter along the sliding surface. This imperfection in the switching mechanism not only generates the undesirable high-frequency components in the state trajectory but also may excite unmodeled high-frequency system dynamics. Consequently, it could make the system unstable, and in many cases, chattering must be minimized. To reduce the effect of chattering by smoothing out discontinuous control, various investigators (e.g., see [7-46]) introduced a boundary layer near the sliding surface. The boundary is defined by the set $L(x) = \{x \mid \|s(x)\| \leq \epsilon, \epsilon > 0\}$ where ϵ is the thickness of the boundary layer and s is sliding surface.

Outside the boundary layer, control input is chosen such that attractiveness to the boundary layer is guaranteed. Inside the boundary, discontinuous input sgn(s) is replaced by $\{s(x)\}/\epsilon$.

Generally, there is a trade off between a fast response and overshoot in control design. However, SMC potentially can alleviate this trade off. If states are driven to a sliding surface and slide along it keeping the angle of attack at desired value as in Fig. 7-1, the state finally arrives at a desired point p without overshoot in an ideal sliding-mode control.

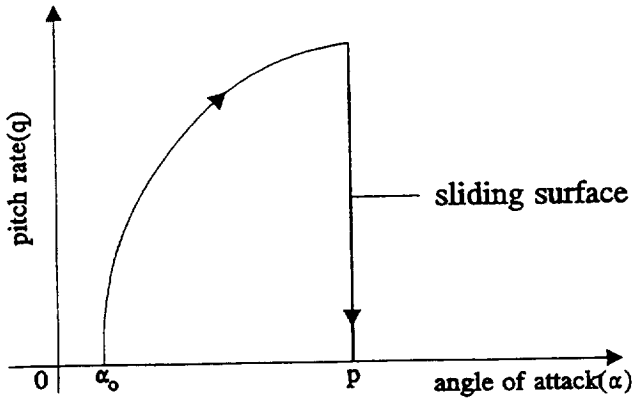

Fig. 7.1 Ideal sliding-mode control

If continuous sliding-mode control (CSMC) is used and the reachable speed is adjusted within a boundary layer the effect of chattering can be reduced and a better result can be obtained without overshoot. This nonlinear control law uses a sliding surface which is described in the form of the equation of error between actual output and desired output. This control law is then applied to the nonlinear longitudinal motion of a high performance and highly nonlinear aircraft, HARV (F-18), and as a result, the rise time can be reduced and the output reaches its final terminal point without overshoot. CSMC also shows some robustness to parameter uncertainty and to disturbances with given bounds.

7.2 Methodology

Usually, sliding-mode control with discontinuous input which includes the sgn(•) function induces chattering. To reduce the effect of chattering, a continuous control law is adopted. This continuous control law can be expanded to not only the decoupled input-output system but also to a multi-input multi-output system. Further more, it can be applied to systems with constraints of control by modification.

The main purpose of this control is for rapid maneuvers with large changes in angle of attack and to keep it at the final value while the aircraft is not trimmed. Here, only two controlled outputs — angle of attack α and pitch rate q will be selected. During this control, the thrust magnitude will be scheduled. The desired trajectories of angle of attack α and pitch rate q are selected so that pitch rate converges when angle of attack approaches its final terminal. The control scheme is composed of α-q control for rapid variation of α and α-control for settling α at its terminal value.

The control scheme will be described in detail for a difficult but representative maneuver for increasing(or decreasing) angle of attack rapidly between 5° and 60°. Of course, the same control, with appropriate simple algorithmic adjustment, is just as successful for general classes of maneuvers.

7.2.1 System Dynamics

The fifth-order longitudinal motion of the HARV (F-18) described in Appendix B can be represented simply by the state model:

$$\dot{\alpha} = f_1 + g_{11}\,\delta_e + g_{12}\,T_x + g_{13}\,T_z \tag{7.1}$$

$$\dot{q} = f_2 + g_{21}\,\delta_e + g_{22}\,T_x + g_{23}\,T_z \tag{7.2}$$

$$\dot{V} = f_3 + g_{31}\,\delta_e + g_{32}\,T_x + g_{33}\,T_z \tag{7.3}$$

$$\dot{\theta} = q \tag{7.4}$$

$$\dot{h} = V\sin(\gamma) \tag{7.5}$$

where

initial value $[\alpha_o\ q_o\ V_o\ \theta_o\ h_o] = [4.3°\ 0\ 4.3°\ 500\ 15000]$,

α : angle of attack (degree), q : pitch rate (degree/second), V : total speed (feet/sec),

θ : pitch angle (degree), δ_h : stabilator angle (degree), γ : climb angle (= θ-α),

h : altitude (feet), T_x : x-direction thrust magnitude (lbs), T_z : z-direction thrust magnitude (lbs), and δ_v : thrust angle (= $\tan^{-1}(T_z/T_x)$) (degree).

$$F = [f_1\ f_2\ f_3]^T \tag{7.6}$$

and

$$G = [G_1\ G_2\ G_3] = \begin{bmatrix} g_{11} & g_{12} & g_{13} \\ g_{21} & g_{22} & g_{23} \\ g_{31} & g_{32} & g_{33} \end{bmatrix} \tag{7.7}$$

are functions of angle of attack, pitch rate, speed, mach number and altitude through the corresponding stability derivatives.

Assumed limits of the stabilator angle and the thrust angle include those used in Section 3. Here, however, the admissible thrust angle constrained is 80°/sec. Since this was the most recent information available.

7.2.2 Design of Controller

While the control algorithm can be computered for any given flight path, an initial $\alpha_o = 4.3°$ and terminal $\alpha = 60°$ is discussed as typical end conditions.

The purpose of this CSMC is to drive the concerned states to a sliding-surface which is represented by errors between the concerned states and their desired states. For this, control inputs δ_h, δ_v, scheduled-thrust magnitude are used and all the states (α,q,θ,V,h) are feedbacked as shown in Fig. 7.2. The control scheme is composed of two parts. In the first stage, an α-q control scheme is used until the error e between the final terminal value α_{final} and α is less than some error e assumed to be 5°, that is, α arrives at nearly 55° while α and q follow the desired α_d and q_d. During this stage, stabilator angle, thrust angle and scheduled-thrust magnitude are used as control inputs.

Obviously, there is some trade off between α and q. Here, the major state-variable is angle of attack not pitch rate. Therefore, the α-q control scheme is changed to an α-control scheme when the error e between α_{final} and α is less than 5°. In this stage, a fast approach toward the sliding surface may bring out a big oscillation because of constraints of control inputs. Therefore, the reachable speed should be adjusted using error $e = \alpha_d - \alpha$ and time derivative of angle of attack, $\dot{\alpha}$, to make angle of attack approach its sliding surface slowly. During this stage, stabilator angle, thrust angle and scheduled-thrust magnitude are also used as control inputs.

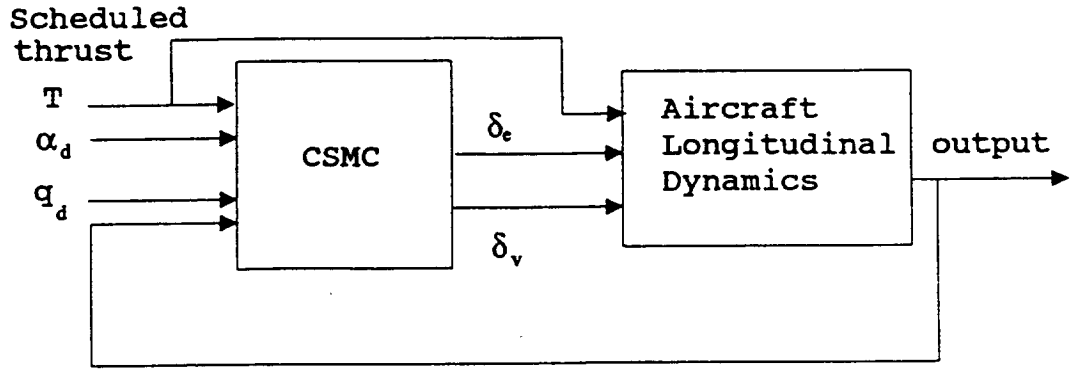

Figure. 7.2 Control structure of CSMC

α-q Control

Select an error sliding surface

$$s = \left[(\alpha - a_d)(q - q_d)(V - V_d)\right] = 0 \tag{7.8}$$

and the time derivative of it assuming that $V = V_d$ is given by

$$\dot{s} = \left[(\dot{\alpha} - \dot{\alpha}_d)(\dot{q} - \dot{q}_d)(\dot{V} - \dot{V}_d)\right] = [\dot{s}_1\ \dot{s}_2\ 0] = 0 \tag{7.9}$$

Algebraically, $\dot{s}$ can be separated as follows with $\dot{s}_3 = 0$

$$\dot{s} = (\dot{\alpha} - \dot{\alpha}_d) = (f_1 - \dot{\alpha}_d + g_{11}\,\delta_e + g_{12}\,T_x + g_{13}\,T_x) \tag{7.10}$$

$$\dot{s}_2 = \dot{q} - \dot{q}_d = (f_2 - \dot{q}_d + g_{21}\,\delta_e + g_{22}\,T_x + g_{23}\,T_x)\ . \tag{7.11}$$

The reachability condition takes the following expression:

$$s\dot{s}^T = s(F' + Gu) = sF' + sGu = sG\left[u + \frac{(sG)^T}{\|sG\|^2}\,sF'\right] \tag{7.12}$$

where

$u = [\delta_h\ T_z\ T_x]^T$, $\|\cdot\|$ is Euclidean vector norm,

$$G = [G_1\ G_2\ G_3] = \begin{bmatrix} g_{11} & g_{12} & g_{13} \\ g_{21} & g_{22} & g_{23} \\ g_{31} & g_{32} & g_{33} \end{bmatrix}$$

and

$$F' = \begin{bmatrix} F_1' \\ F_2' \\ F_3' \end{bmatrix} = \begin{bmatrix} (f_1 - \dot{\alpha}_d) \\ f_2 - \dot{q}_d \\ f_3 - \dot{V}_d \end{bmatrix} \tag{7.13}$$

If

$$u = -\frac{(sG)^T}{\|sG\|^2} sF' - K(sG)^T \tag{7.14}$$

then $s\dot{s}^T = -(sG)K(Sg)^T < 0$ where

$$K = \begin{bmatrix} k_1 & 0 & 0 \\ 0 & k_2 & 0 \\ 0 & 0 & k_3 \end{bmatrix}$$

is a positive definite matrix.

But $s\dot{s}^T$ can be modified for practical application with bounded control inputs such as

$$s\dot{s}^T = [M_1 \; M_2 \; M_3] \left[u + \frac{[M_1 \; M_2 \; M_3]^T}{M_1^2 + M_2^2 + M_3^2} sF' \right] = M[u + L] \tag{7.15}$$

where

$$SG = M = [M_1 \; M_2 \; M_3] \tag{7.16}$$

$$\|M\|^2 = M_1^2 + M_2^2 + M_3^2 \tag{7.17}$$

and

$$L = \begin{bmatrix} \frac{M_1 sF'}{\|M\|^2} \\ \frac{M_2 sF'}{\|M\|^2} \\ \frac{M_3 sF'}{\|M\|^2} \end{bmatrix} = \begin{bmatrix} L_1 \\ L_2 \\ L_3 \end{bmatrix} \tag{7.18}$$

$s\dot{s}^T$ is a function of δ_h and T_z because $T_x^2 = T^2 + T_z^2$

By equation (7.15)~(7.18), the reachability equation for the system (7.1)~(7.5) can be expressed by

$$\begin{aligned} s\dot{s}^T &= M_1(\delta_h + L_1) + M_2(T_z + L_2) + M_3(T_x + L_3) \\ &= M_1(\delta_h + L_1) + M_2(T_z + L_2) + M_3\left[\sqrt{T^2 - T_z^2} + L_3\right] \\ &= s\dot{s}_1(\delta_h) + s\dot{s}_2(T_z) \end{aligned} \tag{7.19}$$

That is, $s\dot{s}_1$ is a function of δ_h and $s\dot{s}_2$ is a function of T_z or δ_v.

The control scheme is composed of two parts to satisfy the sliding-surface reachability condition $s\dot{s}_1(\delta_h) < 0$ and $s\dot{s}_2(T_z) < 0$ separately.

At every step where sampling time $\Delta t = 0.03$, stabilator angle δ_h is constrained to the interval $[\delta_{hmin}, \delta_{hmax}]$ and T_z is constrained to the interval $[T_{zmin}, T_{zmax}]$ where $\delta_v = \tan^{-1}(T_z / T_x)$.

(1) Control for $s\dot{s}_1(\delta_h) < 0$

For $s\dot{s}_1(\delta_h) = M_1(\delta_h + L_1)$, if $\delta_h = -L_1 - k_1 M_1$ is selected where k_1 is a positive constant $s\dot{s}_1(\delta_h) < 0$ is satisfied.

Case 1: $-L_1 \notin [\delta_{hmin}, \delta_{hmax}]$ and $s\dot{s}_1 > 0$ or $s\dot{s}_1 < 0$ regardless of bounded input δ_h

If $-L_1$ is outside of $[\delta_{hmin}, \delta_{hmax}]$ one of δ_{hmin} and δ_{hmax} is selected to make α and q approach the error sliding surfaces as fast as possible considering the sign of M_1. That is, δ_{hmin} and δ_{hmax} is selected as inputs for $M_1 > 0$ and $M_1 < 0$, respectively.

Case 2: $-L_1 \in [\delta_{hmin}, \delta_{hmax}]$

We choose δ_h depending on the sign of M_1

$$\delta_h = -L_1 - k_1 M_1 = \frac{\delta_{hmin} - L_1}{2}, \qquad \text{if } M_1 > 0$$

and

$$\delta_h = -L_1 - k_1 M_1 = \frac{\delta_{hmax} - L_1}{2}, \qquad \text{if } M_1 < 0$$

such that the reachability condition $s\dot{s}^T < 0$ is satisfied.

After δ_h enters into the inside of the input bound, k_1 is calculated by

$$k_1 = \left| \frac{\delta_{hmin} + L_1}{2M_1} \right| \qquad \text{if } M_1 > 0$$

$$k_1 = \left| \frac{\delta_{hmax} + L_1}{2M_1} \right| \qquad \text{if } M_1 < 0$$

At the next step, k_1 is used in case that $-L_1$ is within the input bound. If k_1 is so large that δ_h is outside of $[\delta_{hmin}, \delta_{hmax}]$, k_1 is reset to some value by the above method again to make δ_h be within the input constraints satisfying $s\dot{s} < 0$.

(2) Control of $s\dot{s}_2(T_z) < 0$

At every step $T_z = T \sin(\delta_v)$ is bounded because δ_v is constrained to $[\delta_{vmin}, \delta_{vmax}]$ for $-(\pi/2\} \le \delta_v \le \pi/2$.

Case 1: $-L_2 \notin [T_{zmin}, T_{zmax}]$ and $s\dot{s}_2 > 0$ or $s\dot{s}_2 < 0$ regardless of T_z

One value is selected between T_{zmin} and T_{zmax} to make α and q approach their sliding surfaces.

Case 2: $-a \le s\dot{s}_2 \le b$ for T_z and $a,b > 0$

In this case,the reachability condition is $-a \le s\dot{s}_2 \le 0$. Therefore, the range of T_z to satisfy $-a \le s\dot{s}_2 \le 0$ is changed to $T_{z1} \le T_z \le T_{z2}$ where T_{z1} is T_z which satisfies one between $-a = s\dot{s}_2$ and $s\dot{s}_2 = 0$ and T_{z2} is T_z which satisfies the remained one.

The relation of T_{z1}, T_{z2}, T_{zmin} and T_{zmax} is $T_{zmin} \le T_{z1} \le T_z \le T_{z2} \le T_{zmax}$ because $T_z = T \sin(\delta_v)$ is increasing function for $-(\pi/2) \le \delta_v \le \pi/2$. The control input is calculated by the same method as that applied in case that $s\dot{s}_1 < 0$ with $T_z \in [T_{z1}, T_{z2}]$ which is given by

$$T_z = -L_2 - k_2 M_2 = \frac{T_{z1} - L_2}{2}, \qquad \text{if } M_2 > 0$$

$$T_z = -L_2 - k_2 M_2 = \frac{T_{z2} - L_2}{2}, \qquad \text{if } M_2 < 0$$

and different k_2 depending on the sign of M_2 which is given by

$$k_2 = \left| \frac{T_{z1} + L_2}{2M_2} \right| \qquad \text{if } M_2 > 0$$

$$k_2 = \left| \frac{T_{z2} + L_2}{2M_2} \right| \qquad \text{if } M_2 < 0$$

Case 3: Case that $s\dot{s}_2 < 0$ and $-L_2 \in [T_{zmin}, T_{zmax}]$

The above same method is used with $T_z \in [T_{zmin}, T_{zmax}]$.

This control scheme can be explained simply in flow chart as shown in Fig. 7.3. The control of $s\dot{s}_1$ $(\delta_h) < 0$ is depicted by Loop 1 in Fig. 7.4.

α-Control

The α-q control scheme is switched to α-control scheme when error $e = \alpha_{final} - \alpha$ between final terminal α_{final} and α is less than 5° for keeping angle of attack near its final terminal.

According to CSMC scheme, select the sliding surface $s = (\alpha - \alpha_d) = 0$.

The equation (7.1) can be expressed using thrust angle

$$\dot{\alpha} = f_1 + g_{11}\,\delta_h + g_{123}\sin(\alpha - \delta_v) \tag{7.20}$$

Using equation (7.20), the reachability condition is given by

$$s\dot{s} = s g_{11}\left[\delta_h + \frac{g_{11}}{|g_{11}|^2}\left(f_1 - \dot{\alpha}_d + g_{123}\sin(\alpha - \delta_v)\right)\right] \tag{7.21}$$

If

$$\delta_h = -\frac{g_{11}}{|g_{11}|^2}\left(f_1 - \dot{\alpha}_d + g_{123}\sin(\alpha - \delta_v)\right) - k_1\, s g_{11}$$

then $s\dot{s} = -k_1(s g_{11})^2 < 0$, where k_1 is a positive constant.

The equation (7.21) can not be applied directly because the control inputs - stabilator and thrust angle are bounded at every step as $\delta_{hmin} \le \delta_h \le \delta_{hmax}$ and $\delta_{vmin} \le \delta_v \le \delta_{vmax}$.

Let

$$l = \left[-\frac{g_{11}}{|g_{11}|^2}\left(f_1 - \dot{\alpha}_d + g_{123}\sin(\alpha - \delta_v)\right)\right] \tag{7.22}$$

Then, $s\dot{s} = s g_{11}(\delta_h - l)$ (7.23)

Here, the control purpose is to make the angle of attack approach its sliding surface slowly without big oscillation satisfying the reachability condition $s\dot{s} < 0$. For this, the reachable speed will be reduced slowly for some time, which means that $\dot{\alpha}$ is decreased satisfying $s\dot{s} < 0$. To adjust reachable speed, multiple boundary layers are set in the neighborhood of sliding surface and the reachable speed is adjusted in each boundary layer satisfying the reachability condition as follows:

- $|\text{error} = \alpha_{final} - \alpha| > 1°$: adjust reachable speed so that $\dot{\alpha} = \pm 0.1°/\Delta t$
- $0.2° < |\text{error} = \alpha_{final} - \alpha| \le 1°$: adjust reachable speed so that $\dot{\alpha} = \pm 0.01°/\Delta t$

Flow Chart

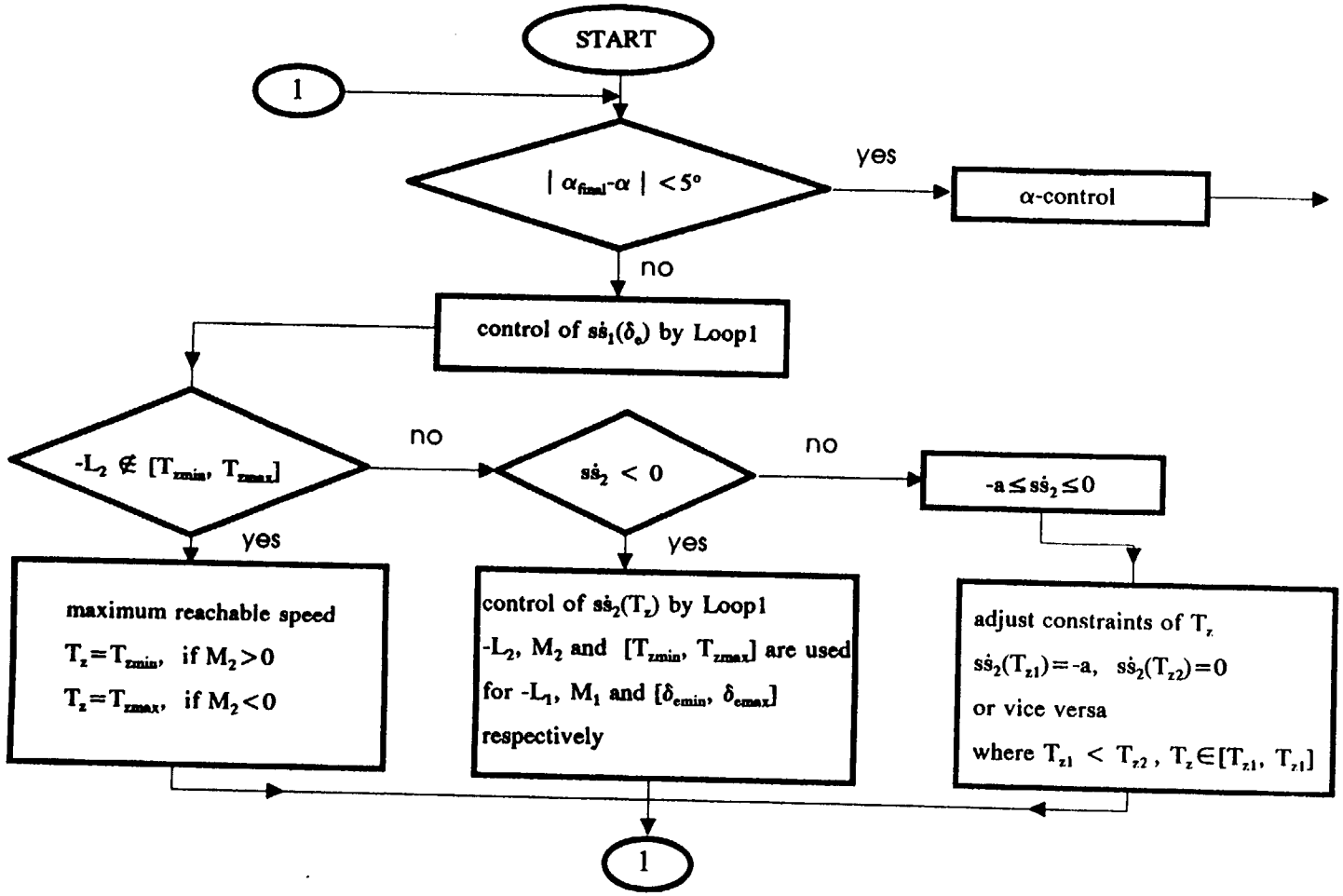

Figure 7.3 Flow chart of α-q control

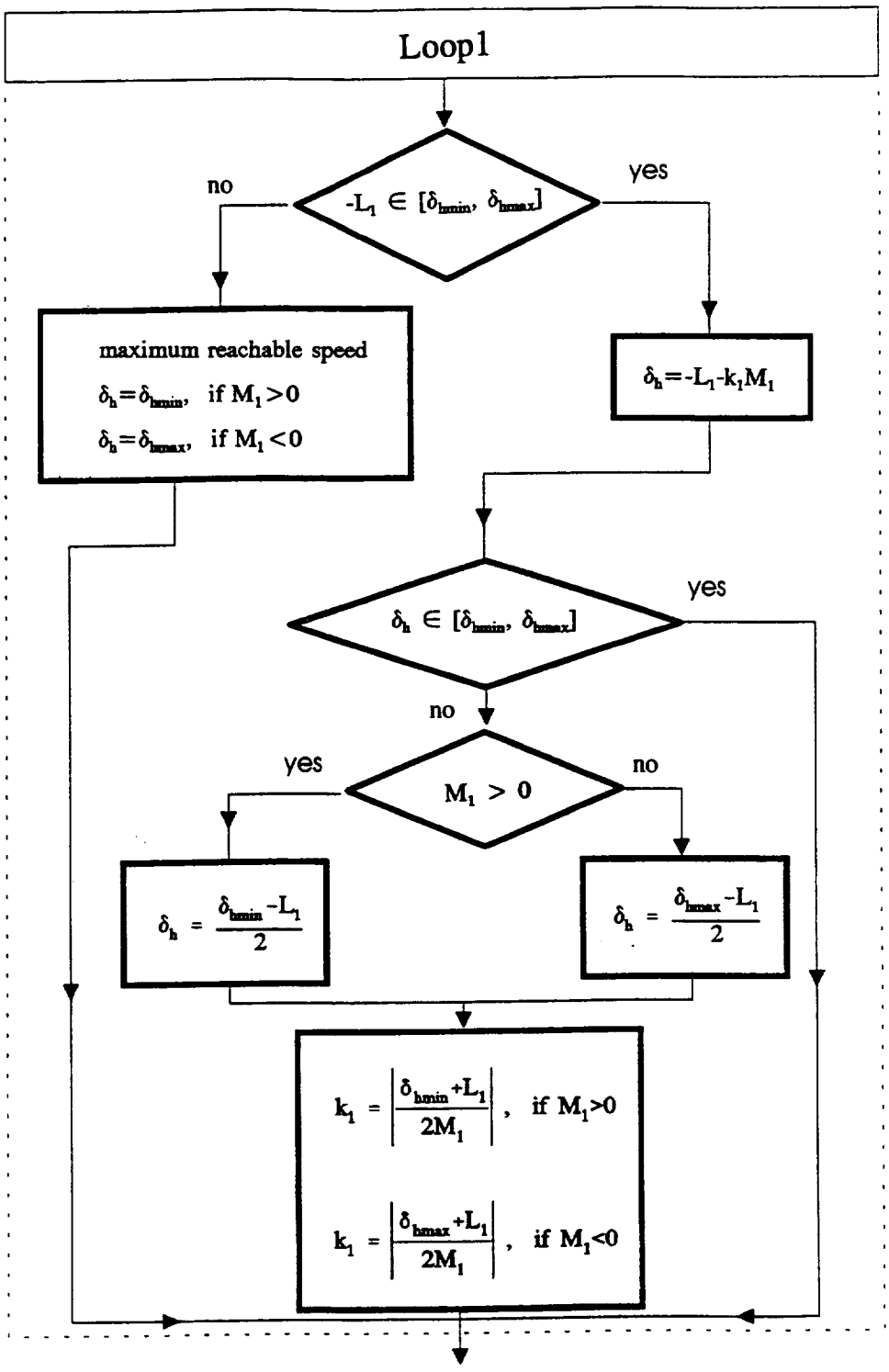

Figure 7.4 Flow chart of Loop1

- $0° \leq |\ \text{error} = \alpha_{final} - \alpha\ | \leq 0.2°$: adjust reachable speed so that $\dot{\alpha} = \pm 0.0001°/\Delta t$

where Δt (0.03 second) is sampling time.

When $\dot{\alpha}$ becomes zero approximately interval $[\delta_{hmin},\ \delta_{hmax}]$ enters into $[l_{min},\ l_{max}]$ or interval $[\delta_{hmin},\ \delta_{hmax}]$ intersects interval $[l_{min},\ l_{max}]$. From this time, the reachable speed of angle of attack can be adjusted linearly in time. α-control scheme is expressed simply by the flow chart in Fig. 7.5.

When the aircraft maneuvers from high angle of attack to low angle of attack the same method is applied except that angle of attack should be decreased with maximum speed by α-q control. For uncertain system, CSMC also can be applied by adjusting the reachable speed in the neighborhood of the sliding surface.

7.3 Simulation

CSMC scheme is applied to the MIMO system with constrained control inputs. In this case, desired trajectories have to be selected appropriately considering the characteristics of the system.

Scheduled thrust magnitude and desired trajectories of angle of attack and pitch rate for maneuvers from initial $\alpha = 4.3°$ to $\alpha = 60°$ and $\alpha = 60°$ to $\alpha = 5°$ have to be selected appropriately considering the system dynamics. Here, it is assumed that the pilot adjusts the scheduled thrust magnitude for the desired maneuver as shown in Fig. 7.6. $|T| = T_o = 1467.19$ lbs for 0.96 second and $|T|$ is increased linearly from T_o to 18000 lbs for $0.96 \leq t \leq 2.94$ sec, and it is kept at 18000 lbs after 2.94 second. Then thrust magnitude is kept at 18000 lbs to 7.98 second. After 7.98 second it is decreased linearly from 18000 lbs to 10234.584 lbs for $7.98 \leq t \leq 8.93$. Constant thrust $T = 10234.584$ is scheduled for $8.93 \leq t \leq 15.84$ second and for $15.81 \leq t \leq 16.65$ second, it is decreased linearly and finally reaches $T = 3000$ lbs.

The main purpose of this CSMC control is to control the angle of attack as fast as possible and keep it at some terminal value. After the rapid α-control phase, it is assumed that the pitch rate should approach zero.

The desired trajectories of angle of attack α and pitch rate q are selected as follows:

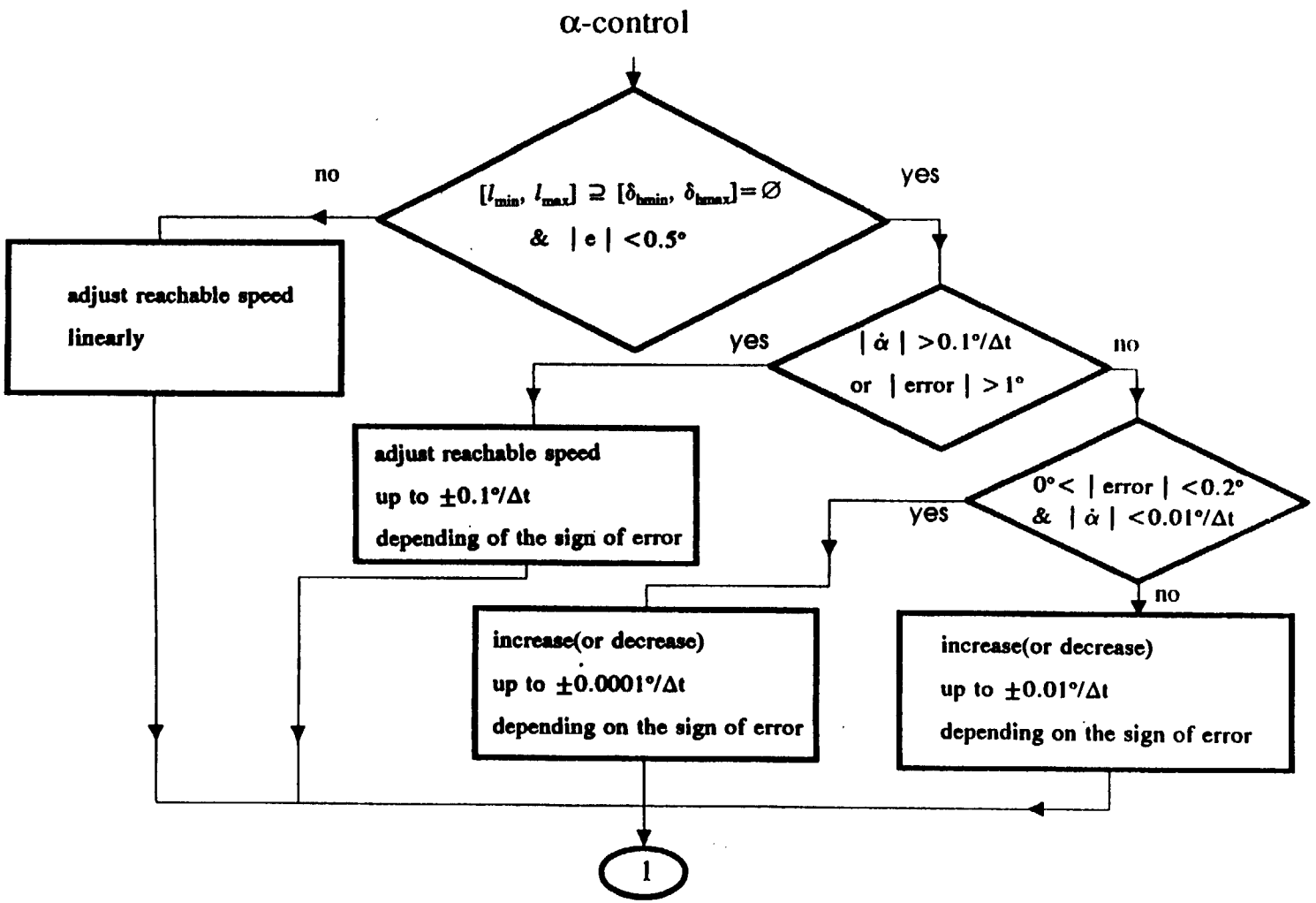

Figure 7.5 Flow chart of α-control

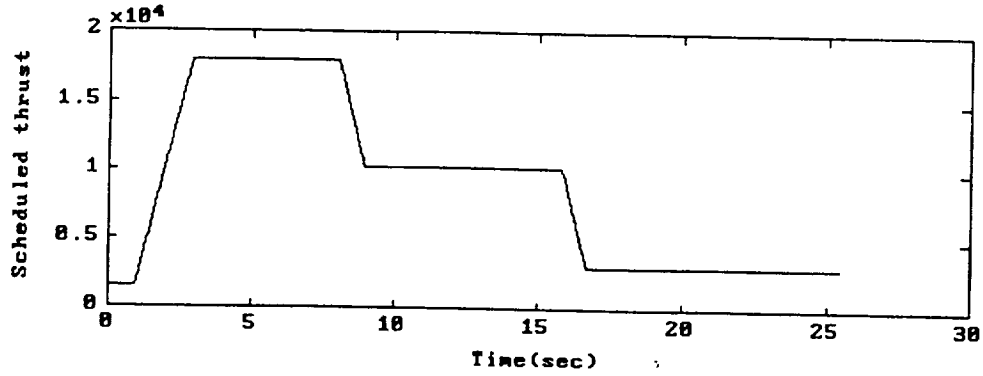

Figure 7.6 The scheduled thrust magnitude(lbs) of maneuver from α_o=4.3° to α=60° and from α=60° to α=5°

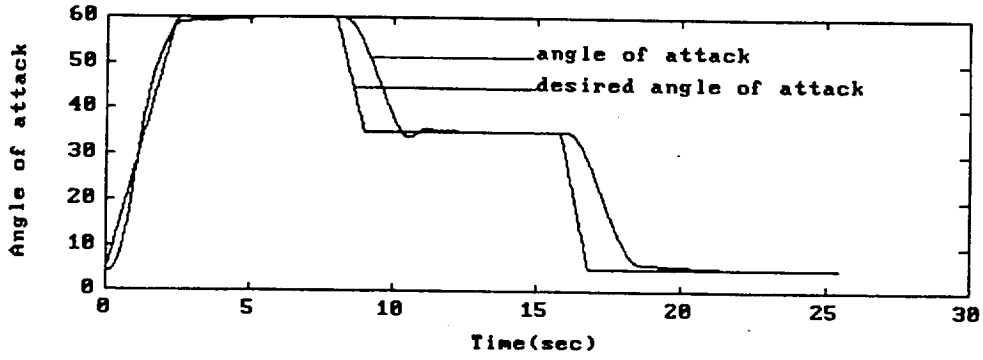

Figure 7.7 The desired angle of attack(deg) of maneuver from α_o=4.3° to α=60° and from α=60° to α=5°

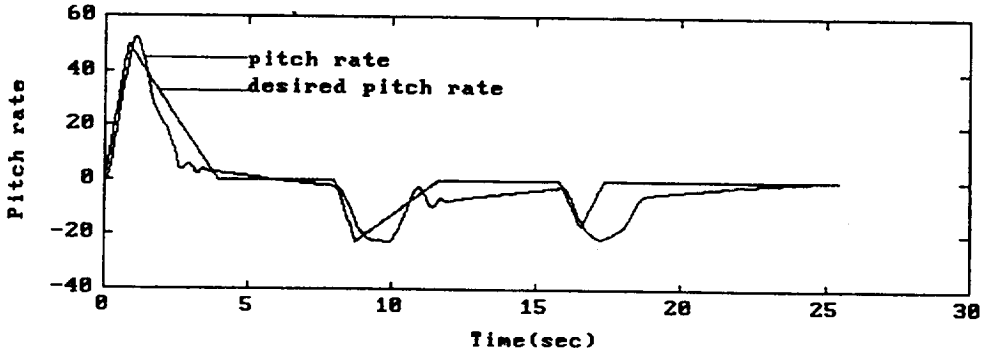

Figure 7.8 The desired pitch rate(deg/sec) of maneuver from α_o=4.3° to α=60° and from α=60° to α=5°

$$
\begin{cases}
\alpha_d = \dfrac{60 - \alpha_o}{2.49} t + \alpha_o , & 0 < t \le 2.49 \\
\alpha_d = 60 , & 2.49 < t \le 7.98 \\
\alpha_d = \dfrac{-25}{8.97-7.98} t + \dfrac{25 \times 8.01}{8.97 - 7.98} + 60 , & 7.98 < t \le 8.97 \\
\alpha_d = 35 , & 8.97 < t \le 15.81 \\
\alpha_d = \dfrac{-(35 - \alpha_o)}{16.8 - 15.81} (t - 15.81) + 35 , & 15.81 < t \le 16.80 \\
\alpha_d = 60 , & 16.80 < t
\end{cases}
\tag{7.24}
$$

where α_o is the initial angle of attack. Figure 7.7 shows the desired angle of attack.

$$
\begin{cases}
q_d = \dfrac{50}{0.81} t , & 0 < t \le 0.81 \\
q_d = \dfrac{-50}{3.96 - 0.81} t + \dfrac{50 \times 3.99}{3.96 - 0.81} , & 0.81 < t \le 3.96 \\
q_d = 0 , & 3.96 < t \le 7.98 \\
q_d = \dfrac{-22.5}{8.73 - 7.98} (t - 7.98) , & 7.98 < t \le 8.73 \\
q_d = \dfrac{22.5}{11.61 - 8.73} (t - 11.61) , & 8.73 < t \le 11.61 \\
q_d = 0 , & 11.61 < t \le 15.81 \\
q_d = \dfrac{-17}{16.59 - 15.81} (t - 15.81) , & 15.81 < t \le 16.56 \\
q_d = \dfrac{17}{17.31 - 16.56} (t - 17.37) , & 16.56 < t \le 17.37 \\
q_d = 0 , & 17.37 \le t
\end{cases}
\tag{7.25}
$$

Figure 7.8 shows the desired pitch rate.

CSMC is applied to maneuvers from low angle of attack to high angle of attack and vice versa. For example, from initial $\alpha = 4.3°$ to $\alpha = 60°$ and $\alpha = 60°$ to $\alpha = 5°$. CSMC shows a fast response (Figs 7.6~7.13). Angle of attack arrives at 55° approximately in 2.19 second and 59° in 2.6 second approximately and approaches the final terminal state without overshoot. However, this control shows a small overshoot for a maneuver from $\alpha = 60°$ to $\alpha = 35°$. This overshoot can be reduced by using appropriate desired trajectories of angle of attack and pitch rate.

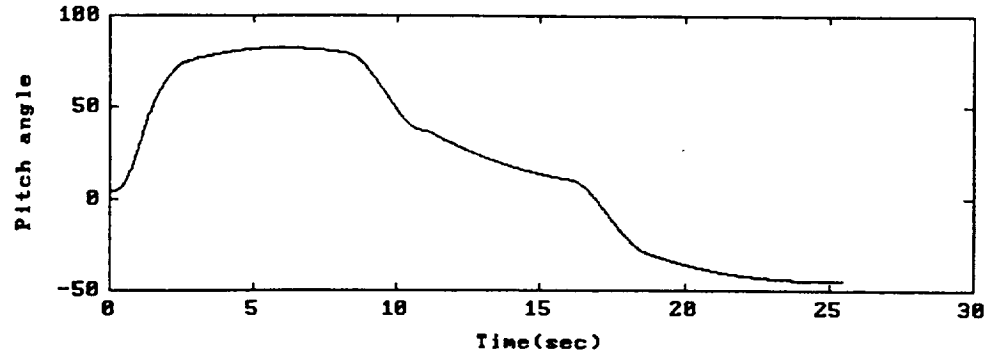

Figure 7.9 Response of the pitch angle(deg) for maneuver from α_o=4.3° to α=60° and from α=60° to α=5°

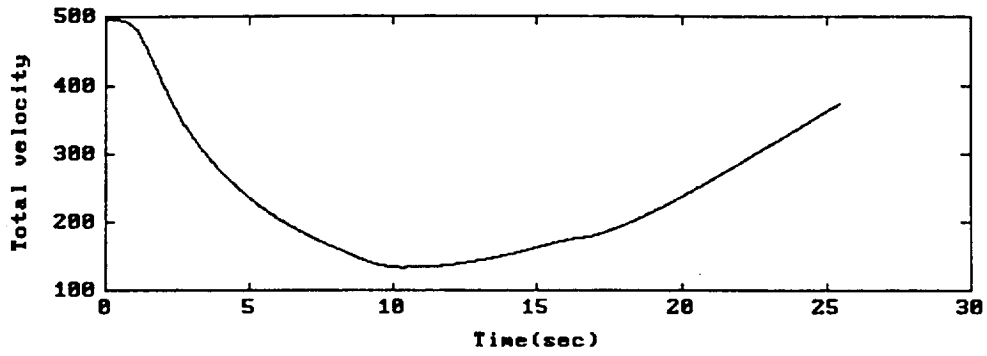

Figure 7.10 Response of the total velocity(feet/sec) for maneuver from α_o=4.3° to α=60° and from α=60° to α=5°

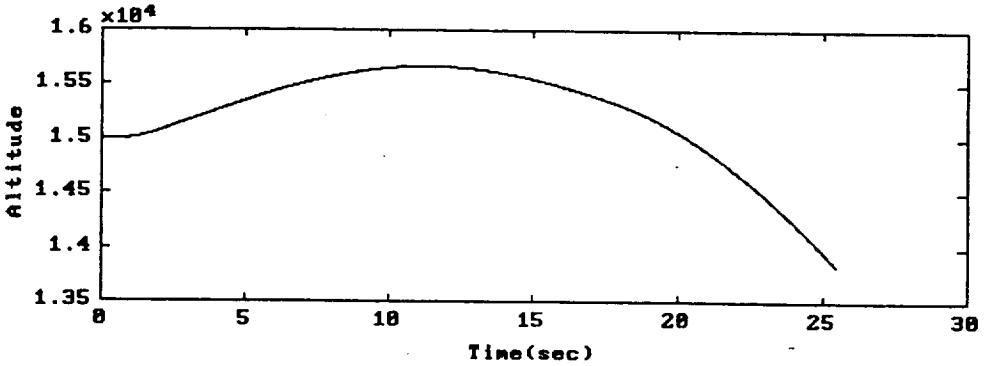

Figure 7.11 Response of the altitude(feet) of maneuver from α_o=4.3° to α=60° and from α=60° to α=5°

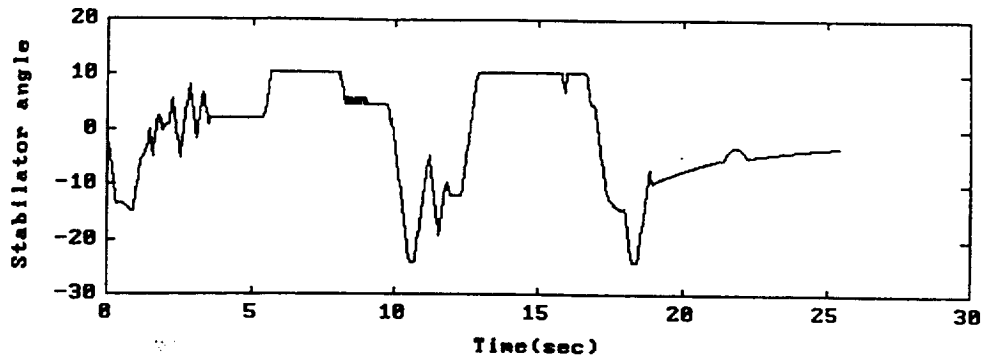

Figure 7.12 Response of the stabilator angle(deg) for maneuver from α_o=4.3° to α°=60° and from α=60° to α=5°

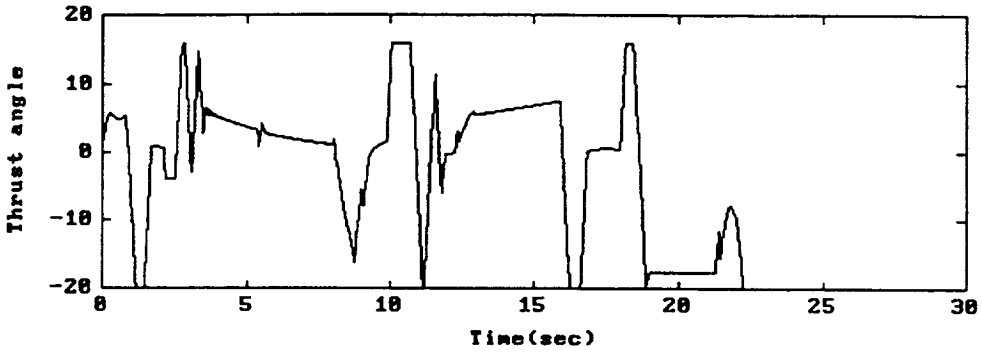

Figure7.13 Response of the thrust angle(deg) for maneuver from α_o=4.3° to α=60° and from α=60° to α=5°

7.4 Conclusion

An effective control design methodology using continuous sliding-mode control (CSMC) of a highly nonlinear maneuverable high performance aircraft, the HARV (F-18), has been presented.

Although not shown here, our simulations show that with only horizontal stabilator control, CSMC works very well without overshoot for maneuvers up to about $\alpha = 20°$. CSMC of the MIMO longitudinal motion of HARV is demonstrated successfully by accurate computer simulations. Similarly, Ostroff [7.39,7.40] investigated the maneuver by utilizing numerous trim-state linearization studies accompanied by scheduled variable gain in PIF controller. CSMC shows, in particular, a fast response from $\alpha(t_o) = 4.3°$ to 55° in 2.19 sec. and settling time to 60° in about 3 sec. compared to the latter case, which shows a rise time from $\alpha(t_o)$ to 55° in about 3.3 sec. and settling time in about 6 sec. Accordingly, CSMC shows that it is very useful for the terminal approach to the high angle of attack reducing overshooting and chattering of control even though control inputs are constrained physically. The response using time-optimal control, of course, is faster, that is, the slightly faster as shown in Section 3. Therefore, better results can be obtained if time-optimal control is used for the fast response in the first stage, and CSMC used for driving output to the final terminal value without overshoot and keeping it in the neighborhood of the sliding surface. CSMC also shows some robustness to parameter uncertainty and disturbance with the known bounds. This is accompanied by a boundary layer in the neighborhood of the sliding surface and adjusting the reachable speed within it so that less chattering of control results for the system with constrained inputs.

7.5 References

[7.1] B.R. Barmish, M.Corless and G. Leitmann, "A New Class of Stabilizing Controllers for Uncertain Dynamical System," *SIAM J. Control and Optimization*, Vol. 21, 246-255, 1983.

[7.2] S. Behtash, "Robust Output Tracking for Non-Linear Systems," *Int. J. Control*, Vol. 51, 1381-1407, 1990.

[7.3] J. Cao, F. Garrett, Jr., E. Hoffman and H. Stalford, "Analytical Aerodynamic Model of a High Alpha Research Vehicle Wind-Tunnel Model," *NASA CR-187469*, 1990.

[7.4] L.-W. Chang, "A MIMO Sliding Control with a Second-Order Sliding Condition," *ASME WAM, Paper No. 90-WA/DSC-5*, Dallas, TX, 1990.

[7.5] L.-W. Chang, "A MIMO Sliding Control with a First-Order Plus Integral Sliding Condition," *Automatica*, Vol. 27, 853-858, 1991.

[7.6] M.J. Corless and G. Leitmann, "Continuous State Feedback Guaranteeing Uniform Ultimate Boundness for Uncertain Dynamic System," *IEEE Trans. Automat. Contr.*, Vol. AC-26, 1139-1144, 1981.

[7.7] M. Corless, "Control of Uncertain Discreet-Time Systems," *Proc. American Contr. Conf.*, Seattle, WA., Vol. 1, 515-520, 1986.

[7.8] M.J. Corless and G. Leitmann, "Continuous State Feedback Guaranteeing Uniform Ultimate Boundness for Uncertain Dynamic Systems," *IEEE Trans. Automat. Contr.*, Vol. AC-26, 1139-1141, 1981.

[7.9] R.A. DeCarlo, S.H. Zak, and G.P. Matthews, "Variable Structure Control of Nonlinear Multivariable Systems: A Tutorial," *Proc. IEEE*, Vol. 76, 212-232, 1988.

[7.10] B. Drazenovic, "The Invariance in Variable Structure Systems," *Automatica*, Vol. 5, 287-295, 1969.

[7.11] O.M.E. El-Ghezawi, A.S.I. Zinober, and S.A. Billings, "Analysis and Design of Variable Structure Systems Using a Geometric Approach," *Int. J. Control*, Vol. 38, 657-671, 1983.

[7.12] H. Elmali and N. Olgac, "Robust Output Tracking Control of Nonlinear MIMO Systems via Sliding Mode Technique," *Automatica*, Vol. 28, 145-151, 1992.

[7.13] H. Elmali and N. Olgac, "Theory and Implementation of Sliding Mode Control with Perturbation Estimation," *Proc. IEEE Int. Conf. on Robotics and Automation*, Nice, France, 1992.

[7.14] B. Etkin, *Dynamics of Flight — Stability and Control*, John Wiley & Sons, Inc., New York, 1982.

[7.15] B. Etkin, *Dynamics of Atmospheric Flight*, John Wiley & Sons, Inc., New York, 1972.

[7.16] B. Fernánandez R. and J.K. Hedrick, "Control of Multivariable Non-Linear Systems by the Sliding Mode Method," *Int. J. Control*, Vol. 46, 1019-1040, 1987.

[7.17] L.-C. Fu and T.-L. Liao, "Globally Stable Robust Tracking of Nonlinear Systems Using Variable Structure Control and with an Application to a Robotic Manipulator," *IEEE Trans. Automat. Contr.*, Vol. AC-35, 1345-1350, 1990.

[7.18] W.B. Gao and J.C. Hung, "Variable Structure Control of Nonlinear Systems: A New Approach," *IEEE Trans. Ind. Electr.*, Vol. 40, 45-55, 1993.

[7.19] S. Gutman and Z. Palmor, "Properties of Min-Max Controllers in Uncertain Dynamical Systems," *SIAM J. Control and Optimization*, Vol. 20, 850-861, 1982.

[7.20] S. Gutman, "Uncertain Dynamical Systems — A Lyapunov Min-Max Approach," *IEEE Trans. Automat. Contr.*, Vol. AC-24, 437-443, 1979.

[7.21] S. Gutman and G. Leitmann, "Stabilizing Feedback Control for Dynamical Systems with Bounded Uncertainty," *IEEE Conf. Decision and Control*, New York, 1976.

[7.22] L. Hsu and R.R. Costa, "Variable Structure Model Reference Adaptive Control Using Only Input and Output Measurements," *Int. J. Control*, Vol. 49, 399-416, 1989.

[7.23] W.A. Herbst, "Future Fighter Technologies," *J. of Aircraft*, Vol. 17, 561-566, 1980.

[7.24] R.A. Horn and C.R. Johnson, *Topics in Matrix Analysis*, Cambridge University Press, Cambridge, 1991.

[7.25] J.Y. Hung, W.B. Gao, and J.C. Hung, "Variable Structure Control: A Survey," *IEEE Trans. Ind. Electr.*, Vol. 40, 2-21, 1993.

[7.26] L.R. Hunt, R. Su, and G. Meyer, "Global Transformation of Nonlinear Systems," *IEEE Trans. Automat. Contr.*, Vol. AC-28, 24-30, 1983.

[7.27] A. Isidori, *Nonlinear Control Systems: Second Edition*, Springer-Verlag, 1989.

[7.28] A. Isidori, *Nonlinear Control Systems: An Introduction*, Springer, New York, 1985.

[7.29] A. Isidori, A.J. Krener, C. Gori-Giorgi and S. Monaco, "Nonlinear Decoupling via Feedback: A Differential Geometric Approach," *IEEE Trans. Automat. Contr.*, Vol. AC-26, 331-345, 1982.

[7.30] Y. Itkis, *Control Systems of Variable Structure*, Wiley, New York, 1976.

[7.31] H. Khurana, S.I. Ahson and S.S. Lamba, "On Stabilization of Large-Scale Control Systems Using Variable Structure Systems Theory," *IEEE Trans. Automat. Contr.*, Vol. AC-31, 176-178, 1986.

[7.32] C. Kravaris and C.-B. Chung, "Nonlinear State Feedback Synthesis by Global Input/Output Linearization," *Proc. American Contr. Conf.*, Seattle, WA, Vol. 2, 997-1005, 1986.

[7.33] D.S. Lee, M.G. Kim, H.K. Kim, and M.J. Youn, "Controller Design of Multivariable Variable Structure Systems with Nonlinear Switching Surfaces," *IEE Proc. Pt. D*, Vol. 138, 493-499, 1991.

[7.34] D.G. Luenberger, "Canonical Forms for Linear Multivariable Systems," *IEEE Trans. Automat. Contr.*, Vol. AC-12, 290-293, 1967.

[7.35] S.M. Madani-Esfahani, R.A. DeCarlo, M.J. Corless and S.H. Zak, "On Deterministic Control of Uncertain Nonlinear Systems," *Proc. American Contr. Conf.*, Seattle, WA, Vol. 2, 1523-1528, 1986.

[7.36] R.R. Mohler, *Nonlinear System: Vol. 2: Applications to Bilinear Control*, Prentice Hall, Englewood Cliffs, NJ, 1991.

[7.37] R.R. Mohler, *Nonlinear System: Vol. 1: Dynamics and Control*, Prentice Hall, Englewood Cliffs, NJ, 1991.

[7.38] R.C. Nelson, *The Flight Stability and Automatic Control*, McGraw Hill, New York, 1989.

[7.39] A.J. Ostroff, "Application of Variable-Gain Output Feedback for High-alpha Control," *Proc. AIAA Guidance, Navigation and Control Conf.*, Boston, MA., Paper No. 89-3576, 1989.

[7.40] A.J. Ostroff, "High-Alpha Applications of Variable-Gain Output Feedback Control," *Journal of Guidance, Control, and Dynamics*, Vol. 15, 491-497, 1992.

[7.41] S. Richter, S. Lefebvre and R. DeCarlo, "Control of a Class of Nonlinear Systems by Decentralized Control," *IEEE Trans. Automat. Contr.*, Vol. AC-27, 492-494, 1982.

[7.42] S.Z. Sarpturk, Y. Istefanopulos and O. Kaynak, "On the Stability of Discrete-Time Sliding Mode Control Systems," *IEEE Trans. Automat. Contr.*, Vol. AC-32, 930-932, 1987.

[7.43] H. Sira-Ramirez, "Differential Methods in Variable-Structure Control," *Int. J. Control*, Vol. 48, 1359-1390, 1988.

[7.44] J.-J.E. Slotine, "Sliding Controller Design for Nonlinear Systems," *Int. J. Control*, Vol. 40, 421-434, 1984.

[7.45] J.-J.E. Slotine, and L. Weiping, *Applied Nonlinear Control*, Prentice-Hall, 1991.

[7.46] J.-J.E. Slotine and S.S. Sastry, "Tracking Control of Nonlinear Systems Using Sliding Surfaces, with Application to Robot Manipulators," *Int. J. Control*, Vol. 38, 465-492, 1983.

[7.47] S.K. Spurgeon, "Hyperplane Design Techniques for Discrete-Time Variable Structure Control Systems," *Int. J. Control*, Vol. 55, 445-456, 1992.

[7.48] H. Stalford, W.T. Baumann, F.E. Garret, T.L. Herdman, "Accurate Modeling of Nonlinear Systems Using Volterra Series Submodels," *Proc. American Contr. Conf.*, Minneapolis, MN, Vol. 2, 886-891, 1987.

[7.49] V.I. Utkin, *Sliding Modes and Their Application in Variable Structure Systems*, Mir (in English), Moscow, 1978.

[7.50] V.I. Utkin, "Variable Structure System with Sliding Modes," *IEEE Trans. Automat. Contr.*, Vol. 22, 212-222, 1977.

[7.51] V.I. Utkin, "Equations of the Sliding Regime in Discontinuous Systems, 2, " *Automation and Remote Contr.*, No. 12, 211-219, 1972.

[7.52] V.I. Utkin and K.-K.D. Young, "Methods for Constructing Discontinuity Plants in Multidimensional Variable Structure Systems," *Automation and Remote Contr.*, Vol. 39, 1466-1470, 1978.

[7.53] V.I. Utkin, "Sliding Mode Control Design Principles and Applications to Electric Drives," *IEEE Trans. Ind. Electr.*, Vol. 40, 23-36, 1993.

[7.54] V.I. Utkin, "Variable Structure Systems: Present and Future," *Automation and Remote Contr.*, Vol. 44, 1105-1120, 1983.

[7.55] F. Zhou and D.G. Fisher, "Continuous Sliding Mode Control," *Int. J. Control*, Vol. 55, 313-327, 1992.

8. CONCLUSIONS AND DIRECTIONS

Much more was accomplished with respect to high-performance aircraft control by this project than was originally proposed. However, less was accomplished on stability methodology development than anticipated. Although, it is apparent that stability criteria, such as those desired for bilinear systems with nonlinear feedback [8.1], can be applied to the aircraft dynamics with feedback, we were not able to find relevant practical design criteria in the time allowed. Unfortunately, the desired sufficient conditions are overly constraining. On the other hand, a new linear perturbation study was made for a second-order short-period model with a range of admissible feedback gains derived in conjunction with that model. This result is reported in our Phase 2 Annual Report [8.2].

The research presented here does show the potential role of nonlinear control for high performance aircraft. Indeed, the time-optimal and quadratic-optimal controls investigated make full use of nonlinear dynamics, as shown in Section 3. Nonlinear adaptive controls (Sections 4 and 5), neural-net controls (Section 6), and sliding-mode controls (Section 7), all use nonlinear feedback to effectively control, in many cases nearly optimally, the nonlinear longitudinal aircraft motion [8.3].

The neural-net-based nonlinear feedback control was trained according to simulated optimal flight trajectories in Section 4. Unfortunately, the lengthy computations can not be accomplished on-line with present technology. Still, if used in conjunction with more classical on-line feedback control, such intelligent controls could be effective in a practical sense. Other nonlinear adaptive schemes (Sections 5 and 6) can be done in real time, but do depend on sufficient disturbance (naturally or in terms of persistent self-excitation). In some cases such excitation may not be available or not tolerated and, again, off-line "learning" may be used.

The tradeoffs between on-line and off-line computations, between natural and self-excitation, between robustness and optimal performance all need to be investigated in more detail. Convenience to the pilot in using the controllers also needs to be studied.

Perhaps of immediate interest for controller, and even aircraft and engine configuration design, is the optimization analysis and the developed optimization software. This methodology and corresponding software can provide information on the most performance sensitive design parameters and constraints as well as providing precise control and performance data.

8.1 References

[8.1] X. Yang, L. Chen, and R. Mohler, "Stability of Bilinear Systems," *IEEE Tans. Autom. Control*, Vol. AC36, 1310-1315, 1991.

[8.2] R. Mohler, et al., *Phase 2 Annual Report on Nonlinear Stability and Control Study of Highly Maneuverable High Performance Aircraft*, OSU-ECE Report NASA 92-02, Corvallis, OR, August 1992.

[8.3] R.R. Mohler, "Nonlinear Control of High Performance Aircraft," *Proc. American Control Conf.*, San Francisco, 1993, pp. 1395-1399.

APPENDIX A

Project Publications and Contributors

A. PROJECT PUBLICATIONS AND CONTRIBUTORS

A.1 Project Publications (Supported Wholly or in Part by NASA Grant)

1. R.R. Mohler, *Nonlinear Systems: Vol. 2 Applications to Bilinear Control*, Prentice Hall, Englewood Cliffs, NJ, 1991.
2. R.R. Zakrzewski and R.R. Mohler, "On Nonlinear Model Algorithm Controller Design," *Proceedings* IFIP Conf. Sys. Modeling and Optimiz., Zurich, 1991.
3. R.R. Mohler, V. Rajkumar, and R.R. Zakrzewski, "Nonlinear Time-Series Based Adaptive Control Applications," *Proceedings* IEEE Conf. Decision & Control, Brighton, 1991.
4. R.R. Mohler, V. Rajkumar, and R.R. Zakrzewski, "On Discrete Nonlinear Self-Tuning Control," *Proceedings* Korean Control Conf., Seoul, 1991.
5. R.R. Mohler, R. Zakrzewski, S. Cho, and C. Koo, "New Results on Nonlinear Adaptive High Alpha Control," Comcon 3, Victoria, 1991.
6. J.E. Kurek, "Analysis of Nonlinear Stability Using Robust Stability Analysis for Linear Systems," submitted to *IEEE Trans. Autom. Control*, 1993.
7. R.R. Mohler and R.R. Zakrzewski, "Suboptimal Intelligent Control with High Alpha Aircraft Application," *Proceedings* IFIP Conf. Sys. Modeling & Optimiz., Compiegne, France, 1993.
8. R.R. Mohler, "Nonlinear Control of High Performance Aircraft," *Proceedings* American Control Conf., San Francisco, 1993.
9. A. Khapalov and R. Mohler, "Reachable Sets and Controllability of Bilinear Time-Invariant Systems," submitted to *IEEE Trans. Autom. Control*, 1993.

Three other journal papers are being prepared on adaptive/intelligent aircraft control.

A.2 Project Contributors

Senior Staff

1. R.R. Mohler, P.I., Professor
2. A. Khapalov, Visiting Professor
3. J. Kurek, Visiting Professor
4. M. Boasson, Visiting Professor
5. A. Yagen, Visiting Research Associate
6. J. Dory, Visiting Research Associate

Students

1. R. Zakrzewski*, Graduate Research Assistant (GRA)
2. D. Collins, NASA Fellow/NSF REU
3. S. Cho, GRA
4. C. Koo, GRA
5. J. Young**, NSF (REU)
6. D. Aaberg**, NSF (REU)
7. H. Travis**, NSF (REU)
8. S. Bloom**, NSF (REU)

---

*NASA-NSF support

**NSF support

APPENDIX B

Equations of Motion and Aerodynamic Model

B. EQUATIONS OF MOTION AND AERODYNAMIC MODEL

B.1 Introduction and Notation

In the following the equations of motion of an airplane in the longitudinal mode will be derived from the basic six degrees of freedom equations of a rigid body. The curve fitting technique for the stability derivatives will also be presented.

Coordinate System

Figure B.1 depicts the body axes coordinate system used in this work.

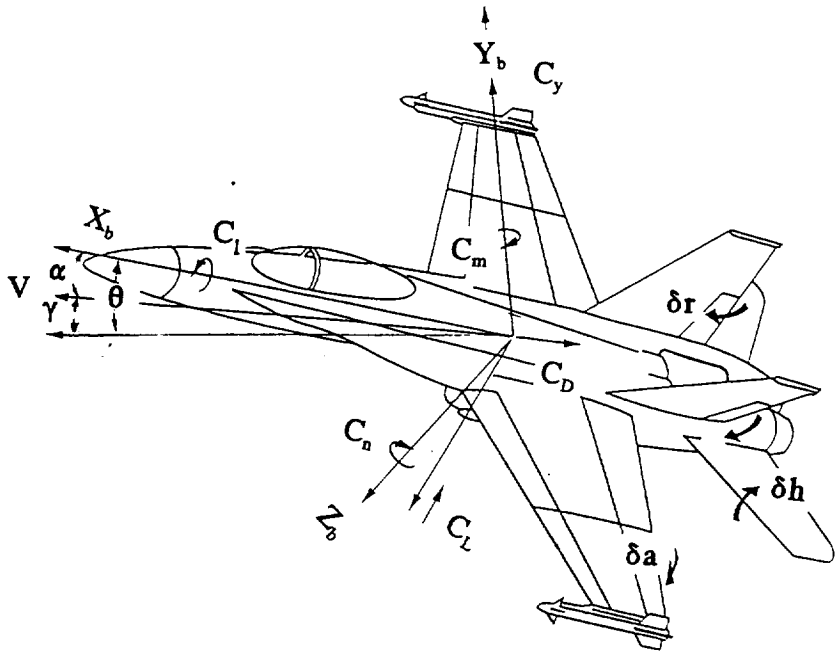

Figure B.1. Coordinate System (body axes)

XYZ: Aerodynamic forces in X_b, Y_b, Z_b directions

FR, FQ, FP: Aerodynamic moments in X_b, Y_b, Z_b

The aerodynamic lift and drag forces are defined in Fig. B.1. Also, the flight path angle (γ), pitch angle (θ), and angle of attack (α) are related, as shown in Fig. B.1.

The side slip angle β is the angle between V_T (the velocity vector) and the X_bZ_b plane. Angle of attack, α, is the angle between the projection of V_t on the X_bZ_b plane and X_b.

The following relations are defined

$$\alpha = \tan^{-1}\left[\frac{w}{u}\right] \qquad \beta = \sin^{-1}\left[\frac{v}{V}\right] \tag{B.1}$$

$$V^2 = u^2 + v^2 + w^2$$

Nomenclature

b, b′	reference length for lateral derivative (span, ft)
$\bar{c}$	reference length for stability derivatives (MAC, ft)
c.g.	center of mass (gravity)
C_{ij}	coefficients, functions of moments of inertia, I_{xx}, I_{yy}, I_{zz},I_{xz}
C_m	pitching moment coefficient
C_D	drag coefficient
C_L	lift coefficient
D	drag force (lb)
F_x, F_y, F_z	external force components (lb)
FP, FQ, FR	angular acceleration components (lb-ft)
g	gravitational acceleration (ft/sec^2)
h	altitude (ft)
I_{xx}, I_{yy}, I_{zz}	principal moments of inertia (slugs·ft^2)
I_{yz}	cross product of inertia (slugs·ft^2)
L	lift force (lb)
$\ell_{x\ell}$, $\ell_{y\ell}$, $\ell_{z\ell}$	position vector from c.g. to engine thrust center (ft)
ℓ_x, ℓ_y, ℓ_z	position vector from c.g. to aerodynamic center (ft)
M	mach number
M_x, M_y, M_z	external moment components (lb-ft)
m	aircraft mass (slug)
p	roll rate (rad/sec)
q	pitch rate (rad/sec)
$\bar{q}$	dynamic pressure (lb/ft^2)
r	yaw rate (rad/sec)
S	reference area ((wing area) ft^2)
T_x, T_y, T_z	engine thrust components (lb)

u	velocity component in x_b direction (ft/sec)
v	velocity component in y_b direction (ft/sec)
w	velocity component in z_b direction (ft/sec)
X, Y, Z	force components in x_b, y_b, z_b directions (lb)
α	angle of attack (rad or degree)
β	angle of side slip (rad or degree)
γ	flight path angle (rad or degree)
θ, ψ, ϕ	Euler angles (pitch, yaw, roll) (rad)*
ρ	air density (slug/ft^3)
δh, δa, δr	deflection angles of stabilator, ailerons, and rudder (·)
σ	standard atmosphere density ratio
δ_T	throttle setting (·)

B.2 General Equations of Motion (GDOF)

The general, GDOF equations of motion derived from Newtons laws are given in many references. The form used in [B.1] is shown here for the force and moment equations and in [B.2] for the Euler equations.

Force Equations

$$\begin{aligned} \sum F_x &= m(\dot{u} - vr + wq) \\ \sum F_y &= m(\dot{v} - wp + ur) \\ \sum F_z &= m(\dot{w} - uq + vp) \end{aligned} \tag{B.2}$$

Moment Equations

$$\begin{aligned} \sum M_x &= \dot{p} I_{xx} - \dot{r} I_{xz} + (I_{zz} - I_{yy}) qr - pq I_{xz} \\ \sum M_y &= \dot{q} I_{yy} + rp(I_{xx} - I_{zz}) + (p^2 - r^2) I_{xz} \\ \sum M_z &= \dot{r} I_{zz} - \dot{p} I_{xz} + (I_{yy} - I_{xx}) pq + I_{xz} qr \end{aligned} \tag{B.3}$$

*Get order of rotations: yaw, pitch, roll

Euler Equations

$$\begin{aligned}\dot{\theta} &= q\cos\phi - r\sin\phi \\ \dot{\phi} &= p + q\sin\phi\,tg\,\theta + r\cos\phi\,tg\,\theta \\ \dot{\psi} &= (q\sin\phi + r\cos\phi)\sec\theta\end{aligned} \tag{B.4}$$

Here the aircraft is treated as a rigid, symmetrical body (so only the I_{xz} cross product exits); also (j mean d/(dt) the time derivative.

The GDOF equations can be written in terms of u, v, w and Dyr [B.3].

Force Equations (body axes)

$$\begin{aligned}\dot{u} &= rv - qw - g\sin\theta + X + \frac{T_x}{m} \\ v &= pw - ru + g\cos\theta\sin\phi + Y + \frac{T_y}{m} \\ w &= qu - pv + g\cos\theta\cos\phi + Z + \frac{T_z}{m}\end{aligned} \tag{B.5}$$

Moment Equations (body axes)

$$\begin{aligned}\dot{p} &= C_{41}\,pg + C_{42}\,qr + C_{43}\,FR + C^*\,FP + \frac{C_{43}}{I_{zz}}\left(\ell_{z\ell}\,T_y - \ell_{y\ell}\,T_x\right) + \frac{C^*}{I_{xx}}\left(\ell_{y\ell}\,T_z - \ell_{z\ell}\,T_y\right) \\ \dot{q} &= C_{51}\,pr + C_{52}\left(r^2 - p^2\right) + FQ + \frac{1}{I_{yy}}\left(\ell_{z\ell}\,T_x - \ell_{x\ell}\,T_z\right) \\ \dot{r} &= C_{61}\,pq + C_{62}\,qr + C_{63}\,FP + C^*\,FR + \frac{C_{63}}{I_{xx}}\left(\ell_{y\ell}\,T_z - \ell_{x\ell}\,T_y\right) + \frac{C^*}{I_{zz}}\left(\ell_{x\ell}\,T_y - \ell_{y\ell}\,T_x\right)\end{aligned} \tag{B.6}$$

The three Euler equations (B.4) remain unchanged.

In these equations

$$
\begin{aligned}
X &= [-D\cos\alpha + L\sin\alpha]/m && \text{(normal aerodynamic acceleration)} \\
Z &= [-D\sin\alpha - L\cos\alpha]/m && \text{(axial aerodynamic acceleration)} \\
Y &= \bar{q}\,S\,C_y/m && \text{(aerodynamic side acceleration)}
\end{aligned} \tag{B.7}
$$

and

$$L = \bar{q}\,S\,C_L \quad \text{(lift)} \qquad D = \bar{q}\,S\,C_D \quad \text{(drag)}$$

The aerodynamic accelerations are

$$
\begin{aligned}
FP &= \left[\bar{q}\,Sb\,C\ell + m\left(\ell_y Z - \ell_z Y\right)\right] \Big/ I_{xx} && \text{(rolling)} \\
FQ &= \left[\bar{q}\,S\bar{c}\,Cm + m\left(\ell_z X - \ell_x Z\right)\right] \Big/ I_{yy} && \text{(pitching)} \\
FR &= \left[\bar{q}\,Sb\,Cn + m\left(\ell_x Y - \ell_y Z\right)\right] \Big/ I_{zz} && \text{(yawing)}
\end{aligned} \tag{B.8}
$$

Note that reference length for roll and yaw is b (wing span) and for pitch is $\bar{c}$, mean aerodynamic chord (MAC).

The inertia moments are assumed to be constant and their coefficients are defined as follows

$$
\begin{aligned}
C^* \equiv C_{40} &= I_{xx}\cdot I_{zz} \Big/ \left(I_{xx}I_{zz} - I_{xz}^2\right) \\
C_{41} &= C^*\, I_{xz}\left(I_{zz} + I_{xx} - I_{yy}\right) \Big/ I_{xx}I_{zz} \\
C_{42} &= C^* \left[I_{zz}\left(I_{yy} - I_{zz}\right) - I_{xz}^2\right] \Big/ I_{xx}I_{xz} \\
C_{43} &= C^*\, I_{xz} / I_{xx} \\
C_{51} &= \left(I_{zz} - I_{xx}\right) / I_{yy} \\
C_{52} &= I_{xz} / I_{yy} \\
C_{61} &= C^* \left[I_{xx}\left(I_{xx} - I_{yy}\right) + I_{xz}^2\right] \Big/ I_{xx}I_{zz} \\
C_{62} &= C^*\, I_{xz}\left(I_{yy} - I_{zz} - I_{xx}\right) \Big/ I_{xx}I_{zz} \\
C_{63} &= C^* I_{xz} / I_{zz}
\end{aligned} \tag{B.9}
$$

B.3 Form of Aerodynamic Coefficients (Stability Derivatives)

The aerodynamic coefficients, also called stability derivatives, are written in the following form:

$$\text{Drag Coefficient} \quad C_D = C_{D_o}(\alpha, M, h, \delta h)$$

$$\text{Lift Coefficient} \quad C_L = C_{L_o}(\alpha, M, h, \delta h) + \frac{\bar{c}}{2V}\left[C_{L_q}(\alpha, M, h)\, q + C_{L_{\dot{\alpha}}}(\alpha, M, h)\, \dot{\alpha}\right] \tag{B.9}$$

$$\text{Pitching Moment} \quad C_m = C_{m_o}(\alpha, M, h, \delta h) + \frac{\bar{c}}{2V}\left[C_{m_q}(\alpha, M, h)\, q + C_{m_{\dot{\alpha}}}(\alpha, M, h)\, \dot{\alpha}\right]$$

The aerodynamic coefficients C_{D_o}, C_{L_o}, C_{m_o} depend on angle of attack, α, mach, M, altitude, h, and control surface angles, δ, (which are the controlling factor). The damping coefficients C_{L_q}, $C_{L_{\dot{\alpha}}}$, C_{m_q}, $C_{m_{\dot{\alpha}}}$ are dependent on α, M, h but not functions of δ.

B.4 Equations of Motion for the Longitudinal Mode

The case in which the airplane moves without side slip and rolling motion is called the longitudinal mode. In this the motion is restricted to a plane containing the X_bZ_b plane. For this case we may make the following assumptions.

β, $\dot{\beta}$, v, p, r, ϕ, ψ will all be zero identically (B.10)

The equation for longitudinal motion, based on (B.5) and (B.6) are

$$\dot{u} = -qw - g\sin\theta + X + \frac{T_x}{m}$$

$$\dot{w} = qu + g\cos\theta + Z + \frac{T_z}{m} \tag{B.11}$$

$$\dot{q} = \frac{\bar{q}\, S\, \bar{c}\, C_m}{I_{yy}} + \left(m\left(\ell_z X - \ell_x Z\right) + \ell_{z\ell}\, T_x - \ell_{x\ell}\, T_z\right) / I_{yy}$$

and the remaining Euler equation (B.4)

$$\dot{\theta} = q \tag{B.12}$$

It is more convenient to select state variables α, V, q, θ, instead of u, w, q, θ (B.4).

Using the relationship (Fig. B-4, $\beta = 0$)

$$U = V \cos \alpha$$

$$W = V \sin \alpha$$

and $$V^2 = u^2 + w^2$$

By taking derivatives with respect to time, we get

$$\dot{\alpha} = \frac{u\dot{w} - \dot{u}w}{V^2} \Rightarrow \dot{w} = \frac{V\dot{\alpha} + \sin\alpha\,\dot{u}}{\cos\alpha} \tag{B.13}$$

Using the expression for $\dot{w}$ in (B.11), after some algebraic manipulation, we get the equation for $\dot{\alpha}$:

$$\dot{\alpha} = q + \frac{g}{V}(\cos\theta\cos\alpha + \sin\theta\sin\alpha) - \frac{L}{mV} - \frac{T_x}{mV}\sin\alpha + \frac{T_z}{mV}\cos\alpha$$

In a similar fashion we derive expressions for $\dot{V}$, $\dot{q}$, and $\dot{\theta}$:

$$\dot{V} = -g\sin\theta\cos\alpha + g\sin\alpha\cos\theta - \frac{D}{m} + \frac{T_x}{m}\cos\alpha + \frac{T_z}{m}\sin\alpha$$

$$\dot{q} = \frac{\bar{q}\,S\,\bar{c}\,Cm}{I_{yy}} + \frac{D}{I_{yy}}(-\ell_z\cos\alpha + \ell_x\sin\alpha) + \frac{L}{I_{yy}}(\ell_z\sin\alpha + \ell_x\cos\alpha) + \frac{1}{I_{yy}}(\ell_{z\ell}\,T_x - \ell_{x\ell}\,T_z) \tag{B.13}$$

$$\dot{\theta} = q$$

By substitution of the form of aerodynamic coefficients (B.9) and defining

$$q_{11} = -\ell_z\cos\alpha + \ell_x\sin\alpha$$

$$q_{12} = \ell_z\sin\alpha + \ell_x\cos\alpha \tag{B.14}$$

and some more simple algebra, we get

$$\dot{\alpha} = \frac{1}{1 + \rho\frac{S\bar{c}}{4m}C_{L_{\dot{\alpha}}}}\left\{\left[1 - \frac{\rho\,S\,\bar{c}}{4m}C_{L_q}\right]q + \frac{g}{V}\cos\gamma - \bar{q}\frac{SC_{L_o}}{mV} + \right.$$

$$\left. - \frac{T_x}{mV}\sin\alpha + \frac{T_z}{mV}\cos\alpha\right\} \tag{B.15}$$

$$\dot{V} = -g \sin\gamma - \frac{\bar{q} S}{m} C_{D_o} + \frac{T_x}{m} \cos\alpha + \frac{T_z}{m} \sin\alpha$$

$$\dot{q} = \frac{\rho S}{2I_{yy}} \left(\bar{c} C_{m_o} + q_{11} C_{D_o} + q_{12} C_{L_o} \right) V^2 + \frac{\rho S \bar{c}}{4I_{yy}} Vq \left(\bar{c} C_{m_q} + q_{12} C_{L_q} \right) +$$

$$+ \frac{\rho S \bar{c} \left(\bar{c} C_{m_{\dot{\alpha}}} + q_{12} C_{L_{\dot{\alpha}}} \right)}{4I_{yy} \left[1 + \frac{\rho S \bar{c}}{4m} C_{L_{\dot{\alpha}}} \right]} \left\{ \left[1 - \frac{\rho S \bar{c}}{4m} C_{L_q} \right] \frac{g}{V} \cos\gamma - \frac{\rho S C_{L_o}}{2m} V - \frac{T_x}{mV} \sin\alpha + \right. \quad \text{(B.15)}$$

$$\left. + \frac{T_z}{mV} \cos\alpha \right\} V + \frac{\ell_{z\ell} T_x - \ell_{x\ell} T_z}{I_{yy}}$$

$$\dot{\theta} = q$$

These are the four equations of motion used in this work.

B.5 Values of Constants and Aerodynamic Coefficients

The values of the various constants for this airplane were taken from [B.4].

Constants:

aircraft	— McDonnel-Douglas F-18 Fighter		
mass		m	= 1035.308 slugs
weight		w	= 33,310 lb
moments of inertia:			
		I_{xx}	= 23,000 slug·ft^2
		I_{yy}	= 151,293 slug·ft^2
		I_{zz}	= 169,945 slug·ft^2
		I_{xz}	= -2,971 slugs·ft^2
wing area		S	= 400 ft^2
MAC		$\bar{c}$	= 11.52 ft
wing span		b	= 37.42 ft
geometry		ℓ_x	= -0.297 ft
		ℓ_y	= 0
		ℓ_z	= 0.233 ft

	$\ell_{x\ell}$	= -19.37 ft
	$\ell_{y\ell}$	= 0
	$\ell_{z\ell}$	= 0.233 ft
dynamic pressure	$\bar{q}$	= 1/2 ρ V^2
air density	ρ	= 0.0023709 σ

Aerodynamic Coefficients

Reference [B.4] gives the aerodynamic coefficients for this aircraft in the form of curve fits to wind tunnel data. Values are given for the following range of parameters:

angle of attack	$-10° < \alpha < 90°$
side slip	$-20° < \beta < 20°$
mach number	$0.2 < M < 2$
altitude	$0 < h < 60{,}000$ ft
aileron deflection	$-25° < \delta a < 25$
rudder deflection	$-30° < \delta r < 30°$
stabilator deflection	$-24° < \delta h < 10.5°$
throttle setting	$30°$ (idle) $< \delta_T < 131°$ (full afterburner)

The coefficients are given in the form of piecewise arc tangent functions for discrete values of the parameters. Interim values are then interpolated.

Example:

C_{M_o} - pitching moment in Eq. (B.9):

$C_{M_o}(\alpha, M = 0.6, \delta h = 10.5°, h = 15{,}000 \text{ ft}) = C_{M_o} \text{ X } 6\ (\alpha)$

$$C_{M_o} \text{ X } 6\ (\alpha) = (.26/2.75) \tan^{-1} (-(\alpha°\text{-}5)\ 1/10) + (-.39/2.75) \tan^{-1} ((\alpha°\text{-}1)\ 1/8)$$
$$+ (.8/2.75) \tan^{-1} ((\alpha°\text{-}5)\ 1/13) + (.70/2.75) \tan^{-1} (-(\alpha°\text{-}10)\ 1/65)$$
$$+ (1.2/2.75) \tan^{-1} (\alpha°\text{-}49)\ 1/15) + (2.1/2.75) \tan^{-1} (-(-\alpha°\text{-}69)\ 1/15)$$
$$+ (-.45/2.75) \tan^{-1} (-(\alpha°\text{-}77)\ 1/2) - 3.98$$

Similar expressions are given for all the other relevant aerodynamic coefficients. This data is sufficient for the longitudinal case and also for small lateral angles. Ref. [B.4] also shows the accuracy of the curve filled data by comparing it to the actual wind tunnel results. In most cases the agreement between the curve filled and actual data is excellent. Small deviations can be expected in the high angle of attack range ($\beta >$ w-70°).

The values of the aerodynamic coefficients are given for the following range of parameters:

C_{D_o}	$\delta h = 10.5°, 0°, -5°, -24°$			}	$-10° < \alpha < 90°$
C_{L_o}	$h = 15\ k'$	$\delta h = 10.5°$	$M = 0.6, 0.9$		
		$\delta h = -24°$	$M = 0.6, 0.9$		
C_{L_q}	$M = 0.6$	$h = 15\ k'$			
$C_{L_{\dot{\alpha}}}$	$M = 0.6$	$h = 15\ k'$			
C_{mo}	$M = 0.6, 0.9$	$\delta h = 10.5°, 5°, 2°, 0°, -5°, -12.5°, -24°$			$h = 15\ k'$
C_{m_q}	$M = 0.6$	$h = 15\ k'$			
$C_{m_{\dot{\alpha}}}$	$M = 0.6$	$h = 15\ k'$			

Further aerodynamic data can be found in Ref. [B.5] and [B.6] (manufacturers data) and several more reports which are in our hands.

B.6 Future Developments

The method of derivation for the equations of motion shown here can be used for the lateral mode also. In order to check the longitudinal controllers which were developed and to develop lateral controllers (if necessary) for combined pitch, yaw, and roll maneuvers which are needed in modern air combat, it will be necessary to develop a GDOF aerodynamic model, including GDOF equations of motion. This will be done gradually, by first constraining the lateral movements to small side slip angles, as was done by several references — for example, Safanov [B.7] discussing the Herbst [B.5] maneuver and Ostroff [B.9]. One can do this in two ways — either develop the full GDOF equations, from [B.5] and [B.6], and add a small β constraint to the result, or use the small constraint from the beginning to get a somewhat simpler equation system, and move on to the full case later on. For the full GDOF case the data given in [B.4] must be widened by using the full data available in [B.5] and [B.6]. The group has already done preliminary work in this direction. A convenient method for showing results on real time simulations is given in Ref. [B.10]. This method uses spherical mapping to transform the various angular relations to a two-dimensional plane. Future lateral results may be displayed in this form.

B.7 References

[B.1] Perkins, C.D. and Haye, R.E., *Airplane Performance, Stability, and Control*, J. Wiley & Sons, 1949.

[B.2] Atkin, B., *Dynamics of Flight — Stability and Control* (2nd Ed.), J. Wiley & Sons, 1982.

[B.3] Cho, S., Ph.D. Dissertation, to be published in 1993.

[B.4] Cuo, J., F. Garret Jr., E. Hoffman, and H. Stalford, "Analytical Aerodynamic Model of a High Alpha Research Vehicle Wind Tunnel Model," Georgia Institute of Technology, Atlanta, GA, 1990 (Also NASA Grant NAG10959).

[B.5] MDC Rep. No. *A7247* — "F/A 18 Stability and Control Data Report", Vol. I — Low Angle of Attack; Vol. II — High Angle of Attack; August 31, 1981.

[B.6] MDC Report No. *A8575* — "F/A 18 Basic Aerodynamic Data," McDonnel Aircraft Comp., St. Louis, MO, March 31, 1984.

[B.7] Chiang, R.Y., M.G. Safonov, K.P. Madden, and J.A. Tekway, "A Fixed H^{∞} Controller for a Supermaneuverable Fighter Performing a Herbst Maneuver," *Proc. IEEE Conf. on Decision and Control*, Honolulu, December 5-7, 1990.

[B.8] Herbst, W.B., "Future Fighter Technology," *Jr. of Aircraft*, Vol. 17, No. 8, August 1980.

[B.9] Ostroff, A.J., "Application of Variable Gain for Output Feedback for High Alpha Control.

[B.10] Kalviste, J., "Spherical Mapping and Analysis of Aircraft Angles for Maneuvering Flight," NIAH paper *86-2283*.